Heat Transfer Engineering
Publication details, including instructions for authors and subscription information:
http://www.tandfonline.com/loi/uhte20

Dropwise Condensation Studies on Multiple Scales

Basant Singh Sikarwar [a], Sameer Khandekar [a], Smita Agrawal [a], Sumeet Kumar [a] & K. Muralidhar [a]

[a] Department of Mechanical Engineering, Indian Institute of Technology Kanpur, Kanpur, India

Available online: 25 Aug 2011

To cite this article: Basant Singh Sikarwar, Sameer Khandekar, Smita Agrawal, Sumeet Kumar & K. Muralidhar (2012): Dropwise Condensation Studies on Multiple Scales, Heat Transfer Engineering, 33:4-5, 301-341

To link to this article: http://dx.doi.org/10.1080/01457632.2012.611463

Heat Transfer Engineering, 33(4–5):301–341, 2012

ISSN: 0145-7632 print / 1521-0537 online
DOI: 10.1080/01457632.2012.611463

Dropwise Condensation Studies on Multiple Scales

BASANT SINGH SIKARWAR, SAMEER KHANDEKAR, SMITA AGRAWAL, SUMEET KUMAR, and K. MURALIDHAR

Department of Mechanical Engineering, Indian Institute of Technology Kanpur, Kanpur, India

Recent advances in nanotechnology, chemical/physical texturing and thin film coating technology generate definite possibilities for sustaining a dropwise mode of condensation for much longer durations than was previously possible. The availability of superior experimental techniques also leads to deeper understanding of the process parameters controlling the relevant transport phenomena, the distinguishing feature of which is the involvement of a hierarchy of length/time scales, proceeding from nuclei formation, to clusters, all the way to macroscopic droplet ensemble, drop coalescence, and subsequent dynamics. This paper is an attempt to connect and present a holistic framework of modeling and studying dropwise condensation at these multiple scales. After a review of the literature, discussions on the following problems are presented: (i) atomistic modeling of nucleation; (ii) droplet–substrate interaction; (iii) surface preparation; (iv) simulation of fluid motion inside sliding drops; (v) experimental determination of the local/ average heat transfer coefficient; and (vi) a macroscopic model of the complete dropwise condensation process underneath horizontal and inclined surfaces. The study indicates that hierarchal modeling is indeed the way forward to capture the complete process dynamics. The microscopic phenomena at the three-phase contact line, leading to the apparent droplet contact angle, influence the shear stress and heat transfer. The nucleation theory captures the quasi-steady-state behavior quite satisfactorily, although the early atomistic nucleation was not seen to have a profound bearing on the steady-state behavior. The latter is strongly governed by the coalescence dynamics. Visual observation of dropwise condensation provides important information for building hierarchical models.

INTRODUCTION

Dropwise condensation of vapor on and underneath horizontal and inclined surfaces is encountered in many engineering processes. Dropwise condensation is preferred over the filmwise mode when large heat transfer coefficients are required [1, 2]. Hence, formation of drops needs to be promoted by treating the surface in such as way that fluid wetting is inhibited [3, 4]. The growth of drops commences with the deposition of warmer vapor atoms on a cool substrate, which has a suitably engineered surface created by physical or chemical texturing. Drops evolving from nucleation sites first grow by direct condensation of the vapor and then by coalescence till their size get large enough to slide off or fall off on the surface [5, 6]. A fresh round of nucleation and growth commences in the freshly exposed area of the substrate, indicating that dropwise condensation is a cyclic phenomenon [6]. The associated heat transfer rates are also time dependent, being very large at the start of the cycle and reaching a minimum just before the drop is set in motion [7].

At the atomistic level, vapor atoms may impinge on the surface with a directed velocity, or alternatively, the vapor may be quiescent. The individual quiescent atoms may form stable clusters by combining with the neighbors and grow on the surface with time [8]. An atom/molecule bound to the surface is an adatom and a group of adatoms leads to a cluster, as shown in Figure 1a. Although it is also possible to form clusters in the vapor phase before they get deposited on the surface, with large substrate subcooling, one can expect all condensation to occur at the surface level only, i.e., as heterogeneous condensation. The stability of the cluster depends on mutual energy

The authors are grateful to the Board of Research in Nuclear Sciences (BRNS), Department of Atomic Energy, Government of India, for providing the partial financial assistance to carry out this research work. Technical discussions with Dr. L. M. Gantayet and Dr. Jaya Mukherkjee, Bhabha Atomic Research Center, Mumbai, India, are gratefully acknowledged. Contributions by former students, Gagan Bansal, Gaurav Bhutani, Nirmal Kumar Battoo, and Liza Ann Easo, who worked on the project, and technical help provided by C. S. Goswami are also acknowledged. The authors are grateful to the anonymous referee who examined the first version of the paper very critically and provided useful suggestions.

Address correspondence to Professor Sameer Khandekar, Department of Mechanical Engineering, Indian Institute of Technology Kanpur, Kanpur 208016, India. E-mail: samkhan@iitk.ac.in

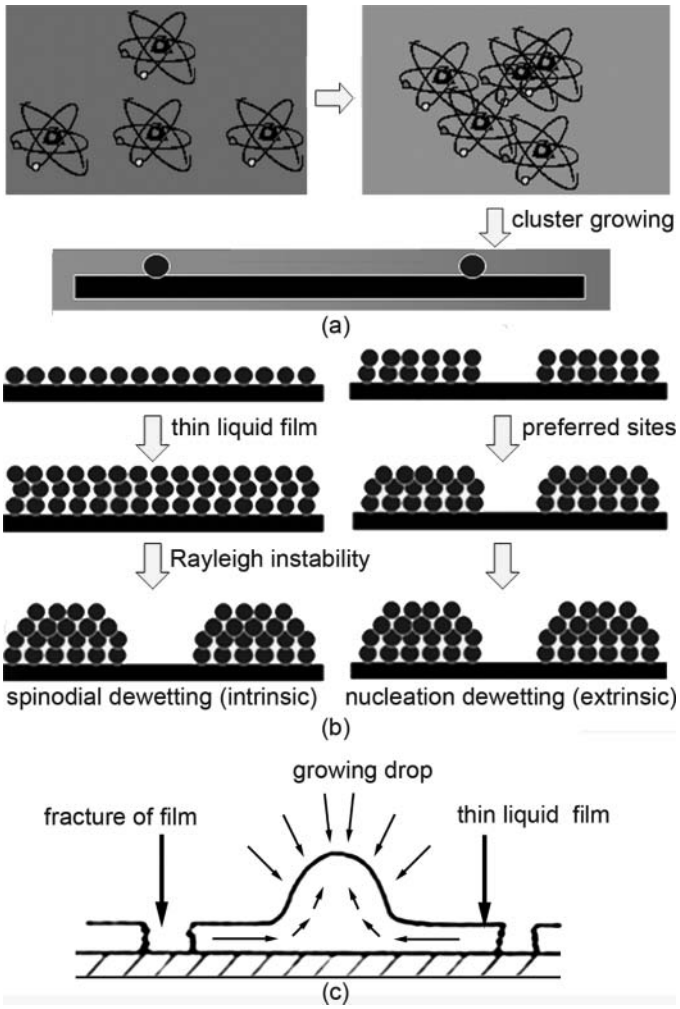

Figure 1 Mechanism of liquid drop formation on cold substrate. (a) At atomic levels from angstroms to nanoscale, individual vapor molecules come closer and a system of adatoms form, a group of adatoms leads to a cluster. (b) Many growing clusters together may form an atomic/molecular monolayer of liquid. At this stage there are at least two possibilities: film formation wetting and droplet formation (dewetting). (c) This liquid film ruptures and converts to droplet formation.

interactions between the cluster, the atoms of the surrounding vapor, and the cold wall. Molecules/atoms approaching the cold wall have a higher temperature—i.e., energy, than departing molecules/atoms that have transferred their energy to the wall [9]. This energy difference determines whether a given cluster clinging to the surface will be stable, will grow with time or diminish in size.

Many stable clusters growing together may form an atomic/molecular monolayer of condensate on the substrate [10]. There are at least two possibilities of drop formation (dewetting) [11], as shown in Figure 1b. In the first model, it is postulated that the condensation initially occurs in a filmwise manner, forming an extremely thin film on the solid surface. As condensation continues in time, the film ruptures due to intrinsic interfacial instabilities and distinct drops are formed, as shown in Figure 1c. The second model is based on the premise that drop formation is a heterogeneous nucleation process. Here, a stable cluster located in a specific nucleation site over the substrate, such as in pits and grooves, grows by incorporating other adjoining clusters. Droplet embryos are postulated to form at the atomic scale and grow in the continuum domain, while the portion of the surface between the growing drops essentially remains dry. Hence, issues such as molecular potential, adatoms dynamics, cluster dynamics, surface diffusion, stable cluster size and nucleation density, film stability and rupture, topography interaction, stable cluster formation, etc. appear, as condensation proceeds from the atomistic scale to the microscale.

In a purely macroscopic model [12], single drops, of the size of the largest cluster determined from atomistic considerations (equal to the minimum thermodynamically stable drop radius), appear at preferred nucleation sites over the substrate. These drops first grow by direct condensation up to a size that is of the order of magnitude of the distance between neighboring nucleation sites. Beyond this point, coalescence between neighboring drops can take place and the subsequent growth of the drops will occur by a combination of direct condensation and coalescence. As a result of coalescence, the number of drops per unit area decreases while the condensing surface area increases. As bare areas are exposed, coalescence between drops also provides a source of hitherto covered nucleation sites [13]. When a certain drop size is reached on an inclined condensing substrate, body forces exceed the surface tension holding the drop to the solid surface. The drop first slides off, then departs and sweeps the surface clear, permitting new nucleation sites to become available. Hence, apart from atomic-level processes in the vapor phase as well as the substrate, subjects of importance in this scale are droplet growth rate, vapor accommodation coefficient, coalescence dynamics, instability and drop motion, shear stresses, pinning, dewetting characteristics, and the influence of surface orientation.

Therefore, the complete condensation cycle begins at the atomic level and leads to macroscopic drops till they slide off or fall off. The process covers a wide spectrum of time and length scales. A complete understanding of condensation is required for the design of textured surfaces that would be suitable for heat transfer applications.

Based on the preceding discussion, research issues that need to be addressed are summarized here.

(i) Mathematical modeling of the entire dropwise condensation process, from atomistic level to the formation of the macroscale drop, followed by the behavior of a population of drops of varying sizes that are in dynamic equilibrium.
(ii) Formation of individual drops, their shape and resulting motion depending on the surface energy distribution, surface roughness and characteristics of thin film coating. Thus, macroscale mechanisms are intrinsically linked to the microscale, indicating the need for hierarchical modeling.
(iii) The mobility of a drop, contact line motion, drop merger and instabilities, contact angle hysteresis, and the

metastable states[1] of the condensing fluid. These subjects pose a challenge in macroscale models.

(iv) Surface texturing to promote dropwise condensation and provide for large heat transfer coefficients. The process of repeated condensation and fluid removal can leach the surface and alter the surface and its energy distributions characteristics. Predicting the wear and tear of the surface is an important consideration from an industry viewpoint.

(v) Heat transfer coefficient. The driving temperature difference in dropwise condensation is small. Hence, the experimental determination of the heat transfer coefficient is a challenge. The statistical nature of drop distribution over the surface, as well as its temporal variations, contributes to the intricacy of analysis and data reduction.

In the present study, the main processes involved in dropwise condensation on physically and chemically textured surfaces over various length and timescales are reviewed. The subjects of interest are the formation of drops at the atomic scale, liquid–substrate interaction, preparation of a lyophobic substrate, predicting the growth of the drops and their motion, interaction between the adjacent drops, and the determination of the local and average heat transfer coefficient and shear stress.

The paper is organized in the following sequence: The first section describes the modeling of dropwise condensation on the atomic scale. This is followed by a discussion of the liquid-substrate interaction, interaction between adjacent drops, preparation of substrate, and the experimental determination of the heat transfer coefficient. A macroscale model of dropwise condensation process is then presented. The review closes with major conclusions arrived at in the study.

CONDENSATION ON THE ATOMIC SCALE

Dropwise condensation of vapor is a phase-change process. It can be homogeneous, namely, distributed in the vapor-phase, or heterogeneous, as in the presence of a cooler solid substrate [12]. It is now generally accepted that phase change, whether homogeneous or heterogeneous condensation, is induced by nucleation, which is triggered by molecular clustering. In view of experimental limitations, the physical picture, right at nucleation, is not very clear. From a heat transfer viewpoint, an important fundamental question is how drops form, grow, and get mobilized over a treated solid surface. For the phase-change process of dropwise condensation, the understanding on the microscale transport of process continues to be deficient. Most of the literature [9–14] suggests that the drop formation during condensation commences with the impingement of vapor atoms on a cold substrate. Some researchers argue that clustering begins in the vapor-phase itself close to the cold wall and that the clusters formed closer to the wall have larger size than those formed in the bulk vapor phase [10, 14]. The thickness of this cluster zone depends on the thermal condition of the molecular system and the energy transfer processes in action. The surface adatoms undergo a sequence of processes such as adsorption, diffusion, reflection, agglomeration, transfer of energy, and formation of stable clusters, eventually manifesting as a distribution of growing condensed liquid nuclei [11, 12, 15]. Wang et al. [16] proposed an idea of critical aggregation concentration of active molecules to describe the situation just before nucleus formation. Tian et al. [17] studied the aggregation of active molecules inside a metastable bulk phase using thermodynamics. The authors derived an expression for the critical aggregation concentration, energy distribution of active molecules inside the bulk phase at superheated and supercooled limits, and used the molecular aggregation theory to describe the gas–liquid phase-transition process.

In the following section, a kinetic population balance model at the atomic level is used to predict the size of critical clusters during condensation of saturated vapor on a sub-cooled substrate. With a given set of process parameters, the model predicts the distribution of stable cluster sizes under steady-state conditions and hence the largest cluster size. The largest cluster size determined from atomistic considerations is interpreted as the smallest drop size appearing on a macroscopic continuum scale.

Atomistic Modeling of Condensation

Consider the following arrangement in which condensation process is in progress (Figure 2a). Saturated vapor is introduced in the chamber at a rate given by the mass flux, F. The substrate is at a temperature lower than that of the saturated vapor. The temperature difference is large enough so that complete condensation of the vapor is ensured on contact, but small enough to prevent condensation rates that would lead to the formation of a liquid film, i.e., reasonable time scales for individual drop formation and subsequent droplet ensemble dynamics are available. A certain amount of condensation may also take place in the vapor phase, just below the substrate. The equivalent microscopic picture is that atomic collisions and binding in the vapor phase lead to clustering. The flux impinging on the substrate comprises not just single atoms or molecules of the vapor phase but also their clusters. The full condensation problem involves developing a mathematical model of vapor condensation in the chamber (homogeneous nucleation) and on the substrate surface (heterogeneous nucleation). The latter also involves growth of clusters over the substrate over a period of time.

In the present work, it is assumed that the no clustering is possible in the vapor phase and hence the flux deposited on the substrate is in the form of single molecules/atoms. The vapor mass flux is obtained in the form of an over-expanded

[1]Condensing vapor that is supercooled below its equilibrium saturation temperature and condensing liquid that is superheated with respect to its equilibrium saturation temperature can prevail for short periods of time and are referred to be in a *metastable* state.

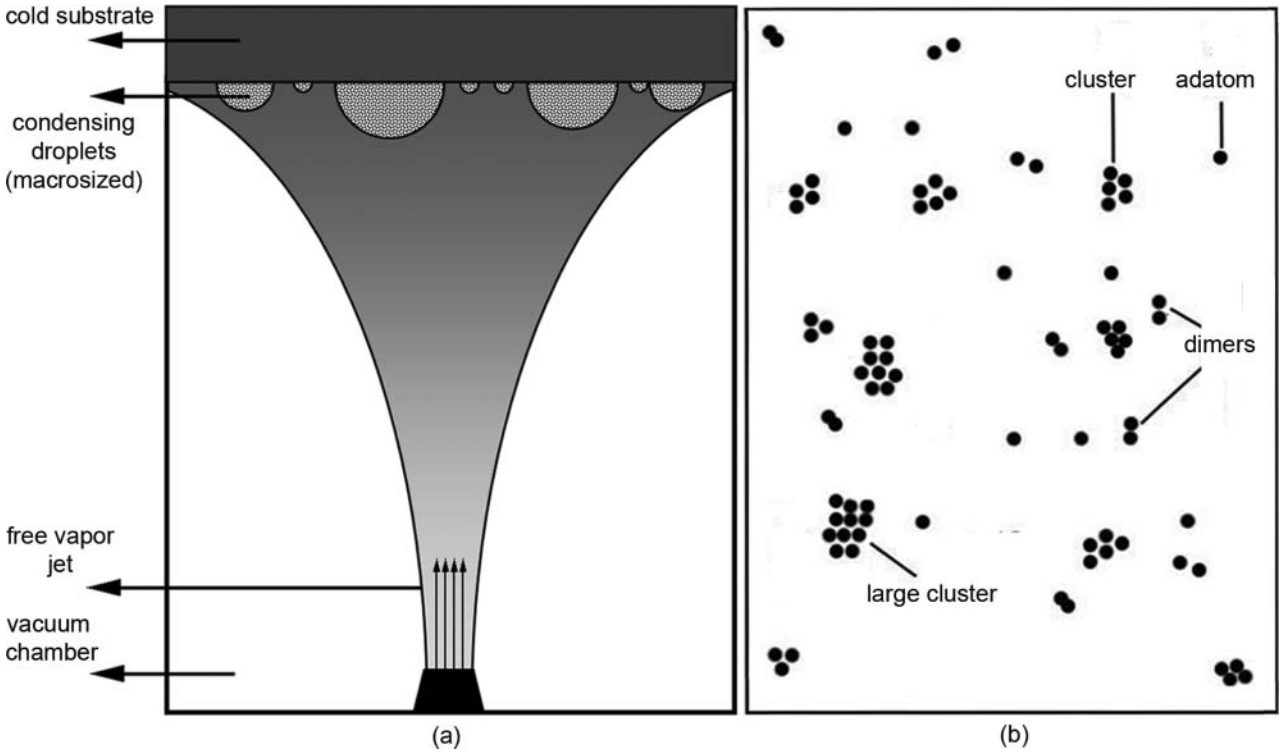

Figure 2 Physical modeling of droplet formation underneath a substrate. (a) Schematic representation of the vapor flux impinging vertically on the underside of a horizontal substrate. (b) Schematic drawing of the distribution of clusters on the substrate.

jet from a nozzle discharging into an evacuated chamber. The substrate on which all the condensation take place is initially clean and free of any condensate. Atoms are deposited on the substrate at a constant rate. An adsorbed layer of atoms, called adatoms, is first formed prior to nucleation. These adatoms can diffuse on the surface with a characteristic time period that is the mean resident time τ_{ads} and then re-evaporate back to the vapor phase. They may collide with other adatoms or clusters during their migration, thus causing nucleation to be initiated. The adatom population on the substrate changes with time due to desorption, capture or release of an adatom by a cluster. The population may redistribute itself over the surface as a result of diffusion at a speed determined by the diffusion coefficient. If two adatoms occupy neighboring sites, they will stick to form a cluster. More adatoms may be captured by a cluster or two clusters may combine to form larger clusters. The population of a cluster of a certain size will thus change due to adatom capture or release, coalescence with other clusters, or breakage into smaller clusters and desorption, as shown in Figure 2b. By way of surface diffusion, the stable nuclei act as efficient adatom sinks, depleting the adatom of a neighborhood. A diffusion zone is established around each stable nucleus. The cluster population may further redistribute itself by diffusion over the substrate [18, 19]. In the growth stages, the condensate clusters grow, not only by capturing adatoms on the surface, but also by direct capture of impinging vapor molecules/atoms.

Other phenomena that are present in the real process include interlayer transport, particle/cluster dissociation, and chemical interactions between adatoms and the surface. These have been neglected in the formulation given next.

Rate Equations for Modeling Cluster Growth

Venables [18], Brune [20], and Oura et al. [21] have reported the following equations to comprehensively depict the time rate of variation of the number density n_j of clusters with j atoms:

$$\frac{dn_1}{dt} = F - \frac{n_1}{\tau_{ads}} + \left(2\delta_2 \cdot n_2 + \sum_{j=3}^{M} \delta_j \cdot n_j - 2\sigma_1 \cdot D \cdot n_1^2 - n_1 \times \sum_{j=2}^{M} \sigma_j \cdot D \cdot n_j \right) - n_1 \cdot \sigma_x \cdot D \cdot n_x \quad (1)$$

$$\frac{dn_j}{dt} = n_1 \cdot \sigma_{j-1} \cdot D \cdot n_{j-1} - \delta_j \cdot n_j + \delta_{j+1} \cdot n_{j+1} - n_1 \cdot \sigma_j \cdot D \cdot n_j \quad j = 2, ..., M \quad (2)$$

$$\frac{dn_x}{dt} = n_1 \cdot \sigma_i \cdot D \cdot n_i \quad (3)$$

The symbols are explained in the nomenclature. The preceding equations are interpreted as follows. Equation (1) describes the time evolution of the adatom density of monomers, namely,

n_1. It denotes an increase in n_1 due to deposition with a flux F and decrease due to desorption at a rate (n_1/τ_{ads}). The terms bracketed together in Eq. (1) represent the supply and consumption rates due to formation and decay of subcritical clusters. The quantity $2\sigma_1 \cdot D \cdot n_1^2$ stands for the loss of monomers that, in turn, lead to the appearance of dimers, with the factor of 2 indicating that in each process, adatoms are supplied or consumed in pairs. The summed terms in Eq. (1) are for the decay and formation of clusters from 3 to M, where M is the largest unstable cluster. The last term is the net capture rate of stable clusters larger than size M. The flux term F appears only in Equation (1), namely for monomers. This is because clustering in the vapor-phase is assumed to be absent and the impinging vapor flux is taken to have monomers alone.

Equation (2) is for the time evolution of number density of subcritical clusters of size j, i.e., $j \leq M$. Four processes affect the number density of the j-sized clusters. First, a new cluster of size j is formed when an adatom is attached to the cluster of size $j-1$. The net flux due to this process is expressed as $\sigma_{j-1} \cdot D \cdot n_{j-1} \cdot n_1$. Second, the detachment of the adatom from the cluster of size $j+1$ produces a cluster of size j and an adatom. Two processes that decrease n_j are: (i) attachment of adatoms to the j-clusters transforming them to $j+1$ clusters with a net rate $\sigma_j \cdot D \cdot n_j \cdot n_1$; and (ii) decay of j clusters producing $j-1$ clusters with a net rate $\delta_j \cdot n_j$.

Equation (3) describes the growth of the density of the stable cluster n_x due to attachment of an adatom to the critical size clusters. Equations (1)–(3) are quite general in the sense that newer physics can be conveniently built into them.

Complete information on the local distribution of clusters is contained in the capture and decay rates, σ_j and δ_j, respectively [18–23]. In the present study, these quantities have been taken to be given parameters. As suggested in the literature, the capture coefficients are nearly constant with $\sigma_1 = 3$ and $\sigma_x = 7$. A first-principles calculation of these parameters involves solving a Helmholtz-type diffusion equation for clusters in two dimensions in the presence of a certain density of stable islands. The analytical expressions obtained with this approach are [18–20]:

$$\sigma_x = \frac{4\pi(1-Z)}{\ln(1/Z) - (3-Z)(1-Z)/2} \tag{4}$$

$$\sigma_1 = 4\pi(1-n_1)\frac{n_x}{n_1}\frac{1}{\ln(1/Z) - (3-Z)(1-Z)/2} \tag{5}$$

Here $Z = \vartheta - \sum_{j=1}^{i} n_j$ is the fraction of the surface covered by the stable clusters. Using the preceding values of σ_1 and σ_x one can obtain the island size distribution for a specified value of i. For the present discussion, it is assumed that dimers as well as clusters with three or more atoms are stable; consequently the decay constants δ_j $(j \geq 2)$ are effectively zero. The assumption is equivalent to stating that clusters that are held together by the long-range van der Waals forces do not have any intrinsic breakup mechanism. The long-range forces appear over length scales of a few nanometers, while repulsive forces become significant over considerably shorter length scales of a few angstroms. Thus, number densities of clusters change purely because of addition of monomers.

Nucleation is the formation of supercritical clusters, namely, clusters larger than a given critical size. The size of the supercritical clusters for various surface textures and flux rates are the quantities of interest to the present work.

Numerical Methodology and Results

When the temperature of the substrate is significantly lower than the saturation temperature, condensation will be complete in the sense that all atoms contained in the vapor-phase stick to the substrate. Under these conditions, certain additional assumptions facilitate the computation of cluster densities. These are listed here:

(i) Adatoms alone diffuse, while dimers and larger clusters are stable, that is, they do not disintegrate or diffuse within the substrate.
(ii) The direct impingement of free atoms on adatoms and clusters and the coalescence of clusters can be neglected. Thus, the atoms and clusters diffusing within the substrate arise exclusively from the condensate and do not have contributions to their population from the vapor phase.

The condition in which complete condensation of the impinging vapor takes place is equivalent to the inequality $\sigma_x \cdot n_x \cdot D \cdot \tau_{ads} >> 1$; it neglects the effect of re-evaporation [18]. For the complete condensation regime modeled here, the mean residence time τ_{ads} is high. It was found that the model predictions reported in the present study were not sensitive to changes in this quantity for $\tau_{ads} \geq 0.1$ s.

The numerical simulation of Eqs. (1)–(3) was run for a large set of cluster sizes varying from adatoms (cluster containing one atom/molecule) to clusters containing 1000 atoms/molecules. The largest cluster with a non-zero number density was found from simulation to have 100–200 atoms/molecules. Hence, the choice of a cluster with 1000 atoms as an upper limit was considered adequate.

Under the approximations already discussed, the rate equations (1)–(3) further reduce to the following [10, 11]:

$$\frac{dn_1}{dt} = F - \frac{n_1}{\tau_{ads}} + (-2\sigma_1 \cdot D \cdot n_1^2 - n_1 \cdot \sigma_x \cdot D \cdot n_x) \tag{6}$$

$$\frac{dn_j}{dt} = n_1 \cdot \sigma_{j-1} \cdot D \cdot n_{j-1} - n_1 \cdot \sigma_j \cdot D \cdot n_j \quad (\text{for } j = 2 \text{ to } 1000) \tag{7}$$

$$\frac{dn_x}{dt} = n_1 \cdot \sigma_i \cdot D \cdot n_i \tag{8}$$

The initial conditions were specified during simulation as $n_j(t = 0) = 0$ (for $j = 1$ to 1000) and $n_x(t = 0) = 0$. The model parameters were taken as $\sigma_1 = 3$ (for $j = 1$), $\sigma_j = 7$ (for $j = 2$ to 1000), and $\sigma_x = 7$.

Brune [20] has showed that the values of the capture coefficients just specified give meaningful results; the corresponding computational effort is also lower since they need not be repeatedly calculated from Eqs. (4) and (5). A vapor flux of $F = 0.005$ per second has been adopted for the study. The diffusion constant D was calculated with the ratio D/F taking on values of 10^5, 10^6, 10^7. The residence time of $\tau_{ads} = 2.3$ s was chosen from numerical experiments to model the complete nucleation regime.

The system of Eqs. (6)–(8) constitutes a set of 1001 coupled ODEs. The fourth-order Runge–Kutta method was implemented in a C-language program to solve the system of simultaneous differential equations. The model and the computer program were extensively validated against benchmark results and are presented next.

The validation of cluster growth simulation is discussed here. The number of islands/clusters of size s can be expressed in terms of the scaling function [22, 24–27]:

$$n_s(\vartheta) = \frac{\vartheta \cdot f_i(s/S)}{S^2} \tag{9}$$

Here, the symbol n_s is the number of islands of size s at coverage ϑ, which is given by:

$$\vartheta = \sum_{s \geq 1} s \cdot n_s \tag{10}$$

The average island size is

$$S = \frac{\sum s \cdot n_s}{\sum n_s} \tag{11}$$

Here, $f_i(s/S)$ is the scaling function for the island size distribution corresponding to the case in which the value of the critical sized island is equal to i.

The variation of the scaled island size distribution with the scaled island size is reported by Shi et al. [22]. Figure 3 shows a comparison of the data generated in the present work against [22]. A close match between the present simulation and the data of [22] is obtained. The variation of monomer density and saturation island density with coverage in Figure 4 also show a good match. Simulation was also conducted for the limiting case of zero flux deposition rate ($F = 0$). The results, plotted in Figure 5, show that the initial spike in the number density distribution vanishes when the deposition rate is zero.

The number density distribution of the condensing clusters on the substrate as a function of the model parameters D, F, and τ_{ads} is shown in Figure 6a and b. The first peak at the origin of the coordinate system corresponds to single adatoms originating from the impingement of the vapor flux. The second peak indicates the most probable cluster size of the condensate. The tail of the distribution shows that sizes beyond a certain value do not appear on the substrate. The size distribution determined from

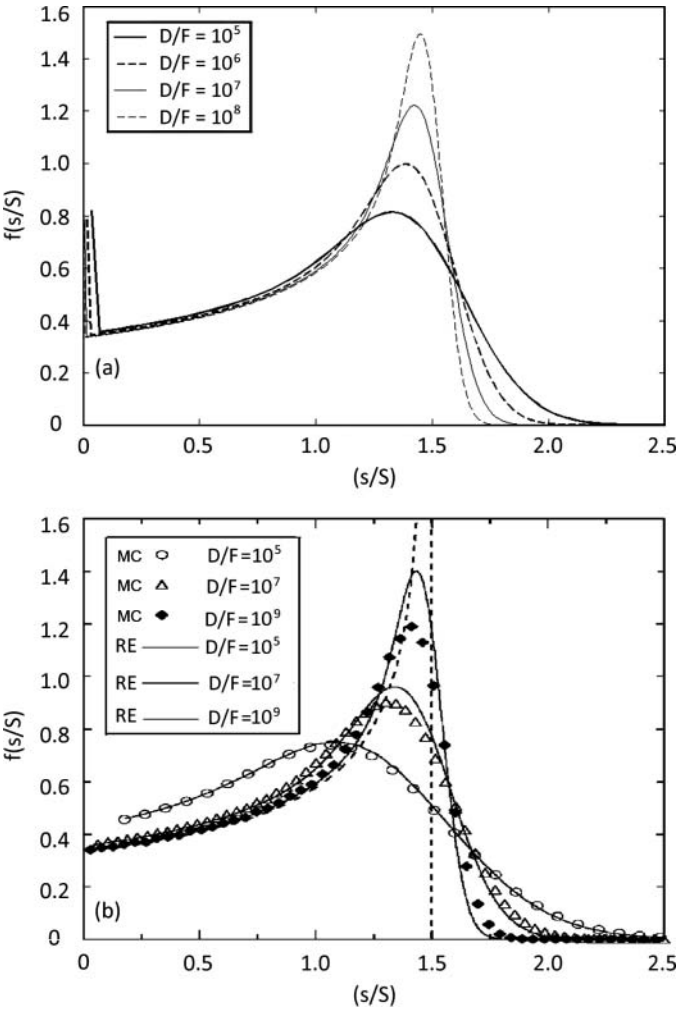

Figure 3 (a) The figure is generated by numerical simulation as described in the text. This set of results was obtained by solving the rate equations governing the nucleation process. (b) The results as given by Shi et al. [22] by using both the rate equations (RE) approach (solid lines) and Monte Carlo(MC) simulation (symbols) are presented here. A close match is obtained between the data of [22] and the present study as can be seen by comparing (a) and (b).

Eqs. (6)–(8) is purely from microscopic considerations and does not include macroscopic influences such as surface tension and gravity. Hence, the largest cluster, corresponding to the smallest number density in Figure 6 (a and b) can be interpreted as the smallest drop that would appear on a macroscopic viewpoint. Beyond this size, factors such as gravity, surface tension, and coalescence would be operative in determining the increase in drop diameter.

The preceding expectation has been examined with reference to the thermodynamic estimate, Eq. (25), as follows. At atmospheric pressure and a surface maintained at 80°C, one can calculate $r_{\min} = 9.617 \times 10^{-10}$ m. The number of molecules in the drop can be found from the relationship

$$n_d = \frac{N_A \pi \cdot r^3}{3\overline{M} \cdot \upsilon_l}(2 - 3\cos\theta + \cos^3\theta) \tag{12}$$

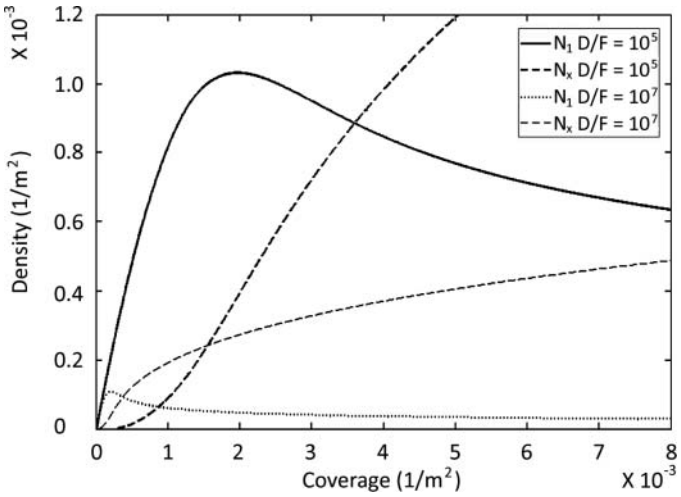

Figure 4 Variation of monomer density (n_1) and saturation island density (n_x) with coverage at various values of *D/F*. Results show a close match with the published data of [22].

Using properties of water, namely, molecular weight $\overline{M}$ of 18 g/mol, N_A the Avogadro number, and $\theta = 90^\circ$, we get

$$n_d = (2\pi \cdot r^3 N_A)/(3\overline{M} \cdot \upsilon_l) \tag{13}$$

The volume referred in Eqs. (12) and (13) is that of the spherical cap of a droplet whose radius is $r_{\min}$ (Eq. (25)) and contact angle is θ. The number of molecules corresponding to the minimum radius of 9.617×10^{-10} m can now be estimated as $n_d = 60$. In the cluster model, the following results were obtained:

$D = 5000$ and $F = 0.005$, $n_d = 53$.
$D = 500$ and $F = 0.05$, $n_d = 58$.
$D = 50$ and $F = 0.5$, $n_d = 62$.

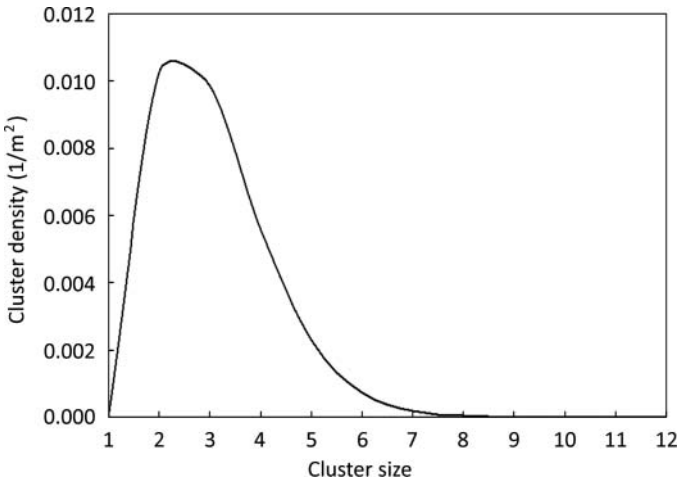

Figure 5 Variation of the number density of clusters with their size. Since vapor flux $F = 0$, the spike due to flux impingement does not appear at a cluster size of unity.

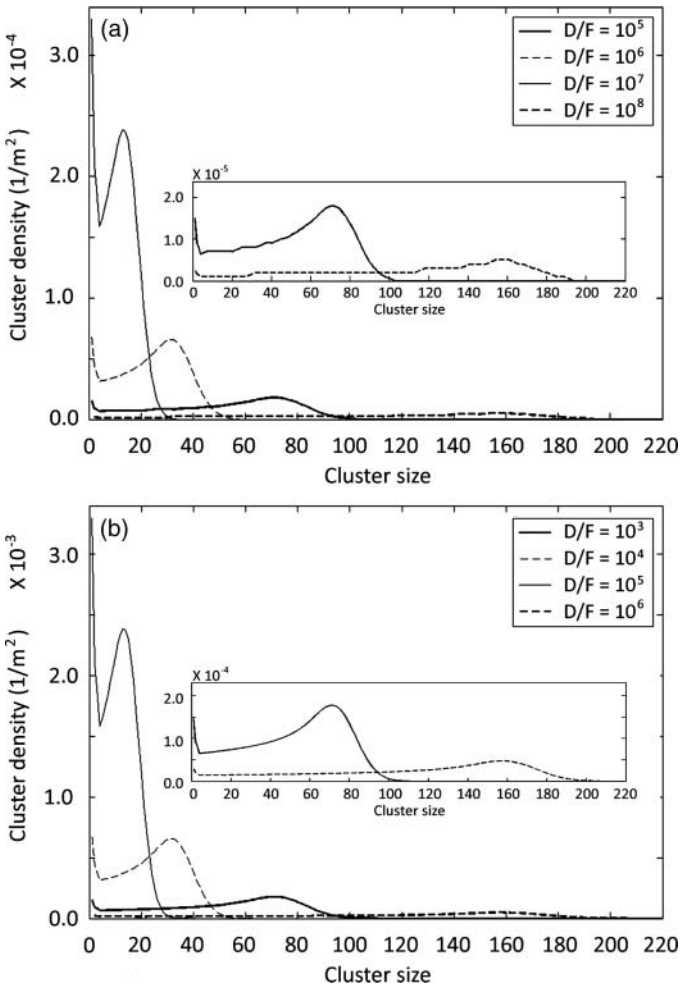

Figure 6 (a) Variation of the cluster density with cluster size at $F = 0.005$ s^{-1}. The cluster size where the number density becomes zero for a particular profile yields the maximum cluster size. The cluster can be assumed to be in the form of a liquid with a corresponding drop radius that is a minimum. Inset shows the details of the island density profiles for $D/F = 10^7$ and 10^8. (b) Variation of the cluster density with cluster size at $F = 0.05$ s^{-1}. Inset shows the details of the island density profiles for $D/F = 10^5$ and 10^6.

The number of molecules thus calculated in the smallest drop corresponds quite well with the data of Figure 3.

The sensitivity of the drop size to the diffusion parameter *D* and the impinging flux *F* are shown in Figure 7a and b. The minimum drop size is seen to increase with *D* as well as *F*, though the change is not substantial. For an increase of four orders of magnitude in the diffusion coefficient, the minimum drop radius increases by a factor of about two. For an increase of one order of magnitude in the vapor flux, the minimum drop radius increases by about 30%. These changes are related to the slight broadening of the cluster density and hence the increase in the size of the largest possible cluster. A higher mass flux increases the number density of adatoms over the substrate and consequently diminishes the extent of diffusion away from the clusters. A higher diffusion constant encourages the association process of monomers and permits clusters of larger sizes to form. Both factors lead to an increase in number of

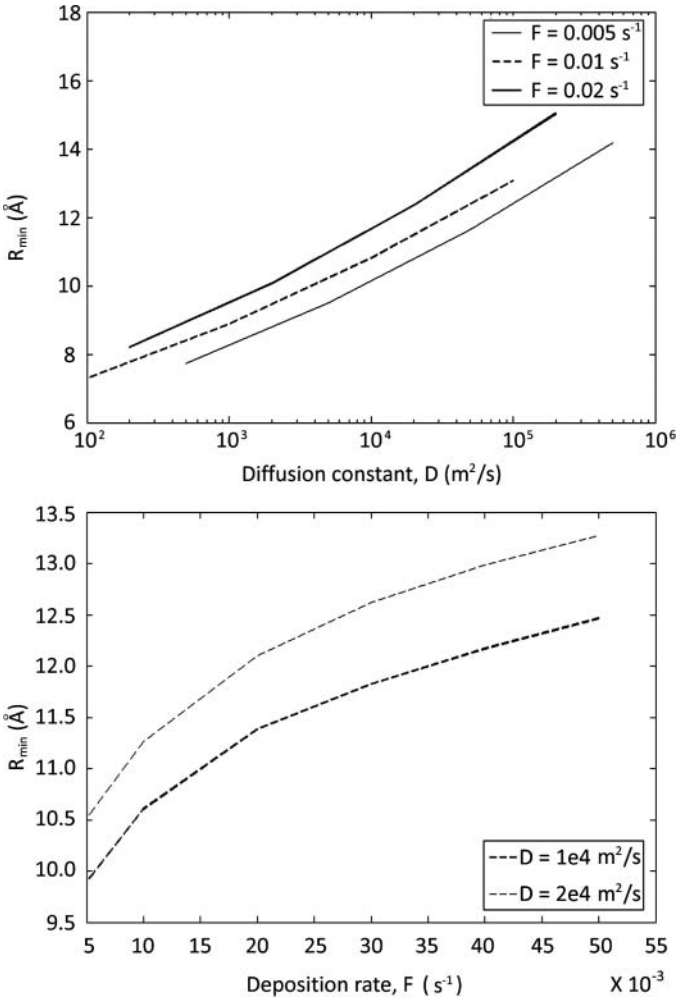

Figure 7 (a) Variation of the minimum drop radius with diffusion constant D at three different values of deposition rate F. (b) Variation of the minimum drop radius with deposition rate F at two different values of diffusion constant D.

molecules in the largest cluster and hence the minimum drop radius.

Apart from the material properties of the condensing medium, the diffusion coefficient is a function of the surface properties and temperature of the substrate. The vapor flux is a process parameter and can be independently controlled. The cluster model given by Eqs. (6)–(8) predicts that by varying D, in effect varying the surface properties, the minimum drop radius is altered. One method available for altering the surface characteristics is physical texturing. As discussed in [28],

$$D \propto 1/\bar{\eta} \tag{14}$$

The symbol $\bar{\eta}$ is the friction coefficient of the surface. When $\bar{\eta}$ is very small,

$$D \propto 1/\bar{\eta}^{0.5} \tag{15}$$

While texturing decreases the friction coefficient, the diffusion coefficient increases, with a corresponding increase in the minimum drop diameter. Figure 7a shows that the increase is, however, marginal. For chemical texturing of a surface, first-principle calculations can be used to predict the diffusion constant [29, 30].

Figure 8 examines the sensitivity of the drop size distribution on the macroscale to the initial minimum drop radius. Of special interest is the question of whether drop size distribution can be influenced by controlling the minimum drop radius. To answer this question, two different r_{min} values were started with, and droplet growth simulation was carried out until drops were large enough for fall-off. The simulation methodology for droplet growth is explained later with water as the working fluid. The two distribution patterns that emerge are practically identical, suggesting that the macroscale drop distribution is determined by coalescence dynamics, rather than the minimum drop radius.

Closing Remarks on Atomistic Modeling

In this section, a cluster model is described in terms of rate equations to obtain the number density distribution of clusters. The residence time is taken to be large enough so that sufficient time is available for all the adatoms existing in the vapor phase to lose their respective latent heats and get condensed. The simulation assumes clusters of a given size to be formed from clusters

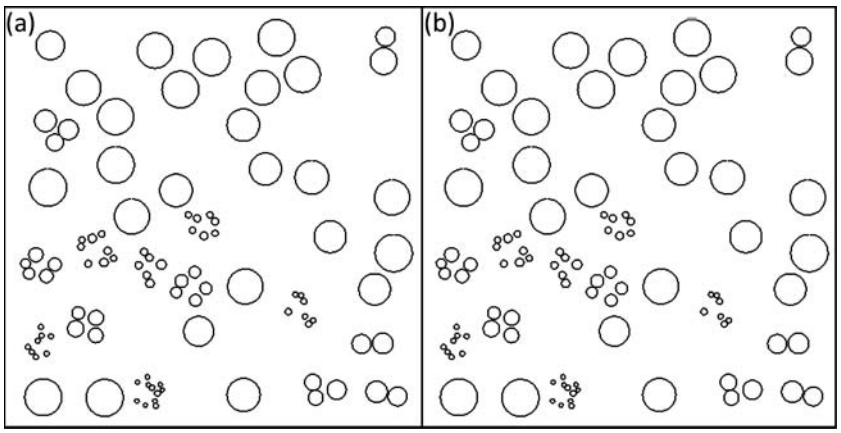

Figure 8 Drop size distribution on a surface for (a) $r_{min} = 10$ A and $r_{max} = 5$ mm, and (b) for $r_{min} = 100$ A and $r_{max} = 5$ mm.

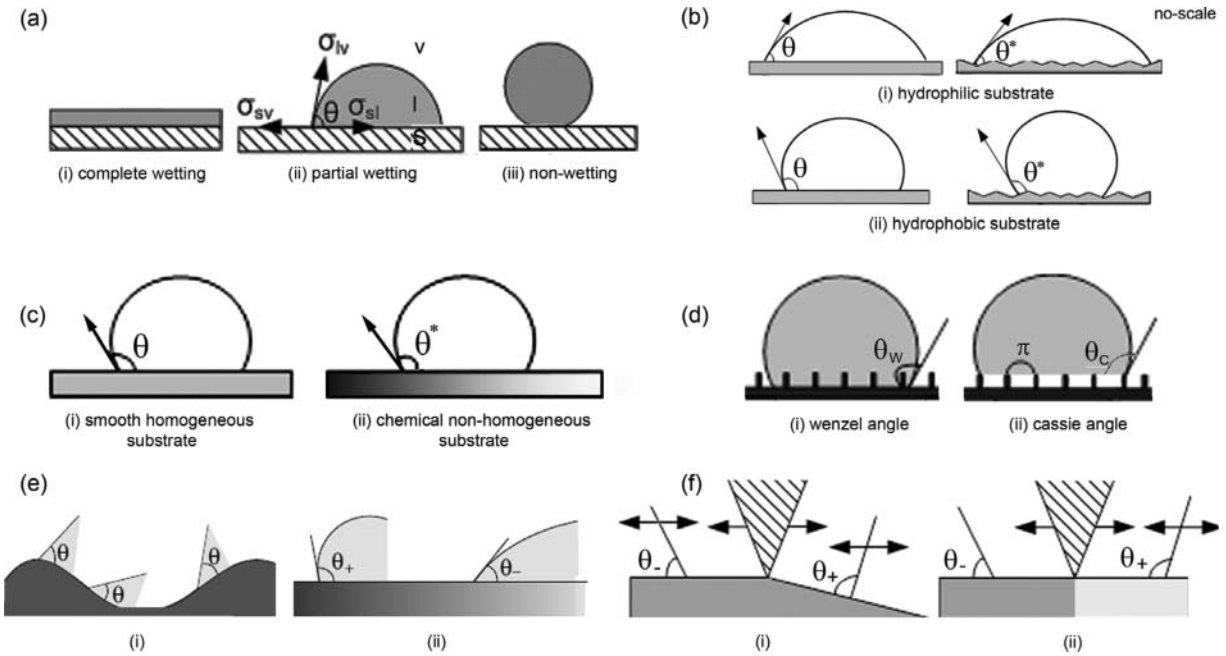

Figure 9 Measurement of contact angle. (a) Droplet on a planar substrate. (b) Effect of roughness on contact angle (Wenzel Law) for a hydrophilic substrate and hydrophobic substrate. (c) Effect of chemical non-homogeneity on local contact angle (Cassie–Baxter relation). (d) Measurement of contact angle when droplet is sitting on a physically textured substrate. (e) The effect of continuously varying wettability. (f) Pinning due to sudden physical or chemical discontinuity.

of smaller sizes but not by the disintegration of larger clusters. The largest stable cluster size in the number density distribution is taken to be representative of the minimum drop radius formed in a dropwise condensation process. Results obtained show that the number density distribution is sensitive to the surface diffusion coefficient and the rate of vapor flux impinging on the substrate. The minimum drop radius increases with the diffusion coefficient and vapor flux but the dependence is weak. The minimum drop radius predicted from thermodynamic considerations (Eq. (25)) matches the prediction of the cluster model, though the former does not take into account the effect of the surface properties on the nucleation phenomena. For a chemically passive surface, the diffusion coefficient and the residence time are dependent on the surface texture via the coefficient of friction. Thus, physical texturing provides a means of changing (within limits) the minimum drop radius. The present study reveals that surface texturing at the scale of the minimum drop radius does not provide controllability of macroscale dropwise condensation at large time scales when dynamic steady state is achieved.

FORMATION OF A LIQUID DROP ON A SOLID SUBSTRATE

An atomistic model captures the initial stage of condensation, which leads to a stable cluster. Once a cluster is formed, bulk thermophysical properties of the liquid become relevant and start influencing the growth process. In this section, the properties of the cluster, viewed as a liquid continuum and located on a solid substrate, are discussed.

Dropwise condensation can be sustained if the condensate does not wet the cold surface, say in a condenser. Wetting characteristics can be established by the measurement of the bulk "apparent" contact angle θ,[2] specific to the pair of the liquid and the surface material. It is defined as the macroscopic angle between the tangents drawn at the liquid/vapor interface and the liquid/solid interface. A liquid is said to wet a solid surface completely if it spreads over a considerable distance with a limiting value of $\theta = 0^\circ$. If a liquid remains a full spherical drop on contact with a solid surface, it is said to be fully nonwetting with a contact angle $\theta = 180^\circ$. In the real context, it is invariably between the wetting and the nonwetting limits. A liquid has a contact angle $0 < \theta < 180^\circ$ over the surface and we obtain the partial wetting regime; a clear liquid/solid interface is formed in this context. Figure 9a shows a schematic diagram, explaining the three wetting cases.

The wettability of a surface by a liquid is a consequence of a combination of complex processes. Some of these originate at the microscale and can be understood in terms of surface chemistry and long-range van der Waals forces. Certain factors are purely statistical and may vary from sample to sample. These include wetting transitions and the pinning of the contact line. Fluid motion inside the droplet commences when it starts moving due to a force imbalance, and then the shape of the droplet will depend on the principles of fluid dynamics as well. As a first step, the solid–liquid interaction in a drop may be characterized uniquely by the apparent contact angle θ and determined

[2]Unless otherwise stated, in this paper we always deal with the apparent contact angle. The molecular contact angle formed by the precursor layer existing at the three-phase contact line is not considered in this discussion [31].

by measurements when the drop has reached force equilibrium. Since the contact angle refers to the shape of the drop and hence its curvature, it can be related to interfacial tension and hence the surface energy of the substrate. It depends on the thermophysical properties of the liquid as well as the physicochemical structure of the solid substrate. The contact angle contains details of the interactions at various interfaces, including solid/liquid, liquid/gas, solid/gas, and solid/liquid/gas. The adoption of the apparent contact angle simplifies analysis and helps understand the behavior of drops from a mechanics perspective. For a given liquid, a wide variety of substrates, natural and engineered, will produce a range of contact angles. These are classified as hydrophilic ($0 \leq \theta \leq 90^\circ$), hydrophobic ($90\ \theta \leq 150^\circ$), and super-hydrophobic substrate ($150 \leq \theta \leq 180^\circ$).

Several important phenomena in condensation rely on partial wetting of the solid substrate. Surface heterogeneities, chemical and topographical, are important in this context. In the following subsections, measurement of the contact angle, contact angle hysteresis, effect of substrate orientation, and the initial nucleation site density on dropwise condensation are discussed.

Measurement of Contact Angle

Three-phase triple contact lines are formed when materials in different phases, e.g., solid, liquid and gas (or vapor) intersect. Common examples are a liquid drop spreading on a solid surface or a liquid meniscus in a capillary tube. In the presence of the third phase (gas or vapor), a liquid spreading on a solid surface can reach two distinct equilibrium states. These are (a) partial wetting and (b) complete wetting. The condition for static equilibrium of a triple contact line involving an ideal solid (perfectly smooth and chemically homogeneous), liquid, and a gas/vapor is stated in the form of Young's equation:

$$\sigma_{1v} \cdot \cos\theta = \sigma_{sv} - \sigma_{sl} \tag{16}$$

Here, the symbol σ_{ab} is the surface tension between phases a and b. Symbols s, l, and v in Eq. (16) indicate solid, liquid, and gaseous phases. The symbol θ is the contact angle at each point of the solid–liquid boundary. Equation (16) holds for an ideally smooth solid surface with no chemical heterogeneities. Real solid surfaces depart from an ideal behavior since they are not perfectly smooth. In addition, their composition may also vary slightly with location. Molecules, atoms, or ions of other chemical species may be adsorbed on the surface. Effectively, the static contact angle turns out to be non-unique on real surfaces and can only be experimentally determined. The experimentally observed contact angle depends on the way the surface was prepared. De Gennes [31], Leger [32], and Huh [33] have shown that a wetting experiment is extremely sensitive to heterogeneities of the solid surface. One of the first attempts at understanding the influence of roughness on wetting is due to Wenzel [34] who proposed the relationship following for the apparent contact angle:

$$\cos\theta^* = f \cdot \cos\theta \tag{17}$$

Here θ^* is the apparent contact angle, f is the degree of roughness (with $f = 1$ for a smooth surface, $f > 1$ for a rough surface), and θ the local contact angle. Equation (17) embodies two types of behavior for rough surfaces. If $\theta < 90^\circ$ (hydrophilic behavior), we will have $\theta^* < \theta$ since $f > 1$. Likewise, if $\theta > 90^\circ$(hydrophobic), we will have $\theta^* > \theta$, as shown in Figure 9b. Shibuichi et al. [35] have shown in their work that the contact angle can be tuned by varying solid roughness in the hydrophilic region ($\theta < 90^\circ$). A similar line of reasoning can be applied to a surface that is planar but chemically heterogeneous. Viewing a chemically heterogeneous surface as composed of distinct patches of various species, the apparent contact angle was proposed to follow the relation:

$$\cos\theta^* = A_1 \cdot \cos\theta_1 + A_2 \cdot \cos\theta_2 \tag{18}$$

In Eq. (18), called the Cassie–Baxter relation, θ^* is the apparent contact angle, θ_1 and θ_2 are the local contact angles for surfaces 1 and 2, respectively, and A_1 and A_2 are the fractional areas occupied by surfaces 1 and 2, respectively. Therefore, the apparent angle θ^* (restricted to the interval $[\theta_1, \theta_2]$) is given by an average involving the cosines of the angles characteristic of each constituent species. The contact angle on chemically homogeneous and nonhomogeneous surfaces is shown in Figure 9c. This discussion clarifies why the three-phase contact line of a liquid drop resting on a surface gets locally deformed: Chemical and topographical heterogeneities play an important role. Certain surfaces have roughness in the form of micro-pillars creating a super-hydrophobic substrate. Here, it has been observed that the drop does not always contact the actual surface and, indeed, may stay on the top of the pillars. This is called the Fakir effect; in such case the contact angle is obtained as follows. If the drop penetrates the pillars, Eq. (17) (Wenzel's law) applies as

$$\cos\theta_w = f \cdot \cos\theta \tag{19}$$

Here θ_w is the Wenzel contact angle and f is the equivalent roughness of the substrate. If the drop stays on the top of the pillars, one can write Cassie's law (Eq. (18)) as

$$\cos\theta_c = f \cdot \cos\theta + (1 - f) \cdot \cos\theta_0 \tag{20}$$

Here θ_c is the Cassie contact angle, θ_0 is the contact angle with the layer of air, and f is the ratio of the contact surface (top of the pillars) to the total horizontal surface. If the pillars are not too far from each other, the value of θ_0 is roughly $\theta_0 = \pi$, as shown in Figure 9d.

Pinning of the Contact Line

Figure 9e shows the sketch of the wetting behavior of a drop of liquid on a substrate with a continuously varying topography and continuously varying wettability. If the drop size is smaller

than the length scale of the topography, Figure 9e (i) shows that the drop shape is not affected by the topography. If the drop is larger than the topographical features, the global shape of the drop will be affected by the deformation of the three-phase contact line. Similarly, for a substrate with a gradient in wettability (chemically nonhomogeneous surface), as in Figure 9e (ii), the drop is deformed due to the peripheral changes in the contact angle of the three-phase contact line.

If the substrate has a sharp topography or wettability pattern, the situation is different. At the discontinuities, Young's equation, Eq. (16), becomes ill-defined and is shown in Figure 9f (i, ii). As a result, the three-phase contact line becomes immobilized. This effect is known as the pinning of the contact line. The contact angle at the boundary can have any value in between the smaller angle θ_- on the hydrophilic part and the larger value θ_+ on the hydrophobic part, Figure 9f. As a consequence, the position of the contact line is fixed to the line of discontinuity as long as the contact angle falls in the range of θ_- to θ_+. The contact angle now depends on the local wettability of the substrate and the global shape of the liquid-vapor interface at equilibrium. Contact angles will change further under dynamic conditions when, owing to fluid motion, a nonuniform pressure field is created within the drop.

Contact-Angle Hysteresis

Partially immersing a thin solid sheet in a liquid and moving it slowly, Carey [12] reported the appearance of two distinct contact angles. These angles are known as the advancing angle θ_{adv} and receding angle θ_{rcd}, depending on the direction of motion of the plate (Figure 10a). Arising from this experiment, a difference between the advancing and receding contact angles is known as contact angle hysteresis. Hysteresis is acknowledged to be a consequence of three factors: (i) surface inhomogeneity, (ii) surface roughness, and (iii) impurities on the surface. Various investigators [36–39] have derived an expression relating the criticality of drop sliding on/underneath an inclined plane in dropwise condensation, as a function of the hysteresis (($\theta_{adv} - \theta_{rcd}$), as follows:

$$\sin(\alpha) = \sigma_{lv} \cdot (R \cdot K/m \cdot g)(\cos\theta_{rcd} - \cos\theta_{adv}) \qquad (21)$$

In Eq. (21), α is the critical sliding angle, σ_{lv} the surface tension, m the mass of the drop, and R and K are a length scale and shape constant for the contour of the drop, respectively. Although Öner and McCarthy [40] made it clear that contact-angle hysteresis can be a qualitative indication of drop mobility, it has been argued by Krasovitski and Marmur [41] and Pierce et al. [42] that advancing and receding contact angles are measured on a level surface and should theoretically not be used in numerical predictions of the sliding angles. Instead, they define the maximum and minimum contact angles (θ_{max} and θ_{min}), which are those at the leading and trailing edges of a drop profile on a surface inclined at the sliding angle (Figure 10b). The modified

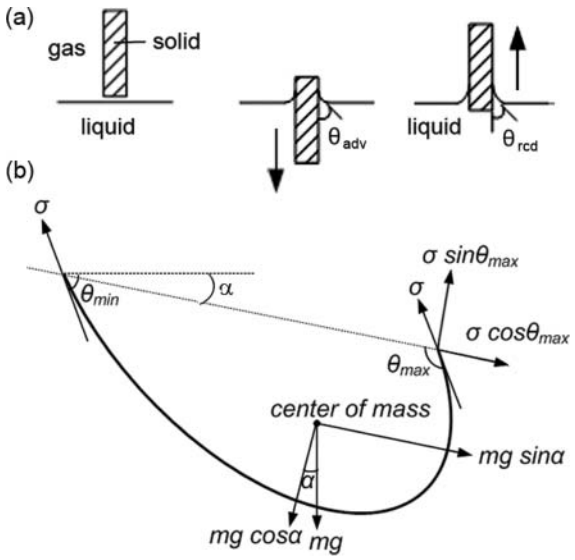

Figure 10 (a) Basic definition of advancing (θ_{adv}) and receding (θ_{rcd}) angle during immersion and removal of a solid plane in a liquid medium. (b) Droplet angle at an inclined plane with leading side angle (θ_{max}) and back side angle (θ_{min}).

form of Eq. (21) is obtained as follows:

$$\sin(\alpha) = \sigma_{lv} \cdot (R \cdot K/m \cdot g)(\cos\theta_{\max} - \cos\theta_{\min}) \qquad (22)$$

Theoretical and experimental evidence suggest that the relationship between θ_{max} and θ_{adv} as well as θ_{min} and θ_{rcd}, respectively, varies with the surface–liquid combination. Elsherbini and Jacobi [43, 44] reported empirical data that exhibit θ_{max} and θ_{min} approximately equal to θ_{adv} and θ_{rcd} for all surface–liquid combinations. Hence, there is some controversy about the value of the leading angle and trailing angle of a deformed drop on an inclined substrate at criticality. This information is quite important from the viewpoint of dropwise condensation and has attracted attention. A few investigators have reported the effect of contact-angle hysteresis in the dropwise mode of condensation. Neumann et al. [45] reported that heat transfer during dropwise condensation of water vapor strongly depends on the hysteresis of the contact angle.[3] The surface conductance increases with decreasing contact-angle hysteresis. Sikarwar et al. [46] reported that heat transfer increases with diminishing contact-angle hysteresis since criticality of drop slide-off/fall-off is inversely proportional to the contact-angle hysteresis. Large hysteresis will provide adequate forces along and normal to the wall and improve the stability of the drop. Conversely, the drop slide-off or

[3]Heat transfer during dropwise condensation depends strongly on the surface properties and surface phenomena, especially on contact angle. To understand this effect, Neumann et al. [45] performed experiments for a coated substrate. Each run was of 300 min duration. The contact angle for horizontal substrate and contact-angle hysteresis for inclined substrate were measured before each run. It was found that after each run the heat flux decreased considerably. The reduction was caused by a deterioration of the condenser surface, which in turn increases the contact-angle hysteresis and size of droplet at slide-off or fall-off. If surface properties remained constant, there would be no change in the heat flux of each run.

fall-off will occur early on a surface that has small hysteresis. The repeated sweep and removal of drops from a surface result in fresh condensation and an overall improvement in the heat transfer rates.

Substrate Orientation

The study of orientation of the cold substrate is important in dropwise condensation and enhancement of heat transfer. Leipertz and Fröba [47] reported the following correlation for the heat transfer coefficient in dropwise condensation as a function of the inclination of the substrate:

$$h_c(\alpha) = h_c(90^\circ) \cdot [\sin\alpha]^\kappa \tag{23}$$

Here, $h_c(\alpha)$ is the heat transfer coefficient of dropwise condensation at angle $\alpha$and $h_c(90^\circ)$ corresponds to that of a vertical substrate. In Figure 11, the value of κ was $\sim$0.270 for the dashed line and $\sim$0.176 for the solid line.

The angle of inclination is defined to be 0° for the horizontally oriented surface with drops on the upper side of the substrate (sessile mode) and 90° for a vertically oriented substrate. From 90° onward, drops form on the lower side of the substrate and the 180° horizontal substrate refers to the pendant mode of dropwise condensation. The heat transfer data for water vapor in dropwise condensation with respect to orientation (sessile and pendant) are shown in Figure 11. It is clear that the pendant mode over a horizontal substrate yields a higher heat transfer coefficient as compared to the sessile mode. The heat transfer coefficient is the highest for a vertical substrate and decreases with increasing inclination. For an inclined substrate, the surface is swept clean of drops, and this renewal of the drop growth process is responsible for a higher heat transfer coefficient. In contrast, drops over a horizontal surface become large and fall off by gravity in the pendant mode or spread over the substrate and cover it by a layer of the condensate liquid, in the case of sessile drops. In both cases, the surface is not regularly refreshed by fresh condensation, resulting in a lower heat transfer coefficient. Briscose and Galvin [37] and Lawal and Brown [48] reported that a pendant drop is less stable as compared to a sessile drop on an inclined substrate, suggesting that heat transfer during dropwise condensation underneath an inclined substrate is marginally better than its counterpart above the surface. Therefore, surface orientation is an important parameter in the enhancement of heat transfer coefficient in dropwise condensation.

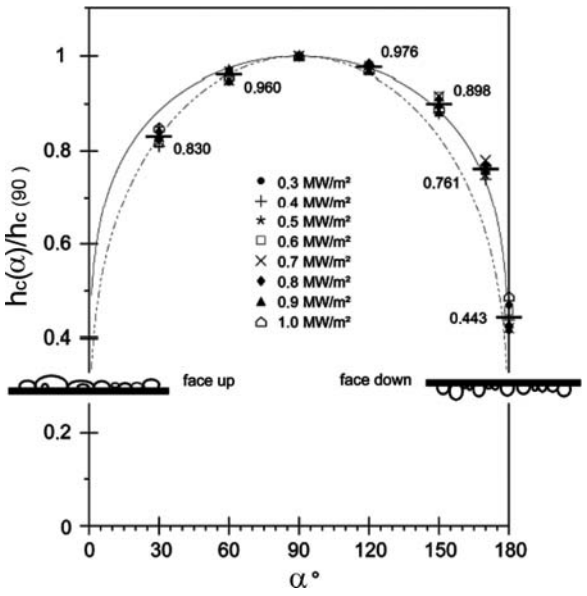

Figure 11 Variation of heat transfer coefficient with respect to angle of inclination of the substrate [47].

Nucleation Site Density

It is difficult to determine the initial nucleation site density from experiments. A theoretical expression for nucleation site density over an untreated surface is given by Rose [49] in the form

$$N = 0.037/r_{\min}^2 \tag{24}$$

Here N is the number of sites on the substrate, per square centimeter, where the initial drop, identifiable as liquid, is formed. The associated drop size is r_{min}, the initial radius of the drop on the substrate. This minimum stable macroscopic drop size is obtained from thermodynamic considerations as:

$$r_{\min} = \left(\frac{2\sigma_{lv}T_w}{H_{lv}\cdot\rho\cdot\Delta T}\right) \tag{25}$$

It is clear that the initial stable drop radius depends on the thermophysical properties of fluid and temperature difference between the substrate and the condensing vapor. Leach et al. [6] reported initial drop densities close to 10^6 cm^{-2} for temperature differences in the range of 50 to 100°C. For condensation of water at 30°C, the initial nucleation site density is in the range of 10^4 to 10^5 cm^{-2} and gradually increases to 10^6 cm^{-2} before the first coalescence. Zhao and Beysens [50] observed no significant difference in the initial nucleation site density with respect to the contact angle. Later, Mu et al. [51] found that the nucleation density varies with surface topography. The rougher substrate can result in a higher nucleation density. Based on the work of Rose [49] and Mu et al. [51], one can conclude that the nucleation density is influenced not only by the degree of subcooling but also by the surface topography. In dropwise condensation, the substrate morphology could be changed by chemical and/or physical texturing. Hence, nucleation density might be influenced by these two factors, i.e., changes in the surface energy induced by a chemical species (chemical texturing) and varying roughness of the substrate (physical texturing). The modified expression for the initial nucleation density of the textured substrate can be expressed as:

$$N_f = f \cdot N \tag{26}$$

Here, N_f is the initial nucleation density of the textured substrate, f is the degree of roughness, and N is initial nucleation

density of a smooth surface as calculated by Rose [49], Eq. (24). For a general textured substrate, factor f needs to be established and is a topic of research.

DROP DYNAMICS

Processes associated with the cycle of dropwise condensation—sessile or pendant—including nucleation, coalescence, sliding as well as fall-off, followed by fresh nucleation, result in heat transfer enhancement [6, 46]. At the initial stages, individual drops grow principally by direct deposition of the condensate onto the surface; secondary growth by coalescence among adjacent drops is also possible. Beyond a certain size of the drop (∼0.01 mm, depending on nucleation site density), coalescence is the primary mechanism of growth in the drop size. When a dynamic quasi-steady state is eventually reached, details of growth by direct condensation make only a small difference to the drop-size distribution [52].

A consequence of the time-dependent processes in dropwise condensation associated with the movement of the drop, first by coalescence and then by sliding motion, is to leach away the promoting layer over the substrate. Accordingly, the long-term sustainability of the process is greatly reduced. Even if there is no chemical reaction between the promoter and condensing liquid, the wall shear stress becomes the primary quantity that controls leaching. The varying shapes of individual drops, as they form and slide on such surfaces, determine the effective shear stress at the wall. A prediction of shear stress requires a complete knowledge of the flow field inside the droplets during growth, coalescence, and sliding motion. Given a shear stress distribution for an individual drop, the net effect due to a drop ensemble can be determined using the time-averaged drop size distribution.

Drop Coalescence

When two or more drops on a cold substrate grow large enough to touch one another, they coalesce and form a single drop of volume equal to the sum of the original, as shown in Figure 12a and b. The growth rate of drops depends on their respective sizes, as in Figure 12c. The figure shows small drops growing due to direct condensation as well as occasional coalescence but large drops grow mainly by coalescence. The growth rate of small drops is related to heat transfer. Smaller drops offer less thermal resistance, thus permitting rapid condensation. Larger drops offer a higher thermal resistance and grow primarily by coalescence [6]. Hence, coalescence plays a primary role in determining the drop size distribution on the macroscale while direct condensation is of secondary importance. Coalescence also plays a direct role in the frequency of attainment of drop criticality, either for sliding motion or fall-off. Subsequently, nucleation occurs over the reexposed area of the substrate. Nucleation, slide-off or fall-off, and droplets coalescence are the prime processes that enhance the heat transfer coefficient at later stages of growth in dropwise condensation. Since the associated heat transfer rates are high, one can imagine

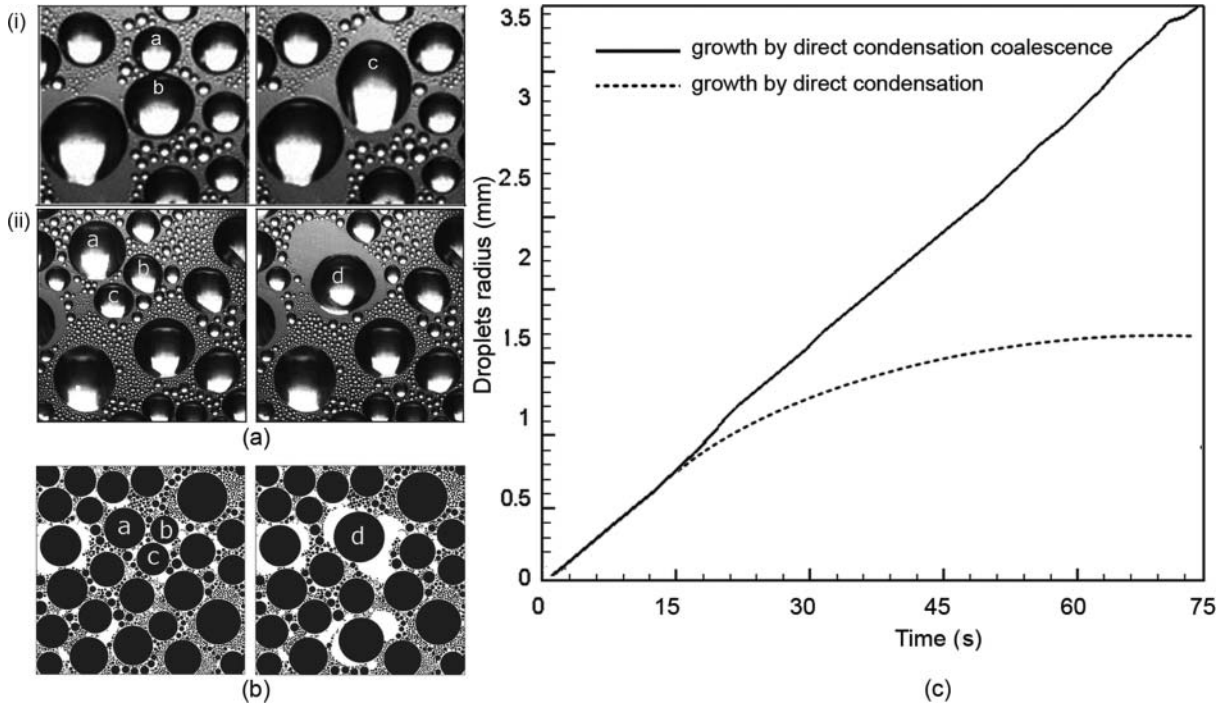

Figure 12 Droplets coalescences. (a) (i) Experimentally observed coalescence of two droplets. Small droplet *a* is sucked by the bigger droplet *b* to form droplet *c*. (ii) Three droplets *a*, *b*, *c* coalesce to form droplet *d*. (b) Numerical simulation of droplet coalescence [37]. (c) Rate of growth of condensing water droplets with respect to time; calculations as per [46].

coalescence dynamics as one of the important factors contributing to enhanced heat transfer during dropwise condensation.

Explicit literature emphasizing the relationship between coalescence of pendant drops and the role of coalescence in heat transfer enhancement is scarce. Much of the research covers the formation of a liquid bridge and the relaxation time of drops after coalescence [53–57]. Leach et al. [6] studied the dropwise condensation of water vapor coming from a hot water reservoir onto a naturally cooled hydrophobic polymer film and silanized glass slide, respectively. The authors reported that the coalescence is affected by surface orientation and composition, vapor and surface temperatures, humidity, and vapor flow rate. The authors experimentally observed smallest detectable droplets that grow and eventually fall off, after repeated cycles of coalescence. The spatiotemporal coalescence scales were not reported. For two drops merging together, Andrieu et al. [53] experimentally captured and theoretically described the kinetics of coalescence of two water drops on a plane solid surface. The final center of mass of the drop was reported to be approximately at the weighted center of mass resulting from the original two drops that coalesced. Immediately after coalescence, an ellipsoidal shape results, eventually relaxing into a hemispherical shape in a few milliseconds. Wu et al. [54] observed that the two liquid drops approach each other with negligible initial velocity, being driven by van de Waals forces that create a tiny liquid bridge. Owing to its large curvature, the bridge quickly expands under the influence of interfacial stresses and pulls the two drops together. The resultant drop has a smaller surface area. Hence, surface-tension-driven flow is a primary factor in drop coalescence and resulting heat transfer enhancement. Liao et al. [55] experimentally studied the effect of inclination on coalescence and reported the variation of contact angle after coalescence. The authors also recorded the oscillation frequency of drops after merging. Narhe et al. [56] reported that the relaxation rate increases with the contact angle. Thoroddsen et al. [57] measured the early interface motion during coalescence of pendant and sessile drops.

A mathematical model that accounts for drop formation at the microscale, all the way to macroscales and fall-off, was developed by the authors; this is described later. The model is capable of predicting the heat transfer coefficient as well.

Against this background, the authors performed an experiment involving the coalescence of two water drops in the pendant mode. The time and length scales of coalescence for various sizes of the drops were observed. Images were recorded by a high speed camera (at 7500 fps). A typical time sequence of snapshots, when two drops of differing diameters merge, is shown in Figures 13–15. The entire time period of the dropwise

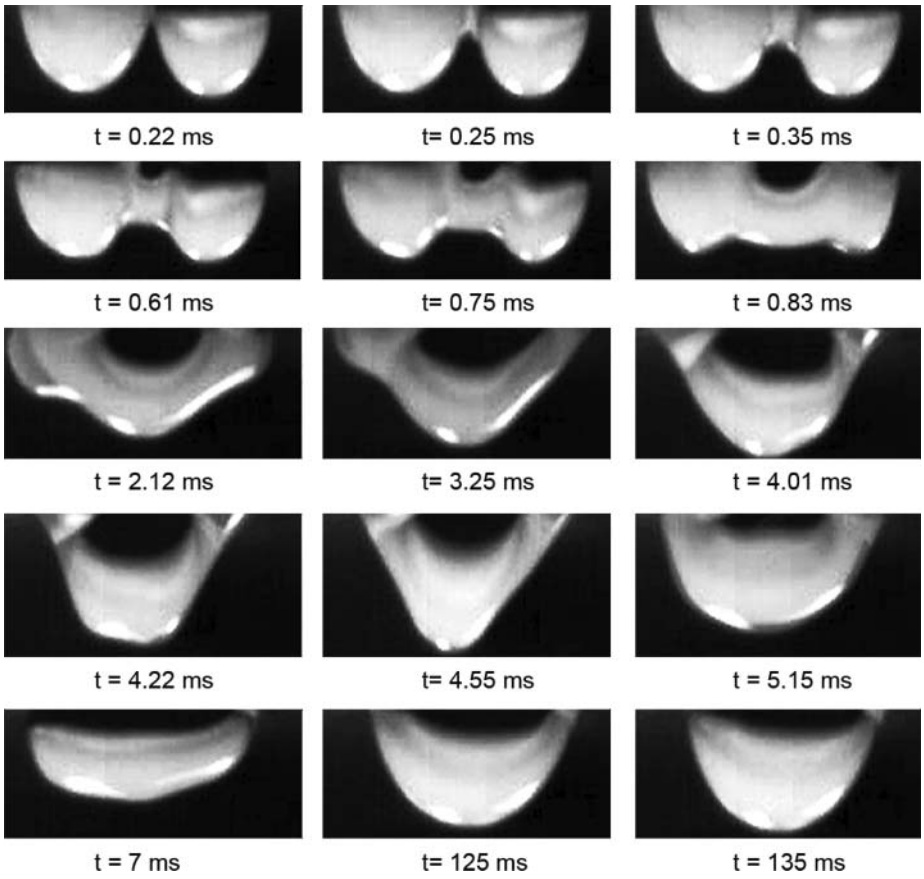

Figure 13 Coalescence of two pendant droplets of water of approximately same volumes (respective diameters are 2.15 mm and 2.00 mm) on a 5° inclined chemically textured substrate. It was observed that the resulting droplet achieves slide-off criticality and starts moving on the substrate.

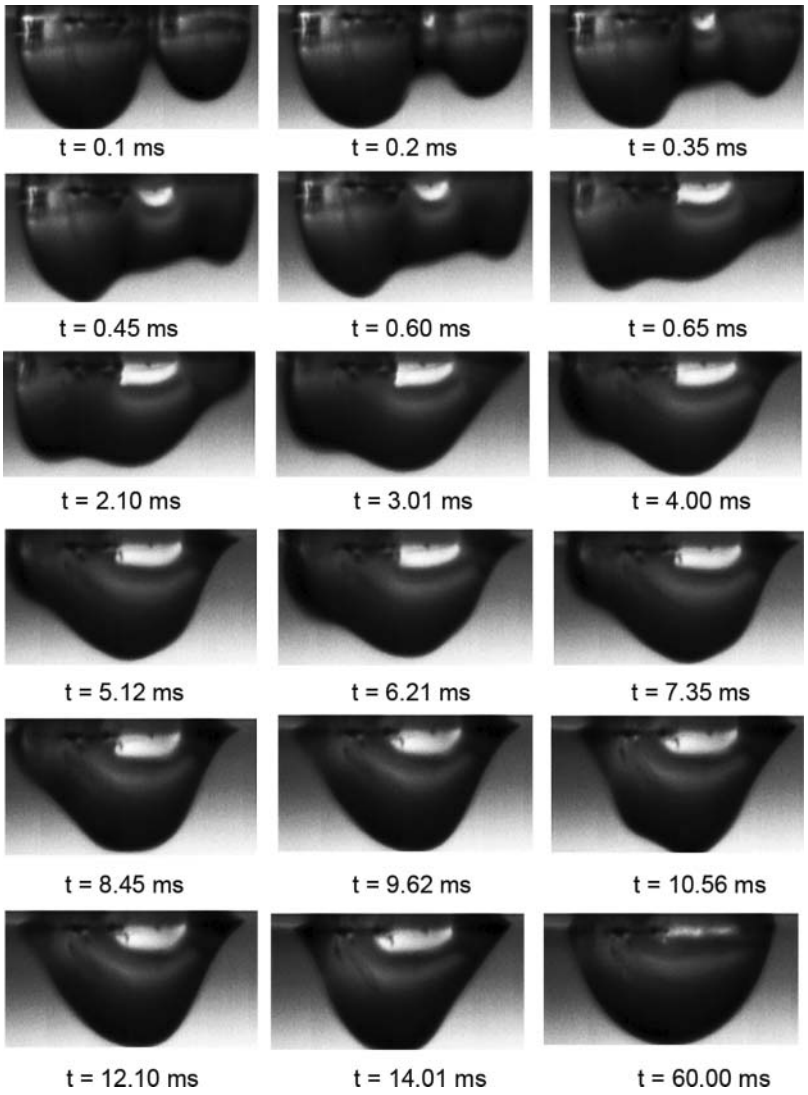

Figure 14 Coalescence of two pendant droplets of water of approximately same volumes (respective diameters are 1.0 mm and 0.45 mm) on a 15° inclined chemically textured substrate. The resulting droplet is stable and tends to achieve static equilibrium.

condensation cycle, from a virgin surface to the first fall-off or a slide-off, is typically of the order of several minutes; in contrast, coalescence of drops happens within ∼5–60 ms [55, 56]. The time scale, though very small, depends on the size of the individual drops and other thermophysical properties such as viscosity, surface tension, contact angles, and surface texture conditions at the operating temperature.

Based on the videographic study, sample images of which are shown in Figures 13–15, the following conclusions have been arrived at in the present work.

(i) When two or more than two drops coalesce, the center of mass of the resultant drop is practically equal to the weighted average mass center of the individual drops, with the discrepancy being attributed to external forces, such as those that pin the contact line.

(ii) The coalesced drop initially has a footprint of an ellipsoid, which relaxes in time to a hemisphere. The relaxation time is found to be of the order of a few milliseconds.

(iii) When the contact angle is large, the new drop relaxes rapidly to the shape of a truncated sphere. If the contact angle is small ($\theta < 20^\circ$), it may not relax to the part-spherical shape at all; the relaxation time here is an order of magnitude larger than for large contact angles.

(iv) Coalescence is accompanied by inertial oscillations visible over the drop surface. Fluid motion is initiated in the liquid bridge joining the original drops. This translates into oscillations of the contact angles as well.

Based on these preliminary observations, we note that: (i) When two drops of different sizes coalesce, the flow is into the larger drop as it is a region of lower pressure. Pressure

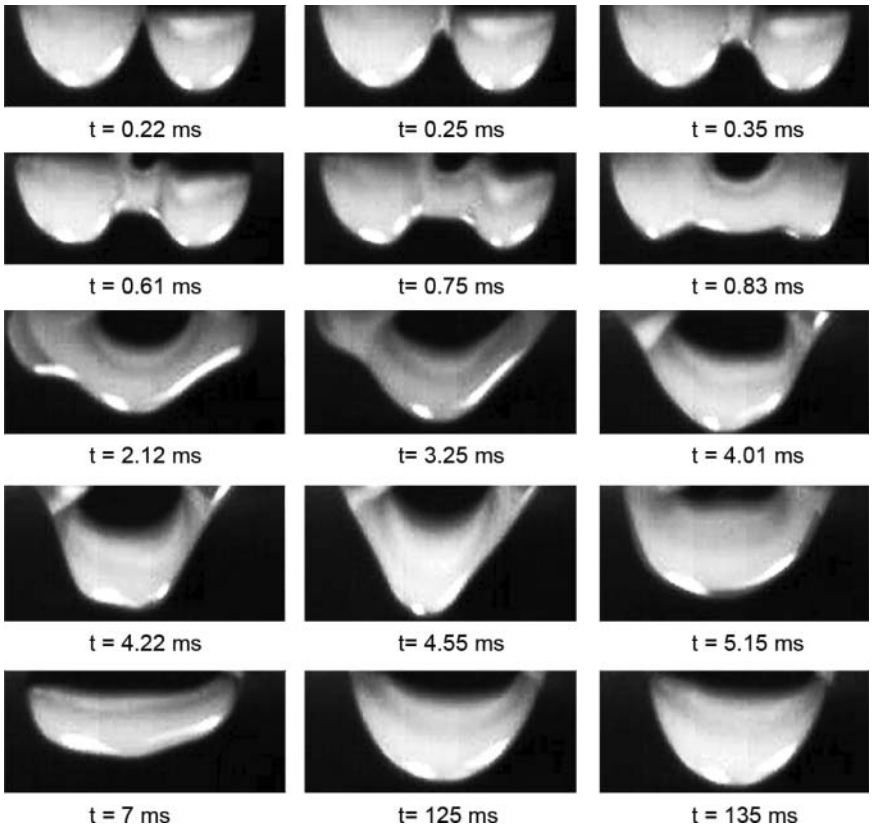

Figure 15 Coalescence of two pendant droplets of water of approximately same volumes (respective diameters are 1.2 mm and 0.95 mm) on a 5° inclined chemically textured substrate.

differences arise from drop curvature, and hence surface tension. A number of new nucleation sites also get exposed on the freshly uncovered condensing surface. (ii) When the two large drops of nearly equal volume coalesce, they form a single drop, and depending on their initial sizes, the newly formed drop may exceed the critical size, resulting in its sliding motion or a fall-off. A number of nucleation sites are once again exposed. (iii) The process of coalescence itself induces fluid motion and enhanced convection. In addition, drop coalescence also momentarily reduces the pressure acting on the surface, creating time-dependent pressure fluctuations. All these factors are believed to enhance local heat transfer coefficient; this needs further numerical, as well as experimental, explicit exploration.

In the preceding discussion, the substrate is taken to be at a constant temperature. Condensation affects the wall heat flux transferred from the vapor to the wall. In practice, wall temperature fluctuations are likely, particularly if the thermal inertia of the substrate matches the timescale of drop instability.

Dynamics of a Single Drop

During condensation, drops grow first by direct deposition of vapor and then by coalescence. At a later stage, the body force exceeds the retention force of surface tension, leading to the sliding motion of the drop or its eventual fall-off. A virgin portion of the substrate is exposed where the next generation of drops begins to grow. While the time-dependent process increases heat transfer, it has a detrimental effect in that the sliding drops leach away the promoting layer over the substrate. There is a possibility of chemical reactions between the promoter and the condensing liquid as well. The shear interaction of growing drops with coalescence followed by sliding motion on textured and coated substrates needs systematic study.

The wall shear stress and heat transfer are primary mechanisms that control physical leaching. To estimate the leaching rate, namely, the rate of removal of the promoter material from the surface, flow and temperature fields in a sliding liquid drop are calculated. The flow field within the sliding drop will determine the wall shear stress and therefore the stripping of the coated promoter layer by mechanical forces. Given a shear stress distribution of an individual drop, the net effect of the drops ensemble can be determined using the time-averaged drop size distribution.

The literature on surface leaching by drop motion is sparse. Most researchers have reported the relationship between the size and shape of the drop with respect to the retentive forces at various angles of inclination of the surface at incipient state before sliding is initiated [38, 39, 58–60]. The shape of the sliding drop and contact angles are also influenced by the velocity and thermal fields in the interior. In this context, Elsherbini

and Jacobi [43, 44] performed experiments to investigate the geometric parameters necessary to obtain the shape of sessile liquid drops on vertical and inclined plane surfaces. Dimitrakopulos and Higdon [61] considered drop shape and forces for a drop that is on the verge of sliding on an inclined plane in low Reynolds number shear flow. The authors minimized the contact-angle hysteresis for a given advancing angle and Bond number, with the condition that pressures from surface tension and gravity are equal at the liquid free surface. Using this approach, no conditions were imposed on the contour of the drop. However, the resulting drop contours showed elongation in the direction perpendicular to gravity (in the cross-sectional plane), a result contrary to experimental observations. Suzuki et al. [62] studied the sliding behavior of water drops on various chemically textured surfaces at a fixed inclination of 35° and reported the sliding displacement of the advancing edge of the drop. Annapragada et al. [63] performed experiments to characterize the velocity dependence of advancing and receding angles as a function of the capillary number.

Though a large volume of work exists on the prediction of the drop shape, its spreading, and stability on an inclined surface, few researchers have reported the sliding behavior of the drop that results from instability [64–71]. Kim et al. [64] performed experiments for measuring the steady sliding velocity of different liquid drops on an inclined surface and reported a scaling law to relate velocity of the liquid drop with its wetting characteristics. Huang et al. [65] used the front tracking method to determine the motion of two-dimensional drops and bubbles on a partially wetting surface which is exposed to external shear flow of air. The authors found the friction parameters and their effect on shape of a drop by introducing a Navier slip condition at the solid–liquid interface. Gao and McCarthy [66] postulated two mechanisms for a drop moving down the plane. Drops can move by sliding, where the particles near the solid–liquid interface exchange their position with those at the gas–liquid interface while the bulk of the fluid remains unaffected. The particle movement along the gas–liquid and solid–liquid interfaces is similar to the motion of a tread of a chain-driven tank. On the other hand, there could be rolling motion where the entire fluid mass undergoes a circulatory movement. Sakai et al. [67] studied rolling versus sliding behavior of a drop on various chemically textured surfaces. In their theoretical analysis, Grand et al. [68] scaled the viscous force as $\mu \cdot U \cdot V^{1/3}$ and reported that the drop sliding velocity along an inclined plane is a linear function of the Bond number.

Yoshida et al. [69] did not consider the viscous force in their study of the sliding behavior of water drops on a flat polymer surface. The authors reported that the sliding motion changes from constant velocity to one of constant acceleration with an increase in the contact angle. Neglecting viscosity for determining the onset of drop motion is not expected to be serious. This is because the resistance to motion is mainly from interfacial tension. Viscous forces are, however, important for determining the tangential force acting on the substrate—over the base area of the drop.

Daniel et al. [70] reported the maximum velocity of the condensing sessile drop on a chemically textured surface. Sakai and Hashimoto [71] experimentally determined the velocity vector distribution inside a sliding sessile drop using PIV. The authors reported that the velocity gradient near the liquid-solid interface is higher than locations elsewhere inside a drop. This analysis was further used to recognize the slipping and rolling components of the sliding velocity and the acceleration of the water drop [72]. Das and Das [73] used smooth particle hydrodynamics to numerically simulate the movement of drops down an inclined plane. The study captured the internal circulation inside a sliding sessile drop. It was shown that the frictional resistance by viscosity at the interface of the solid and the liquid cannot be neglected in estimating the sliding behavior of a drop moving on an inclined substrate. Sikarwar et al. [74] showed the effect of shape of the drop and Reynolds number at a Prandtl number of 5.8 on flow and thermal fields in a pendant drop moving on a hydrophobic substrate. The authors reported that the transport properties such as Nusselt number and friction factor decrease with increasing contact angle.

A computational approach for studying flow and heat transfer inside a pendant drop sliding on inclined substrate as described by Sikarwar et al. [74] is discussed later.

Calculation of the drop shape

The shape of a liquid drop resting on a solid substrate can be determined under static equilibrium conditions by solving the three-dimensional Young–Laplace equation. The additional information needed to solve the governing equation includes the apparent contact angle between the liquid and the surface, the footprint/shape of the three-phase contact line, and the drop volume. The contact angle is fixed by the choice of the substrate and the liquid. On the other hand, the contact angle is an input parameter (a boundary condition) for solving the Young–Laplace equation.

The Young–Laplace equation is highly nonlinear and may not be easily solved even if numerical techniques are employed. Certain simplifications can, however, be enforced and the calculation carried out in two dimensions. For a drop sliding on an inclined surface, the change in its shape because of motion is usually not perceptible and the initial deformation arising from plate inclination can be taken as representative for the drop in motion. Dynamic conditions can also be incorporated to a first approximation by regarding hydrostatic pressure in the equilibrium equation as the total pressure (static + dynamic) arising from fluid motion. This approach couples the shape calculation with that of the flow field.

The simplified determination of the shape of the drop proceeds along the following steps. With reference to Figure 16a, the droplet base is approximated as a circle on planes parallel to the substrate (the *top* plane) while the deformation is restricted to the *frontal* plane in which the plate inclination is visible. On the *cross-sectional* plane normal to the frontal, the drop is

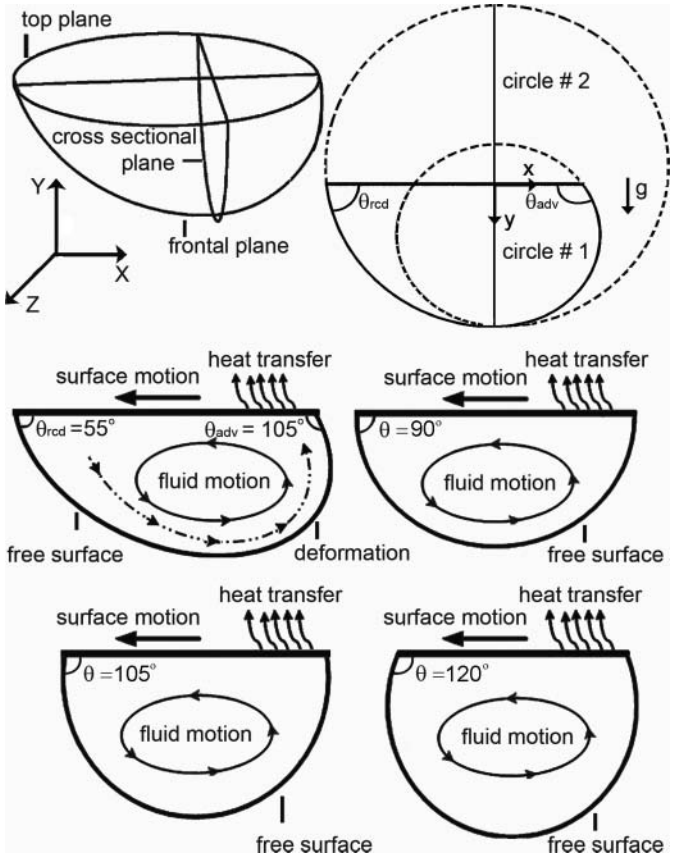

Figure 16 (a) Three planes of a deform droplet, i.e., top, frontal, and cross-sectional plane. Frontal plane is determined by solving the two-dimensional Young–Laplace equation, top is assumed as circular, and cross-section plane is assumed as symmetric part of the drop. (b) The solution of two-dimensional Laplace equation approximate is equal to two-circle approximation [34, 35]. (c) Schematic diagram of the flow inside a drop driven by wall motion. Deformed drop ($\theta_{adv} = 105^\circ$ and $\theta_{rcd} = 55^\circ$), a symmetric drop with contact angle 90°, 105°, and 120°. The volume of drop is conserved and is 134 μl. In dimensional form, wall temperature (T_{wall}) and free surface temperature (T_{free}) are 288 K and 308 K.

taken to be un-deformed and a part of a sphere with the average contact angle $(\theta_{adv} + \theta_{rcd})/2$.

The shape of the drop over the frontal plane is determined by solving the two-dimensional Young–Laplace equation that enforces a balance among the forces due to pressure, weight, and surface tension. The appropriate differential equation for the drop shape *y(x)* and boundary conditions are specified as follows:

$$\frac{\partial^2 y}{\partial x^2} \Big/ \left[1 + \left(\frac{\partial y}{\partial x}\right)^2\right]^{3/2} = A_1 - A_2 y \tag{27}$$

$$x = L_1, \quad \partial y/\partial x = -\tan\theta_{adv}$$

$$x = L_2, \quad \partial y/\partial x = -\tan\theta_{rcd} \tag{28}$$

Here $A_1 = \Delta p/\sigma$ and $A_2 = (\rho_l - \rho_v)g/\sigma$. In general, Δp includes the contributions of the hydrostatic pressure and the dynamic pressure due the fluid motion while σ is the coefficient of surface tension.

Equation (27) is written as a system of two first-order equations and integrated by a fourth-order Runge–Kutta method. While constant A_2 is known in advance, A_1 must be computed as part of the solution by stipulating that the drop shape contains a predetermined liquid volume.

Other methods that circumvent the solution of the three-dimensional Young–Laplace equation include the two-circle approximation [43, 44] shown schematically in Figure 16b.

Mathematical model of fluid flow and heat transfer

The present authors have studied fluid motion and heat transfer in a deformed drop of a given shape. The flow is taken to be steady, laminar, and incompressible, with constant thermophysical properties. The schematic diagram of the three-dimensional drop with an advancing angle of 105° and a receding angle of 55°, as well as symmetric drops of various contact angles (90°, 105°, and 120°), is shown in Figure 16c. The frame of reference is fixed to the liquid drop, with the substrate moving relative to it at constant speed. The boundary conditions applied are those of no-slip at the substrate/wall and free surface (zero shear) elsewhere, as given by Eqs. (31) and (32). Heat transfer rates are obtained for a pair of constant-temperature boundaries at the wall and the free surface, respectively. The boundary condition at the free surface is given by Eq. (32) in spherical coordinates. They need to be transformed from spherical coordinates to Cartesian during numerical implementation.

Using Einstein's summation convention, the equations governing fluid motion in the drop along with appropriate boundary conditions are summarized as follows:

$$\rho\left(\frac{\partial u_i}{\partial t} + u_j\frac{\partial u_i}{\partial x_j}\right) = -\frac{\partial p}{\partial x_i} + \mu\frac{\partial^2 u_i}{\partial x_j^2} \tag{29}$$

$$\rho \cdot C_p\left(\frac{\partial T}{\partial t} + u_j\frac{\partial T}{\partial x_j}\right) = k_c\frac{\partial^2 T}{\partial x_j^2} \tag{30}$$

Viscous dissipation has been neglected in the energy equation, as it was found to be insignificant. Temperature boundary conditions are developed as follows. If the capacity of the cooling system is substantially larger than the latent heat release, nearly uniform temperature will prevail over the substrate. For transient conditions, an additional approximation required is that the substrate should have small thermal inertia. The substrate exposed to vapor would then be at a constant temperature at all times. Thus, at the wall and the free surface of the drop, we get (restricting to only the steady-state situation, as dealt with in the present work):

$$u_x = U_{wall};\ u_y = 0;\ u_z = 0;\ T = T_{wall} \tag{31}$$

$$u_r = 0;\ \tau_{r\theta} = 0;\ \tau_{r\phi} = 0;\ T = T_{free} \tag{32}$$

The wall shear stress is calculated from the velocity field as follows:

$$\left.\begin{aligned}\tau_{xy} &= \mu\left[(\partial u_x/\partial y) + \left(\partial u_y/\partial x\right)\right]_{wall}\\ \tau_{zy} &= \mu\left[(\partial u_z/\partial y) + \left(\partial u_y/\partial z\right)\right]_{wall}\\ \tau_{wall} &= \sqrt{\tau_{xy}^2 + \tau_{zy}^2}\end{aligned}\right] \tag{33}$$

The boundary conditions at the free surface are in spherical coordinates. They need to be transformed from spherical to Cartesian coordinates during the numerical implementation.

The heat transfer rate at the wall and the corresponding heat transfer coefficient are calculated as:

$$q = -k_c\left[\frac{\partial T}{\partial n}\right] = -k_c\left[\frac{\partial T}{\partial y}\right]_{wall} \tag{34}$$

and

$$h = q/\Delta T \tag{35}$$

The symbol ΔT ($= T_{\text{free}} - T_{\text{wall}}$) is the difference of temperature between the vapor and the condensing surface. The convection resistance between the vapor and the free surface of the drop is taken to be small. Consequently, the drop surface is isothermal at the vapor temperature and is slightly higher than the wall temperature. In Eqs. (33) and (34), the derivatives of velocity and temperature are evaluated at the wall.

Fluid flow and heat transfer rates in the drop have been obtained in the present work by numerically solving the unsteady Navier–Stokes and energy equations in three dimensions. Thus, velocity and temperature profiles inside the drop are obtained. From these data, the wall shear stress and heat transfer coefficient are calculated from Eq. (33) followed by Eqs. (34) and (35). The Prandtl number is defined at an average temperature of 298 K, suitable for low-temperature condensation of steam, taken to equal 5.8. Reynolds numbers, based on droplet velocity and base diameter, come out in the range of 10–500.

Solution methodology

The computational approach adopted in the present study is based on finite-volume discretization (FVM) of the three-dimensional unsteady Navier–Stokes equations and energy equation over an unstructured mesh. Between vertex-centered and cell-centered placement of variables, the pressure correction procedure is cell centered, collocated with the fluid velocities [75]. The unstructured mesh is filled with tetrahedral elements of nearly equal volumes. Pressure–velocity coupling is treated using a smoothing pressure correction method that results in a SIMPLE-like algorithm. Convective terms are discretized by a second-order upwind scheme. Geometry-invariant features of the tetrahedral element are used so that the calculation of gradients at cell faces is simplified using nodal quantities of a particular variable. Nodal quantities, in turn, are calculated as a weighted average of the surrounding cell-centered values [76]. The diffusion terms are discretized using a second-order central-difference scheme. The discretized system of algebraic equations is solved by the stabilized biconjugate gradient method (biCGStab) with a diagonal preconditioner. The overall solution algorithm used for the present study is quite similar to that proposed by Date [77]. Points of difference are related to the use of certain invariant properties of the tetrahedral element, and a powerful linear equations solver as well as a parallel implementation of the computer program. Iterations within the code are run until a convergence in terms of the residual of order 10^{-7} is reached.

The computational domain in the present work corresponds to an isolated pendant drop sliding on a hydrophobic substrate. The shape of the drop is defined by its contact angle, and deformed drop shape is calculated by the two-circle approximation method, as was explained earlier. The present three-dimensional numerical investigation reports fluid flow and temperature distribution inside a pendant liquid drop sliding on an inclined surface on the frontal plane as well as the base of the drop, as in Figures 17–20. The fluid flow patterns (velocity vectors and the velocity profile on the frontal plane passing through the mid-section) inside the drop of contact angles 90, 105, and 120° and the deformed drop are shown in Figure 17. The results show that the u velocity variation is nearly linear with respect to the vertical coordinate (y) measured from the base. These results are in general agreement with the PIV studies reported in [71] and the simulation data reported in [73]. With increasing Reynolds number, the vertical location inside the drop, where the x-component velocity changes its sign, shifts toward the base. In this plane, the magnitude of velocity at the free surface nearly matches the imposed wall velocity, though in the opposite direction. Qualitatively comparing drops of contact angles 90, 105, and 120°, we find no major difference in the distributions of velocity components and therefore the overall flow pattern. Deformed drops also show similar qualitative flow distribution at various Reynolds numbers. The point of zero velocity is seen to move closer to the solid wall at Reynolds numbers of 500 and higher.

The contours of nondimensional temperature $(T - T_{wall})/(T - T_{free})$ inside the drops, on selected frontal planes, are shown in Figure 18. The maximum shear stress as well as heat transfer occurs at the drop corners, as in Figures 19 and 20. An attempt is made to correlate the effective average shear stress, i.e., Poiseuille number, and the net heat transfer, i.e., Nusselt number at the base of the drop, with respect to the Reynolds number and drop shape. One can see that Poiseuille number (Po) and Nusselt number (Nu) both increase with increasing Reynolds number. For a given volume, increasing contact angle decreases the transport coefficients, as shown in Figure 21. Such information is vital for estimating leaching rates of drops growing and sliding on a substrate during dropwise condensation. Estimation of the leaching rates is important in many engineering applications, for example, (a) estimation of life cycle of a heat exchanger textured by promoter layers and (b) estimation of substrate life on which heavy liquid metals are being deposited under

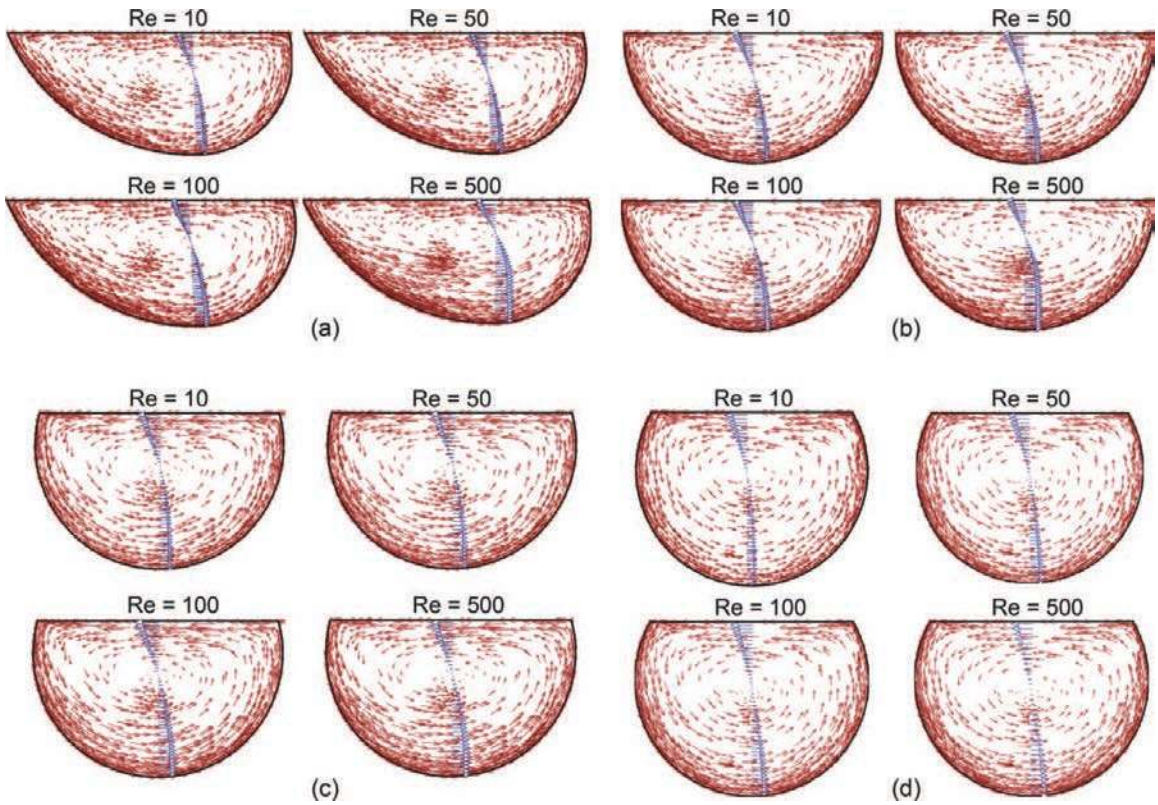

Figure 17 The fluid motion is represented by the resultant of velocity components u_x and u_y; the u_x component with respect to the vertical coordinate at X = 0, in the frontal plane (Z = 0), is also superimposed on the respective vector diagrams. (a) A deformed drop ($\theta_{adv} = 105^\circ$ and $\theta_{rcd} = 55^\circ$), (b) 90°, (c) 105°, and (d) 120° and Pr = 5.8. (Color figure available online.)

vacuum conditions. If the ensemble drop size distribution under dynamic dropwise condensation process is independently known, either from experiments or simulation, the relations proposed in this work for single drops can be used to find the effective shear stress and heat transfer coefficient on the entire physically/chemically textured condensing surface.

SUBSTRATE PREPARATION

In process equipment, dropwise condensation can be realized by suitably treating the condensing surface. The treatment will ensure partial wetting of the surface by the condensate liquid in the sense that the contact angle greater than 90° is achievable. The wetting characteristics of condensate over the cold substrate can be broadly controlled by two different means: (i) modify the surface of the substrate, or (ii) alter the condensing vapor chemically—say, by injecting a chemical that promotes nonwetting behavior.

Other methods that rely on changing the pH value of the condensate can be used so that dropwise condensation can be controlled by using an electrical potential (electro-wetting), changing the condensing temperature, and other similar techniques. Among these methods, substrate modification has emerged as the most popular and effective strategy.

A good drop promoter technique should be long lasting and involve low surface energy, low contact-angle hysteresis, and low thermal resistance. The method should be easy to apply and nontoxic and must be compatible with the system in which it is used; i.e., it should not impair the proper functioning of the other parts of the system. For any technique used for promoting dropwise condensation, the longevity of the textured surface is critical, if it is to be used in any process equipment. With the advent of newer manufacturing/coating and nanoscale fabrication techniques, surface treatment of the substrate holds considerable prospect in terms of providing the required long-term sustainability of dropwise condensation.

There have been two generic methods that can be used to modify the wettability of the substrate. One is chemically grafting or adsorbing molecules with wetting characteristics of their own (chemical texturing of the substrate). The second is to texture the surface by altering the surface topography/roughness or its patterns, which is called as physical texturing. Roughening a surface will increase wettability, in general, unless special patterns of the right scale are employed. In contrast, chemical coatings have gained prominence because of the larger choices available and are reviewed here.

Chemical texturing can be created by coatings such as organic compounds with hydrophobic groups [78, 79], inorganic compounds [80, 81], polymers [82–84], or special surface

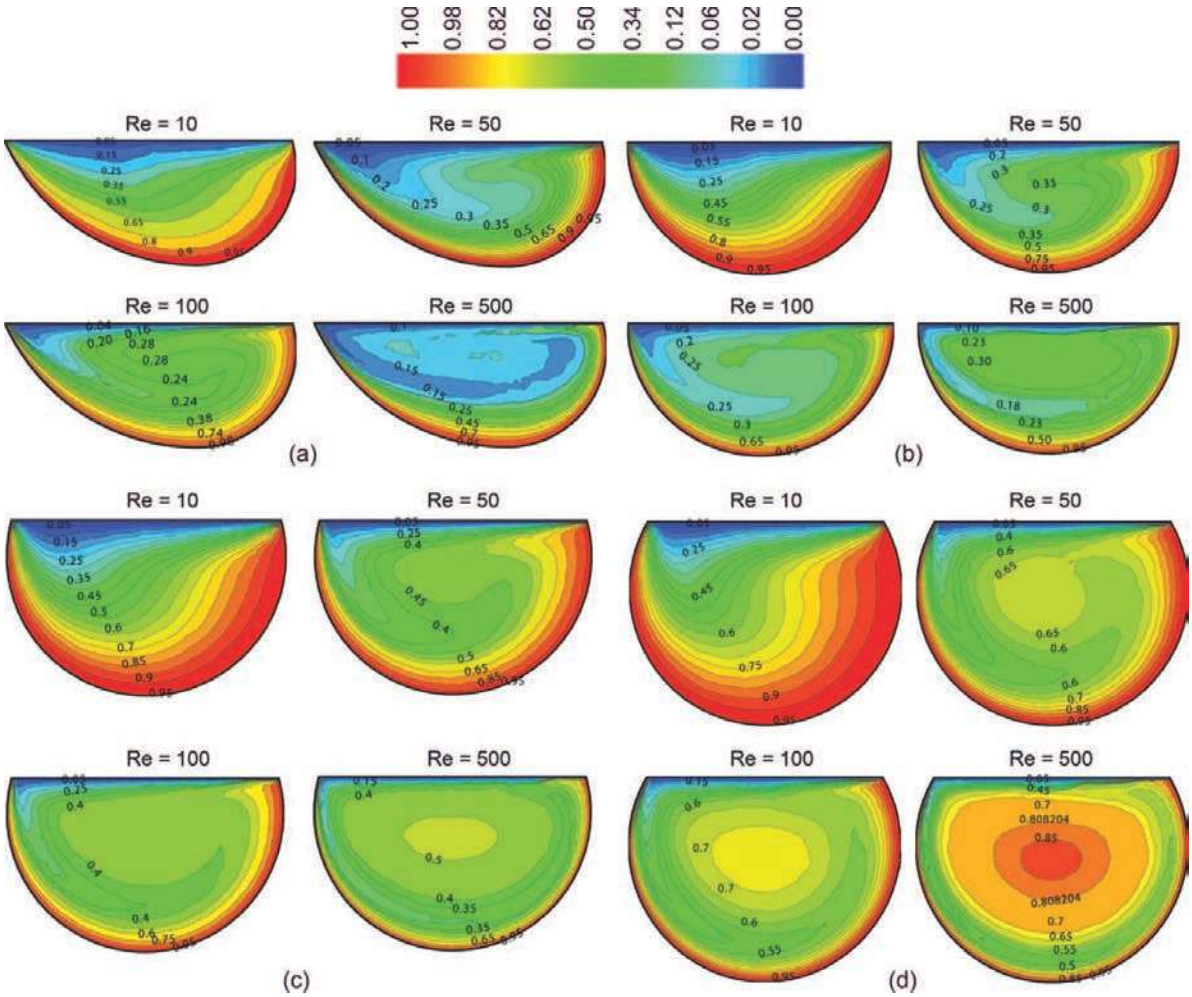

Figure 18 Nondimensional temperature contours in the frontal plane (Z = 0) at various Re and Pr = 5.8. (a) Deformed drop ($\theta_{adv} = 105^\circ$ and $\theta_{rcd} = 55^\circ$), (b) 90°, (c) 105°, and (d) 120°. The highest temperature is at the free surface (= 1) and the lowest temperature at the wall is (= 0). (Color figure available online.)

alloys [85, 86]. Though simple in concept, they suffer from long time sustainability issues that do not allow application to real-life, large-scale processes. Leaching by the motion of drops over the surface can also result in degradation. Recently, amorphous hydrogenated carbon films (a-C:H) with diamond-like mechanical properties have been modified by adding new elements to the film, e.g., silicon or fluorine [87], reducing its surface energy. These coatings have been studied for their heat transfer characteristics. Such coatings are mechanically and chemically stable but introduce an additional thermal resistance. This drawback can be overcome by other surface modifications that do not form any layer. Ion implantation is an example that has been tested successfully by Zhao et al. [85, 88] and Zhao and Burnside [89]. The production procedure is quite complicated and may form alloys in the surface layers. Leipetertz and Fröba [47] and Rausch et al. [90] developed another ion implantation technique, which is much easier to apply. They used fundamental thermodynamic principles of condensation to predict the dopant needed for ion implantation and the corresponding minimum dose for stable dropwise condensation. Vemuri et al. [91] coated a copper substrate with self-assembled monolayers (SAMs) of *n*-octadecyl mercaptan and stearic acid. They reported an increase in the heat transfer coefficient by a factor of three as compared to a bare copper substrate. Das et al. [92, 93] applied an organic self-assembled monolayer coating to enhance the dropwise condensation, with the corresponding increase in the heat transfer coefficient being a factor of four. Koch et al. [94] have reported the effect of hydrophobicity on the heat transfer coefficient in dropwise condensation on a chemically textured vertical substrate. The heat transfer coefficient was found to decrease with an increase in the wettability. Leipertz and Choi [95] reported the heat transfer rates on several metallic substrates (copper, titanium, aluminum, high-grade steel, and hastelloy) treated by ion implantation. Ions considered were nitrogen, oxygen, and carbon ions, with varying ion density. Ma et al. [96] proposed that the heat transfer coefficient increases with the increases of the surface free energy difference between the condensate and the condensing substrate. Hence, surface modifications for promoting dropwise condensation by silanation and ion implantation are of particular

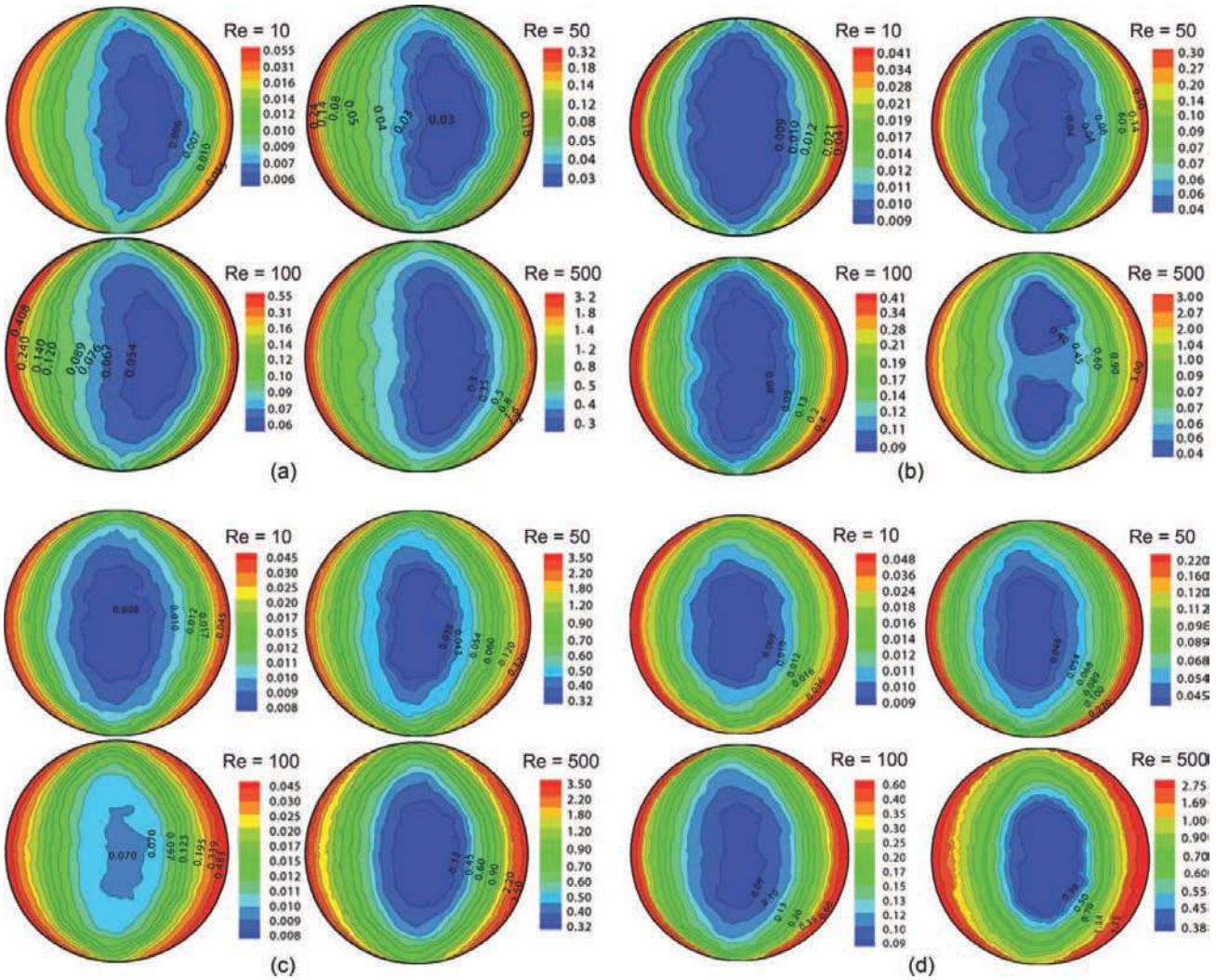

Figure 19 Wall shear stress distribution of (a) a deformed drop ($\theta_{adv} = 105^\circ$ and $\theta_{rcd} = 55^\circ$), (b) 90°, (c) 105°, and (d) 120° (Pr = 5.8 for all cases). (Color figure available online.)

interest. These would yield continuous dropwise condensation along with a high heat transfer coefficient. Recently, Rausch et al. [97] reported that the ion-implanted metallic substrates have stable condensation as well as a high heat transfer coefficient.

In the present study, the authors prepared a hydrophobic surface by coating it with self-assembled monolayers (SAMs). Among the SAMs, octadecyltrichlorosilane (OTS) was found to yield the best quality surface for dropwise condensation because of the smallest contact-angle hysteresis. The detailed preparation of the hydrophobic substrate by self-assembled monolayers is given next.

To obtain surfaces with a variety of surface energies, various treatments of the substrates were performed. A schematic diagram explaining the chemical vapor deposition process of SAM is shown in Figure 22a. The samples were first cleaned by sonicating them in an ethanol, acetone, and toluene bath for 3–10 min, respectively. The substrate was dried carefully with compressed nitrogen gas while changing from one solvent to another. Subsequently, the samples were cleaned by an oxygen plasma torch followed by a dry CO_2 snow-jet [98]. The samples were kept in piranha solution (50% H_2O_2 and 50% H_2SO_4 by volume) for 2–4 h. Piranha solution is highly oxidizing and requires special handling care.

Surface energy modification was accomplished by coating samples with self-assembled monolayers (SAMs). SAMs are formed spontaneously by chemisorption and self-organization of functionalized and long-chain organic molecules on an appropriate surface. Octadecyltrichlorosilane (OTS), dimethylchlorosilane (HMS), trichlorosilane (MTS), and propyltrichlorosilane (HTS) were used as SAMs, as in Figure 22b. To deposit OTS on a surface, the cleaned substrates were kept in a solution of 60 ml bicyclohexane, 35 drops carbon tetrachloride, and 20 drops OTS. During this time, the OTS molecules bond covalently on silicon dioxide substrates. In a few minutes, the substrates were taken out of the silane solution and rinsed with chloroform. To coat the surface with HMS, HTS, or MTS, the

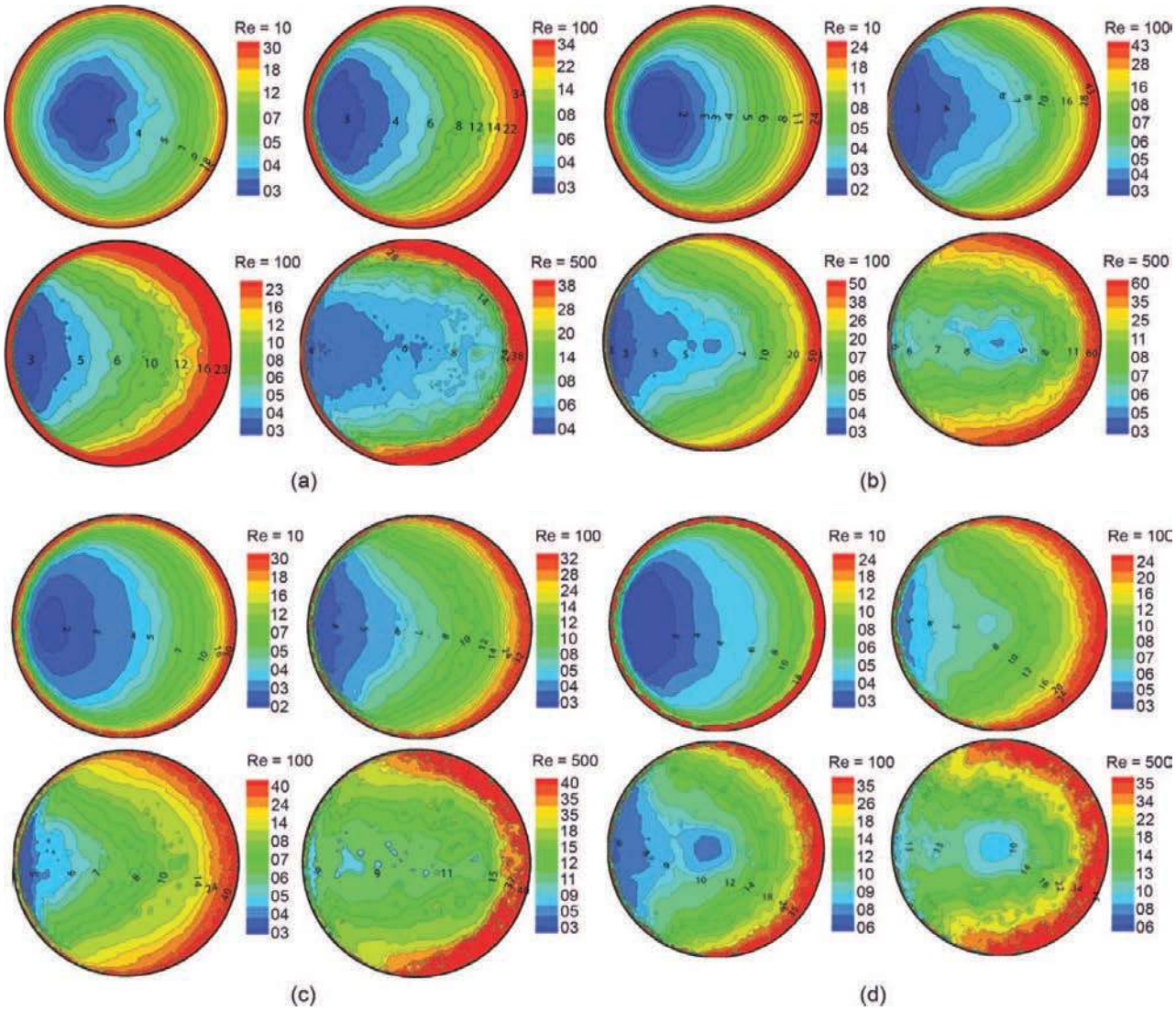

Figure 20 Nusselt number variation at various Re and Pr = 5.8 for (a) a deformed drop ($\theta_{adv} = 105^\circ$ and $\theta_{rcd} = 55^\circ$), (b) 90°, (c) 105°, and (d) 120°. (Color figure available online.)

cleaned samples were kept in a desiccator together with a small quantity of the desired silane. Silane vaporizes in the closed environment of the desiccator and gets deposited on the substrate. After 15–20 min of evaporation, a silane monolayer gets bonded covalently with the oxide surface [99]. After taking out the samples from the desiccators, they should be rinsed by chloroform. Co-evaporation of various silanes can also be carried out to achieve intermediate surface energy but at the cost of a higher contact angle hysteresis. Figure 22, c and d, shows the image of a pendant drop for various chemically textured substrates along with the measurement data. For a good hydrophobic coating, the contact-angle hysteresis should be as small as possible.

Other coating materials include, for example, Teflon. These surfaces are created by preparing a weak solution of Teflon (AF1600) in FC-75. The samples are dip-coated in this solution with different pulling speed to achieve the desired film thickness of Teflon. After the dip-coating, the samples are annealed in a furnace for varying times (∼10 to 30 min) at temperatures ranging from 100 to 300°C [100–102].

MEASUREMENT OF HEAT TRANSFER COEFFICIENT

Despite sustained research in the past two decades, the prediction of the correct heat transfer rate during dropwise condensation over a surface remains a challenge [1, 103], mainly due to lack of complete knowledge of the local transport mechanisms.

Experimental determination of the heat transfer coefficient during dropwise condensation is a demanding task because of the many intricacies involved in the process. Mainly, the driving temperature difference is small, essentially resulting in a high heat transfer coefficient. Further, uncertainties associated with the microscale substructure of contact line shapes and motions, dynamic temperature variations below the condensing drops,

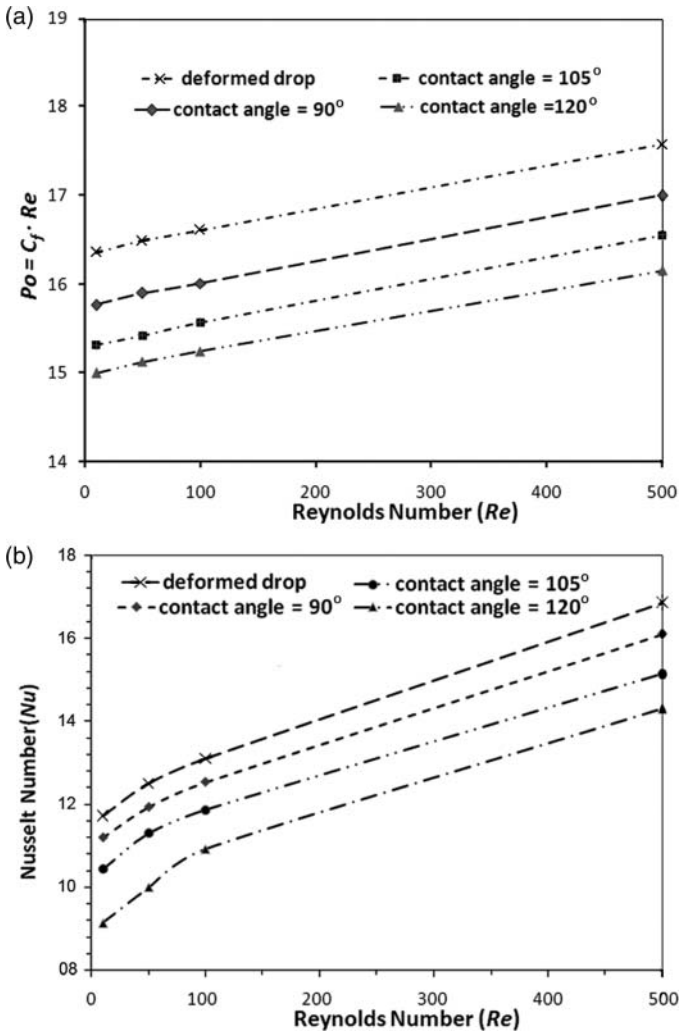

Figure 21 (a) Poiseuille number (Po) = (C_f·Re) versus Re at Pr = 5.8 for various contact angles and deformed drop sliding underneath an inclined surface. (b) Nu versus Re at (Pr) = 5.8 for various contact angles and a deformed drop sliding underneath an inclined surface.

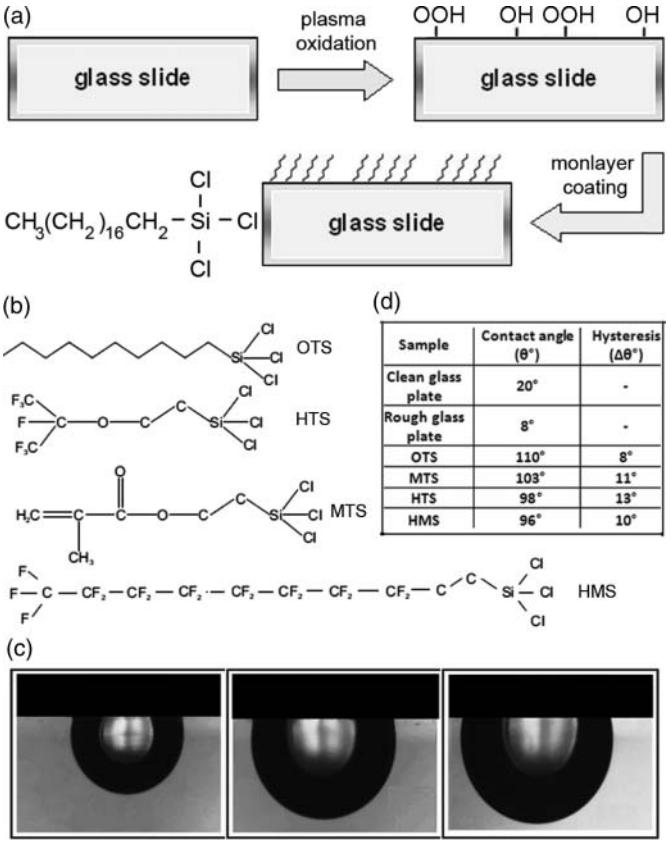

Sample	Contact angle (θ°)	Hysteresis (Δθ°)
Clean glass plate	20°	-
Rough glass plate	8°	-
OTS	110°	8°
MTS	103°	11°
HTS	98°	13°
HMS	96°	10°

Figure 22 (a) Schematic diagram explaining the chemical vapor deposition process. (b) Representations of various self-assembled monolayer (silane) molecules. (c) Image of pendant drop of volume 5 μl, 10 μl, and 15 μl, respectively, on HMS textured substrate. (d) measurement data.

effect of roughness and inhomogeneity of the substrate structure, control of true boundary conditions, microscale instrumentation, and transport dynamics of coalescence, merger, wipe-off, renucleation cycles, and the leaching rates of the promoter layer add to the difficulty in conducting repeatable experiments. Very high heat transfer rates (and therefore a very low temperature differential) coupled with the preceding factors also hinder generation of repeatable experimental data. Consequently, many conflicting experimental results have been published over the years [1, 104]. Some of the results in the literature show considerable scatter (Figure 23).

Typically, the following resistances are considered important during dropwise condensation:

(i) Conduction resistance: The drop in temperature due to conduction heat transfer is determined as:

$$\Delta T_{cond} = (q \cdot r) / \left(4\pi \cdot r^2 \cdot k_c \left(1 - \cos\theta\right)\right) \qquad (36)$$

(ii) Temperature drop due to interfacial heat transfer is:

$$\Delta T_{int} = q / \left(2\pi \cdot r^2 \cdot h_i \left(1 - \cos\theta\right)\right) \qquad (37)$$

(iii) Curvature resistance: This resistance includes the loss of driving temperature potential due to the droplet interface

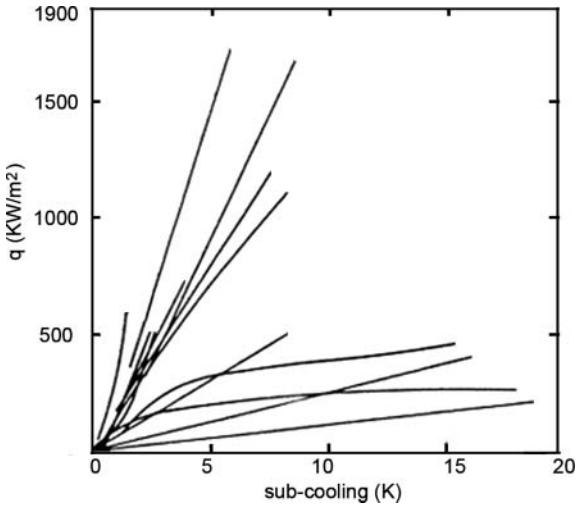

Figure 23 Heat flux versus degree of sub-cooling condensation of water at 1 atm on various engineering materials (with and without promoters/ various roughness characteristics [104]).

curvature and is given as:

$$\Delta T_{curv} = \frac{2v_l \cdot \sigma \cdot T_w}{H_{lv} \cdot r} = \frac{(T_s - T_w)\, r_{\min}}{r} \tag{38}$$

Here, h_i is the interfacial heat transfer coefficient and k_c is the condensate thermal conductivity.
The interfacial heat transfer coefficient is given by [12]:

$$h_i = \left(\frac{2\hat{\sigma}}{2-\hat{\sigma}}\right) \cdot \left(\frac{H_{lv}^2}{T_s v_{lv}}\right) \cdot \left(\frac{\bar{M}}{2\pi \bar{R} T_s}\right)^{1/2} \tag{39}$$

The temperature drop will balance the total available subcooling and so

$$\Delta T_t = \Delta T_{cond} + \Delta T_{int} + \Delta T_{curv} \tag{40}$$

The experiments that concern determination of the heat transfer coefficient during dropwise condensation are quite complex [104–109]. To determine the absolute value of heat transfer it is necessary to understand the mechanism of formation of a drop on an engineered surface involving varied length scales, from atomistic orders at early phases of nucleation to scales controlled by the body force distribution vis-à-vis surface tension [18]. These changes can only be understood when a multiscale modeling approach is adopted [109]. Apart from the factors just described, error in the heat transfer coefficient can also arise due to the presence of no-condensable gases and possibly insufficient accuracy of the measurement of the surface temperature. The thermal inertia of the substrate may also contribute to erroneous estimates.

A common assumption in heat transfer analysis and interpretation of experimental data is the isothermal nature of the substrate on which condensation is taking place. Quite often, the temperature gradient in the normal direction, recorded in the bulk substrate by suitably located thermocouples, is extrapolated to determine the average temperature of the substrate [12, 104]. Subsequently, the average condensation heat transfer coefficient is determined. However, the inherent drop size distribution on the substrate, which in turn is time dependent, results in surface temperature fluctuations during the sequence of condensation, coalescence, and removal of the drop [110]. Tsuruta and Tanaka [111] reported additional resistance between the substrate and the drop caused by the nonuniformity of the surface temperature. The additional temperature drop arises from the constriction resistance between the drop and the substrate. This suggests that neglecting thermal conductivity of the substrate is one of the factors that increase error in heat transfer measurement. There has been considerable controversy over the magnitude of the constriction resistance and the effect of the substrate thermal conductivity on the heat transfer coefficient. Some researchers [112–115] have interpreted their data to indicate a strong effect of thermal conductivity of the substrate on dropwise condensation heat transfer. Others [116–118] have experimentally found that this effect is negligible. For heat fluxes that are greater than $\sim$250 kW/m^2, Rose [1] suggested that the constriction effect is negligible for a high conductivity substrate. The effect of constriction resistance in the context of chemical texturing is not fully established yet.

Although the inherent time dependence of heat transfer in dropwise condensation has been acknowledged in the literature, spatiotemporal determination of temperature fluctuations is not straightforward. Conventional thermometry (e.g., with thermocouples) cannot provide spatial information of temperature distribution. Consequently, more accurate measurements are needed to show consistency of heat transfer measurement in dropwise condensation. For this reason, Bansal et al. [103] used liquid crystal thermography (LCT) to obtain the spatiotemporal thermal behavior of the condensing substrate. The technique was used to determine the thermal behavior at the scale of a single condensate drop. The data of Bansal et al. [103] for measurement of heat transfer is discussed below.

Details of the experimental setup to study dropwise condensation underneath a substrate are shown in Figure 24. The LCT sheet was calibrated and the calibration curve between hue and temperature is shown in Figure 25. Experiments were conducted in such a way that pendant drops form on the underside of the liquid crystal sheet. The spatial distribution of temperature during dropwise condensation over a polyethylene substrate was measured using liquid crystal thermography (view B in Figure 24) simultaneously with actual visualization of the condensation process using videography (view A in Figure 24). View A provides the direct picture of the drop size distribution on the substrate, whereas view B is the liquid crystal thermograph. The latter provides the hue distribution on the selected portion of the substrate as contours. These contours can be transformed into spatial temperature distribution from the hue–temperature calibration curve, as shown in Figure 26. Figure 27 shows the liquid crystal thermograph of a single drop of diameter 2.96 mm condensing on the polyethylene substrate at a vapor saturation temperature 40.3°C. In the LCT image, regions of high heat transfer rates appear as locations of relatively high temperature—for example, the blue ring in Figure 27a. Lower temperature transits toward green and red. The hue distribution over the base of the drop is shown in Figure 27b. Figure 27c shows the variation of heat throughput at the mid plane passing through the single drop, as identified in Figure 27a. Also shown in Figure 27d are examples of other isolated drops recorded during the experiments. Figures 28a and 28b show a pair of adjacent drops, condensing at the vapor saturation temperature of 40.3°C, and the associated hue distribution on the base area (note the elliptic shape of the droplet base). Figures 27c and d depict the instantaneous heat transfer rates on planes passing through these individual drops. It is clear from the experimental images that smaller drops have a lower thermal resistance per unit area than the larger drops. Therefore, the temperature distribution is nonuniform on the condensing substrate and constriction resistance may affect heat transfer data.

In the absence of noncondensable gases, one can conclude that the periphery of the droplet base line was seen to provide the path of least resistance for heat transfer. Average heat transfer

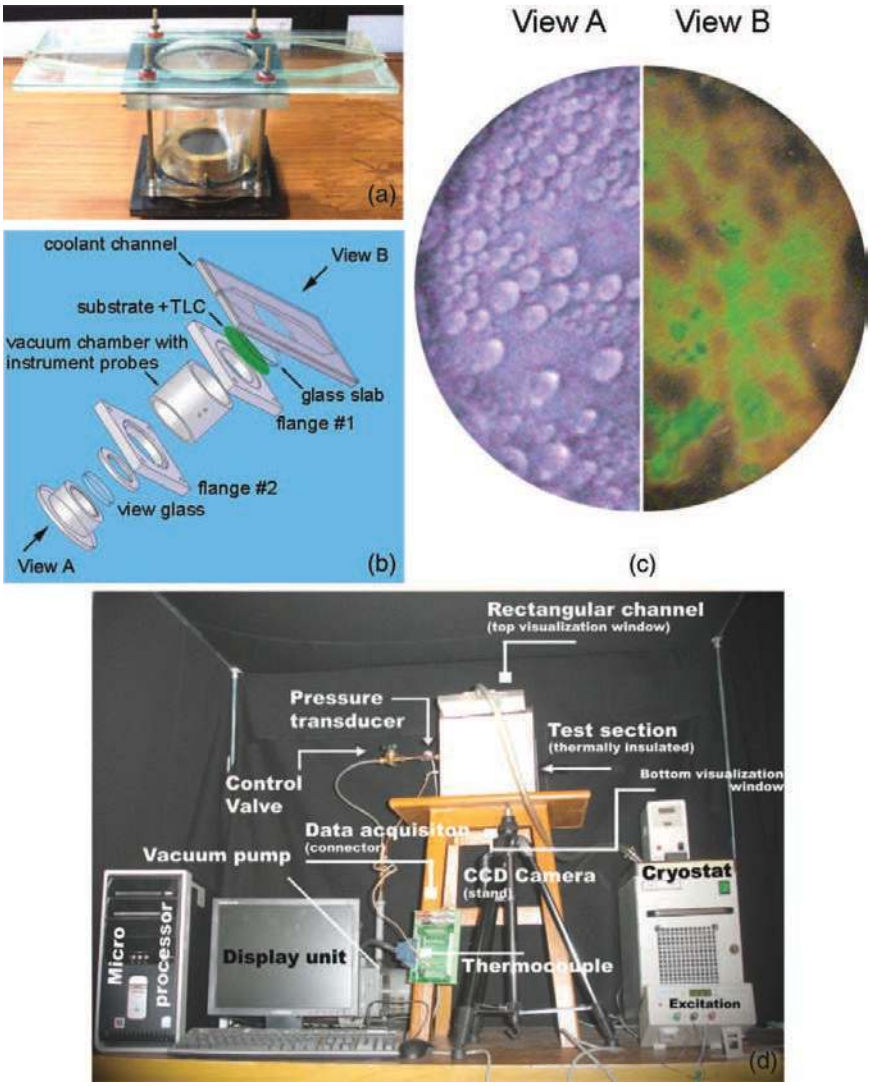

Figure 24 Details of the experimental setup to study dropwise condensation on the underside of a substrate. (a) Photograph shows the details of the main condensing chamber; (b) exploded view of the condensing chamber showing all the components. (c) Camera view A (refer to (b)) from the bottom gives the actual photograph of the condensing droplets, whereas Camera view B provides the RGB image of the TLC. (d) Details of the peripheral systems of the setup [103]. (Color figure available online.)

rate increases with increase in subcooling and saturation pressures. The principal finding of this study is that thermal imaging of dropwise condensation patterns over a surface is adequate for obtaining the heat transfer coefficient. These base images of the wall temperature distribution can be used to estimate local and average heat transfer coefficients by including the relevant thermal resistances between the condensing vapor and the subcooled substrate. Microscale measurement of small temperature differences continues to be a challenge for accurate estimation of heat transfer during dropwise condensation. Although liquid crystal thermography stretches the limit of spatial resolution to microscales, temperature differentials are too small below this limit for correct and repeatable experimental determination. Numerical techniques become essential at smaller length scales.

SPATIOTEMPORAL MACROSCOPIC MODEL OF DROPWISE CONDENSATION

The condensation of saturated vapor on a cold substrate is a cyclic process that begins at the atomic level, all the way to the formation of macroscopic drops, and finally manifests as drop sliding motion and/or fall-off. The complete modeling of dropwise condensation in one step is complex because of various processes distributed over length scales and time scales involved.

Mathematical modeling of dropwise condensation has been carried out by the authors of the present study by considering the following three steps: (i) drop formation at initial nucleation on a cold substrate; (ii) growth from nucleation to the critical size of the drop when sliding motion or falling off, underneath

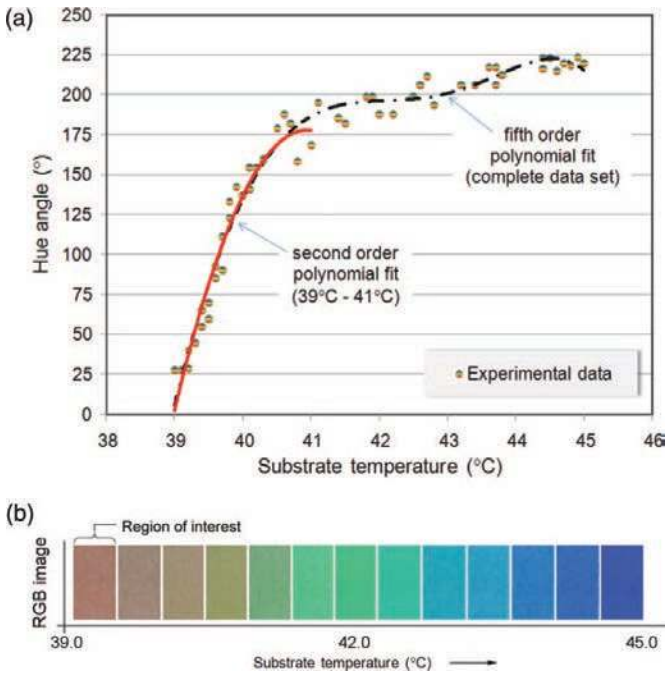

Figure 25 (a) Typical calibration curve of the liquid crystal sheet relating the substrate temperature to the hue scale. (b) The picture shows the RGB images obtained during the calibration step. These are further processed to get the HSI images [103]. (Color figure available online.)

horizontal and inclined substrates, gets initiated; and (iii) drop motion over the surface after reaching criticality. To the best of the knowledge of the authors, an integrated model that combines the three steps, as done in this paper, has not been reported in the literature, though subsystem-level modeling, with a range of assumptions, is available.

Macroscopic modeling of dropwise condensation requires careful understanding of the processes and subprocesses observed during experiments [46], as shown in Figure 29. The microscale studies of McCormick and Westwater [119] and Peterson and Westwater [120] and the experimental studies of Umur and Griffith [121] and Ivanovskii et al. [122] clarify the origin of the smallest drops on the surface. It is conclusively seen that the drops form by growth of clusters, which are created at specific locations, called nucleation sites. This proposal has been supported by other researchers as well [6, 12, 123]. In the macroscale, one can start building a condensation model with nucleation sites being occupied by the drops of the smallest possible radius. These drops are allowed to grow by direct condensation. Subsequently, coalescence of adjacent drops accelerates growth, until the drop attains the critical size for either fall-off (horizontal substrate) or sliding (inclined substrate). New drops form on the site vacated by coalescing drops and those that have left the surface by sliding/fall-off. The interaction among the drops other than coalescence barely counts in the final quasi-steady-state pattern and drop size distribution. On the basis of this approach, mathematical modeling of dropwise condensation mechanism has been attempted by several investigators [6, 46, 124–131]. Their model skeleton has been explained in detail by Van Carey [12]. Quantities such as the initial nucleation density, minimum size of drops at initial nucleation density, the growth rate equation, and criticality for incipient drop motion are to be provided as inputs to the model.

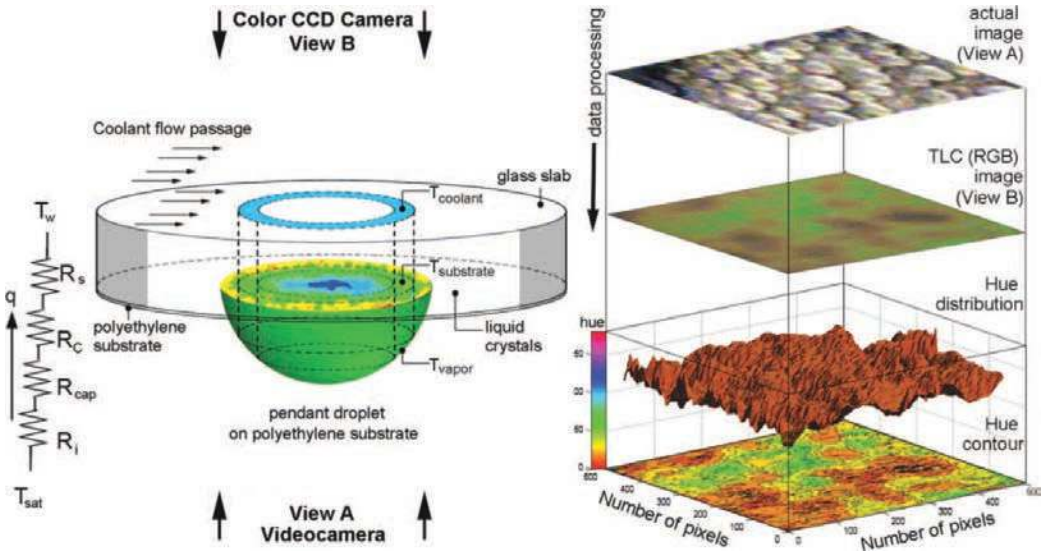

Figure 26 (a) The schematic shows the overall scheme for the estimation of the local heat transfer coefficient for dropwise condensation occurring on the underside of the substrate. View A provides the direct picture of the drop, whereas view B provides the liquid crystal thermograph. (b) The figure shows the series of operations employed for data reduction. The image of condensing droplets is obtained from camera view A, and the corresponding TLC RGB image is simultaneously obtained from camera view B. The latter image provides the spatial hue distribution on the selected portion of the substrate, the contours of which can be transformed into spatial temperature distribution from the hue-temperature calibration curve [103]. (Color figure available online.)

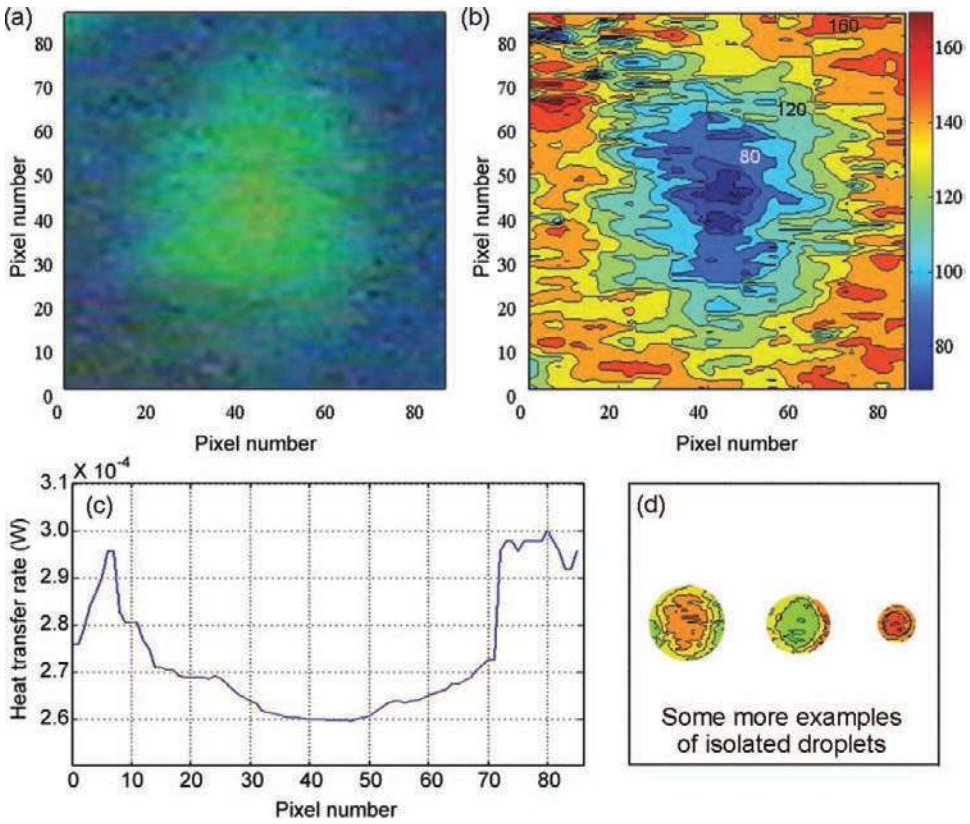

Figure 27 (a), (b) The figures show the TLC-RGB image of an isolated pendant droplet (D = 2.96 mm) during dropwise condensation process, at vapor saturation temperature of 40.3°C, and its corresponding hue contour plot. Images have been recorded after steady state has been attained. (c) The heat transfer rate at a plane passing through the middle of the droplet is shown as a function of position. (d) Examples of hue profiles of three other isolated droplets of smaller sizes [103]. (Color figure available online.)

The first mathematical formulation of dropwise condensation was reported in 1966 by Le Fevre and Rose [124] with drops seen as portions of a sphere. The theory was criticized for using a large number of adjustable constants. Glicksman and Hunt [125] simulated the dropwise condensation cycle in a number of stages, covering the equilibrium drop size to the departing drop size, thus achieving a large number of nucleation sites. The initial stage accommodated a nucleation site density of 10^8 m^{-2} by employing 1000 sites on a surface of size 33 μm × 33 μm. The area of the second stage was increased 10 times and the drops from the first stage were redistributed. In this way the simulation was repeated until the departure drop size was reached. Thus, a large number of nucleation sites were achieved, but an artificial redistribution between two consecutive stages destroyed the natural distribution of the drops. Wu and Maa [126] used the population balance method to find the size distribution of small drops that grow mainly by direct condensation. They estimated the heat transfer coefficient by considering only the conduction resistance through the drop. Abu-Orabi [127] incorporated the resistance due to heat conduction through the promoter layer, too. Since curvature resistance was not included, the error in heat transfer rates increased for large temperature differences. Rose and Glicksman [128] proposed a universal form of the distribution function for large drops that grow primarily by coalescence with smaller drops, though smaller drops mainly grow by direct condensation. Gose et al. [129] carried out computer simulation on a 100 × 100 grid with 200 randomly distributed nucleation sites. Burnside and Hadi [130] simulated dropwise condensation of steam from an equilibrium drop to a detectable size on 240 μm × 240 μm surface with 60000 randomly spaced nucleation sites. Vemuri and Kim [131] modeled dropwise condensation by the population balance method for hemispherical drops which mainly grow by direct condensation. The important resistances to heat transfer, such as vapor–liquid interface resistance were considered in developing the model. The derivation of steady-state distribution for small drops within the size range of negligible coalescence was based on the conservation of the number of drops with no accumulation. Contact angle other than 90° was not considered in this model. Leach et al. [6] fixed the initial size of the drops at 0.5 μm and suggested that the small drops grow by the accretion of drops of liquid molecules diffusing along the surface, while drops larger than about 50 μm in diameter grow principally by the accretion of vapor directly onto the drop surface.

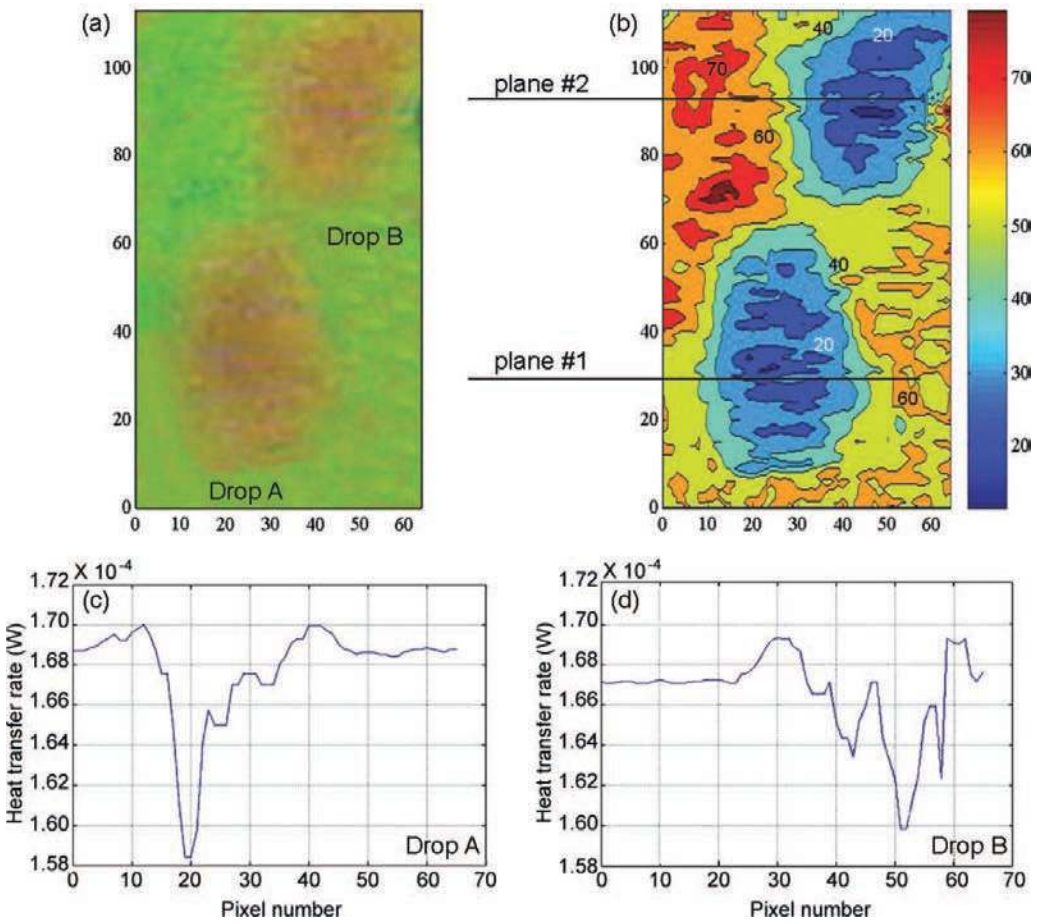

Figure 28 (a), (b) The figures show the TLC-RGB image of two adjacent pendant droplets during the dropwise condensation process and the corresponding hue contour plot at vapor saturation temperature of 40.3°C. Images have been acquired at steady state. (c), (d) Heat transfer rate through plane 1 (drop A) and plane 2 (drop B) is presented as a function of position [103]. (Color figure available online.)

Mathematical Model: Condensation Underneath Horizontal Surfaces

Recently, the authors of the present study have built a detailed mathematical model that captures all the major physical processes observed during dropwise condensation experiment underneath a surface [46], as shown in Figures 12 and 29. These include direct condensation growth, coalescence, sliding, fall-off, and the renucleation of droplets. The effects arising from lyophobicity, viz., the contact angle variation, inclination of the substrate, contact-angle hysteresis, and saturation temperature at which the condensation is carried out, have been incorporated (Figures 30 and 31). The following assumptions are considered during the development of the mathematical model.

(i) Nucleation sites are randomly distributed on the surface. Initial nucleation site density of 10^9 m^{-2} is assumed.
(ii) For a specified wall subcooling ($T_s - T_w$), a thermodynamically constrained smallest radius is taken as the minimum radius in the simulation (Eq. (25)). Initially, the substrate is clear of all condensate and all nucleation sites are instantaneously occupied by the droplet of minimum radius.
(iii) Prior to reaching the critical volume for fall-off or slide-off, all drops are located at the weighted center of mass of the coalescing droplets.
(iv) Heat transfer resistances include those due to the liquid–vapor interface, curvature and conduction, as described in the sixth section of this paper. Constriction resistance is neglected. Convective transport of thermal energy inside the drop is neglected.
(v) The accommodation coefficient is prescribed as a constant; see Appendix.
(vi) Coalescence is instantaneous and smooth; inertia effects and change of shape of droplet due to acceleration are neglected.
(vii) All drop shapes are approximated by an equivalent spherical cap approximation.
(viii) The dynamic variation of contact angle is neglected. For a particular surface–liquid combination, its value is taken to be constant and prescribed.

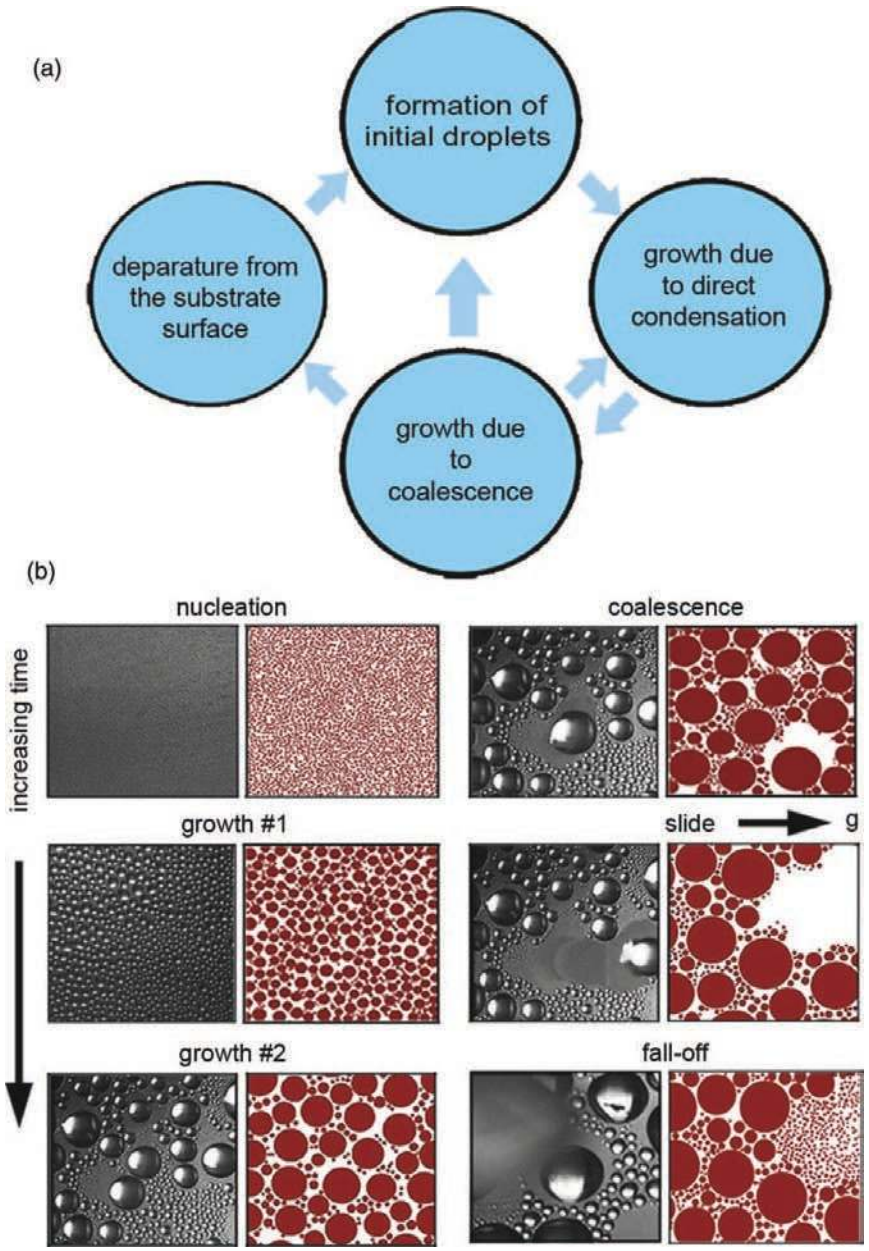

Figure 29 Complete cycle of sub-processes of dropwise condensation as observed in experiment and as captured in simulation [46]. (Color figure available online.)

(ix) Partial fall-off of droplets is neglected; on instability, the complete volume of the critical drop is removed from the surface.
(x) The entire substrate is assumed to be at constant temperature; any local variation in temperature due to drop dynamics is neglected.

While not in the context of condensation, Chatterjee [132, 133] has studied the size of a small oil drop at detachment from metal surfaces placed in an aqueous medium. The author reported the critical Eötvös number for buoyancy-induced oil drop detachment based on shape analysis. Similarly, Lexmond and Geld [134] studied the effect of plate thickness, surface tension, and vapor velocity on the size of drop detachment in compact condensers. It is noted that there is no explicit relation between the size of the drop at fall-off and its contact angle and the substrate inclination. Against this background, the size of the drop at fall-off underneath horizontal and inclined surfaces was determined as follows.

The forces acting on a drop normal to the surface include surface tension, gravity, and pressure. As the drop size increases, the pressure within decreases until, in the limiting case, the pressure difference across the drop surface is practically zero.

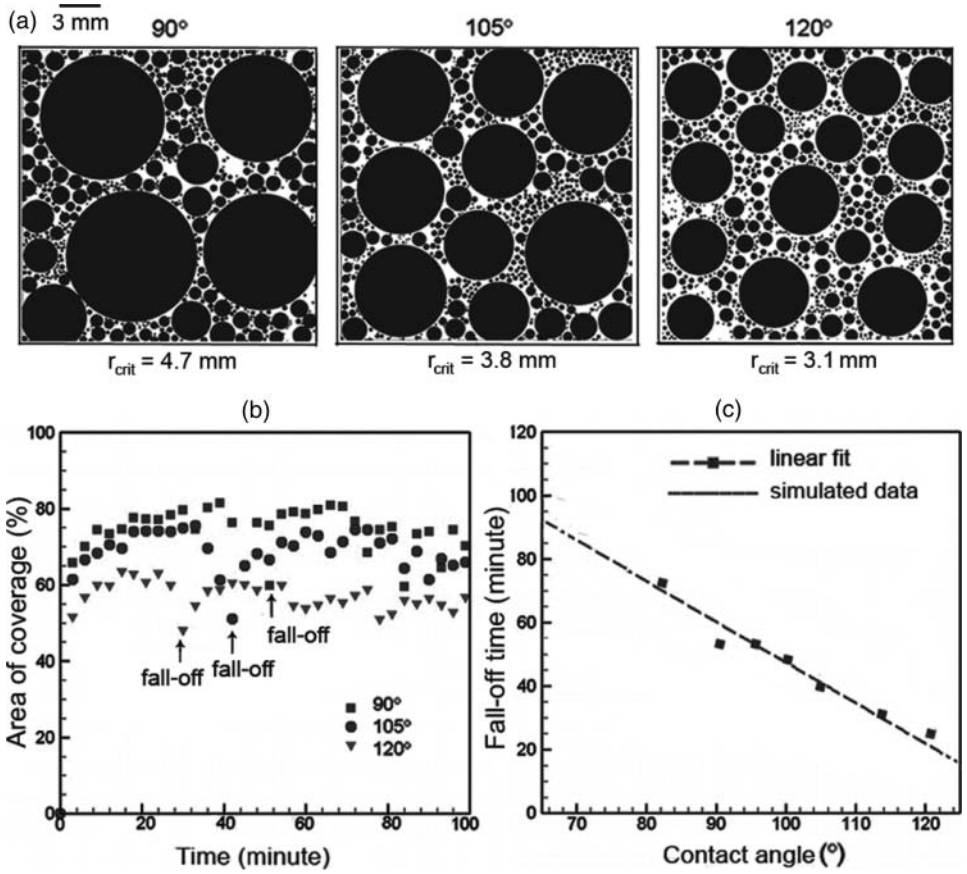

Figure 30 Effect of wettability. (a) Simulated spatial droplet distribution just before fall-off of a drop underneath a horizontal substrate of 20 mm × 20 mm area for contact angles of 90°, 105°, and 120°, respectively. (b) Temporal variation of coverage area of drops. (c) Fall-off time of the drop as a function of the contact angle (for all cases working fluid: water; $T_{sat} = 30°C$, $\Delta T_{sat} = 5°C$) [46].

Thus, the largest drop size is obtained as a limiting condition when gravity equals the normal component of surface tension. The maximum drop diameter is thus calculated from balancing the surface tension with the weight of the drop and is given by[4]:

$$r_{\max} = \sqrt{\left(\frac{6\sin^2\theta}{2-3\cos\theta+\cos^3\theta}\right)\cdot\left(\frac{\sigma}{g\cdot(\rho_l-\rho_v)}\right)} \quad (41)$$

This equation can be interpreted as the modified Bond number criterion, applicable for a pendant droplet, which takes into account the effect of contact angle in the force balance. In case of a horizontal substrate, there is no contact-angle hysteresis. The usual definition of Bond number is given by:

$$Bo = (2\cdot r)\left(\sqrt{(g(\rho_l-\rho_v))/\sigma_{lv}}\right) \quad (42)$$

The heat flux through a single droplet is given by:

$$q = \left(\pi r^2\cdot\rho_l\cdot H_{lv}\right)\cdot\left(2-3\cos\theta+\cos^3\theta\right)\cdot(dr/dt) \quad (43)$$

[4]The actually observed critical drop radius during the experiment by Sikarwar et al. [46] was slightly higher than that predicted by Eq. (41). Factors such as local droplet pinning and physicochemical inhomogeneities of the substrate, which are not considered in Eq. (41), are believed to be responsible for this discrepancy.

From the preceding equation, the rate of growth of individual droplets is derived as:

$$\frac{dr}{dt} = \left(\frac{4\Delta T_t}{\rho_l\cdot H_{lv}}\right)\cdot\left[\frac{\left(1-\frac{r_{\min}}{r}\right)}{\left(\frac{2}{h_i}+\frac{r}{k_c}\right)}\right]\cdot\left(\frac{(1-\cos\theta)}{(2-3\cos\theta+\cos^3\theta)}\right) \quad (44)$$

Here, the total temperature drop ΔT_t is taken from Eq. (40).

Equation (43) can be integrated in time to determine the growth of the droplet due to direct condensation. Along with the direct condensation growth loop in the simulator, a parallel coalescence loop was also monitored at each time step. The time for coalescence was taken to be much smaller than the other relevant timescales. Hence, as soon as two droplets contacted each other (or three droplets, or, very rarely, four droplets contact each other simultaneously), they were substituted with an equivalent single droplet with volume conserved, located at the weighted center of mass of the individual coalescing droplets. At each time step, the nucleation sites which were covered by drops were checked and flagged as hidden sites. In this manner, the randomly distributed droplets were allowed to grow to a stage where their weight exceeds the retention surface force,

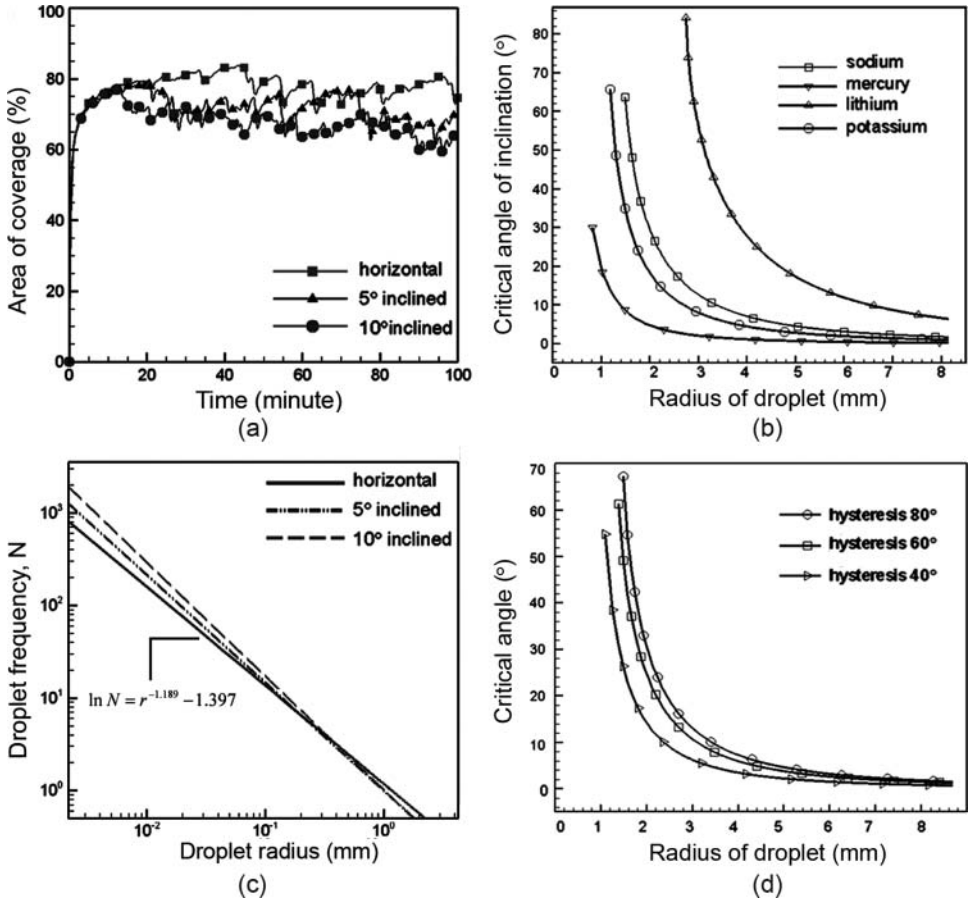

Figure 31 Effect of substrate inclination. (a) Temporal variation of area coverage of drops during condensation of water in the pendant mode. (b) Drop size distribution just before fall-off (for horizontal substrate) or slide-off (inclined substrate). For this simulation, the wettability of the substrate is such that $\theta_{adv} = 106^\circ$ and $\theta_{rcd} = 74^\circ$ for angle of inclination 5° and $\theta_{adv} = 110^\circ$, $\theta_{\text{rcd}} = 61^\circ$ for angle of inclination 10°; the droplet is assumed to be a part of a sphere on a horizontal surface; $T_{sat} = 30^\circ$C, $\Delta T_{sat} = 5^\circ$C. (c) Critical angle of inclination of the substrate as a function of the drop size with respect to fall-off (horizontal substrate)/slide-off (inclined substrate). (d) Effect of contact angle hysteresis on the critical radius of the drop [46].

yielding the critical Bond number criterion given by Eq. (42). At this juncture, droplets fall off. The critical drop was then removed and all hidden nucleation sites underneath the drop become active and were instantaneously supplied with thermodynamically stable droplets of minimum radius. The simulation tracked multiple generations of the droplets—nucleating, growing by direct condensation, by coalescence and some falling off when the virgin surface thus exposed got renucleated. This cyclic process was repeated for a long duration till a dynamic quasi-steady state was reached.

Mathematical Model: Condensation Underneath an Inclined Substrate

Inclining the substrate causes imbalance in the forces and results in drop deformation to achieve necessary static balance. As the droplet grows in size, the gravity force component parallel to the substrate exceeds the force component due to surface tension and eventually causes the droplet to slide underneath the substrate. As droplets slide, they encounter other growing droplets on their path. This process results in a very rapid mass accumulation, as the sliding droplet sweeps away a large population of drops located ahead of it. The critical drop diameter at which sliding commences depends not only on the thermophysical properties of the liquid but also on the contact-angle hysteresis and physicochemical properties of the substrate. Moreover, under dynamic conditions of dropwise condensation, the applicability of static force balances is questionable due to the presence of capillary waves, distortion in local equilibrium droplet shapes, droplet pinning, variation in dynamic contact angle due to inertia effects, sudden local acceleration, and three-dimensional flow structures inside the droplets. Therefore, there is considerable debate in the literature on the applicability of static conditions on the real-time condensation process. The bulk composite effect of these real-time dynamic situations and local contact line perturbations is usually manifested in the form of varying hysteresis of advancing and receding angles. Therefore, the static force balance conditions are assumed to be representative of the dynamic situation, as absolute contact angles and hysteresis are accounted for. The contact-angle

hysteresis, namely, the variation from the advancing to the receding contact angle, is taken to vary linearly along the contact line.

By incorporating this strategy, the critical radius of the droplet at slide-off on the inclined substrate has been calculated as:

$$r_{crit} = \sqrt{\left(\frac{3\sin^3\theta_{avg}}{\pi\left(2-3\cos\theta_{avg}+\cos^3\theta_{avg}\right)}\right)\left[\begin{array}{l}\dfrac{\pi}{2\pi-\theta_{rcd}-\theta_{adv}}\{\sin(2\pi-\theta_{rcd})-\sin\theta_{adv}\}\\ \quad+\dfrac{\pi}{\theta_{adv}+\theta_{rcd}}\{\sin\theta_{rcd}+\sin\theta_{adv}\}\end{array}\right]\left(\frac{\sigma_{lv}}{(g\sin\alpha)(\rho_l-\rho_v)}\right)} \tag{45}$$

The maximum radius of the drop at fall-off was obtained by balancing the forces perpendicular to substrate and is given as:

$$r_{\max} = \sqrt{\left(\frac{6\left(\sin^3\theta_{avg}\right)(\cos\theta_{rcd}+\cos\theta_{adv})}{\left(2-3\cos\theta_{avg}+\cos^3\theta_{avg}\right)(\pi-\theta_{rcd}-\theta_{adv})}\right)\left(\frac{\sigma_{lv}}{(g\cdot\cos\alpha)(\rho_l-\rho_v)}\right)} \tag{46}$$

On an inclined surface, critical-sized droplets first begin to slide off, as against falling off on a horizontal substrate. Criticality is achieved by direct condensation growth or, alternatively, by coalescence. Thus, depending on the length scale of the substrate and the time scales of direct growth and growth due to coalescence, various possibilities on an inclined substrate emerge:

(i) Slide-off criticality is achieved and during the entire slide-off on the substrate, fall-off criticality is not achieved.
(ii) Slide-off criticality is achieved and during the slide-off on the substrate, fall-off criticality is also achieved before the droplet traverses the complete substrate length scale.

Both these possibilities were incorporated in the mathematical model. During slide-off, the body forces accelerate the droplets and in the process many droplets on the path are swept away. The acceleration of the droplet was calculated by computing local forces at the contact line, i.e., gravity force, force due to shear stress at the wall, and the retention force due to surface tension. By assuming a linear velocity distribution inside the moving drop and the maximum velocity at its centre of mass [46, 73, 74, 135], the shear stress that produces surface leaching could thus be obtained. Finally, closure was obtained by externally supplying the wettability characteristics of the substrate, i.e., its average contact angle for a horizontal substrate and the advancing–receding angles for the inclined substrate, both from experimental data.

Using the preceding set of equations, the entire dropwise condensation process was simulated underneath a horizontal and an inclined substrate, from initial nucleation to a dynamic quasi-steady state. Some of the results obtained from this macroscopic model are discussed next (for detailed results, refer to [46]).

The effect of the wettability of the condensing liquid on the substrate is explored in Figure 30a, where the spatial drop distribution underneath a horizontal chemically textured substrate of 20 mm × 20 mm area, just before fall-off, is pictorially depicted. A reduction in wettability leads to a smaller base circle of the drop and, therefore, smaller surface forces holding the drop. Thus, two effects are clearly visible: (i) The droplet volume at the time of fall-off is smaller. The area coverage of the drops, seen in Figure 30b, is smaller as well. The quasi-steady-state area coverage varies with contact angle from 73.3% for 90°, to 67.1% for 105°, and 52.4% for 120°, respectively. (ii) With increasing contact angle, the drops achieve fall-off criticality earlier in the cycle, as shown in Figure 30c. All other conditions remaining unchanged, the fall-off time for a pendant drop is seen to be a linear function of the contact angle.

Figure 31a shows the effect of substrate inclination on the temporal distribution of coverage area. Substrate inclination facilitates easier movement of drops by sliding, leading to droplet sweeping action. Therefore, the effective steady-state coverage is smaller for inclined substrates, changing from 67.4% for the substrate with 10° inclination to 71.2% for 5° inclination and 76.1% for a horizontal substrate. At the instant of the first fall-off (for the horizontal substrate) and the first slide-off (for the inclined substrate), Figure 31b depicts the drop size distribution, as a function of radius, for various inclination angles. The distribution follows a power law with the negative slope increasing with angle, reflecting the repeated appearance of small drops at fresh nucleation.

The variation of the critical angle of inclination for the commencement of sliding with respect to the droplet radius, for various liquid metals, is shown in Figure 31c. The advancing and receding angles are taken to be known quantities for the purpose of simulation. For a given drop radius, the ordinate represents the angle that the substrate makes with the horizontal. At this stage of criticality, the weight of the drop exceeds the surface force holding it, resulting in either a fall-off or a slide-off. Increasing the angle of substrate inclination decreases the radius at which droplet slide-off commences. The critical angle of inclination also depends on the surface tension of the liquid; larger surface tension liquids have a greater critical inclination angle before sliding starts. The effect of the contact-angle hysteresis on the critical angle of inclination is seen in Figure 31d. As the contact-angle hysteresis is reduced, the critical angle of inclination for sliding motion reduces.

CONCLUSIONS

The heterogeneous condensation phase-change process is one of the most efficient ways of heat transfer in engineering systems, with the heat transfer coefficients being orders of magnitude larger than single-phase convective paradigms. This phase-change process may result, under quasi-steady-state conditions, in either (i) the formation of a distinct droplet ensemble mode of condensing fluid, (ii) the formation of a continuous film on the cold substrate, or (iii) there can be a mixed mode, having fuzzy overlapping characteristics of drops and a film simultaneously. The heat transfer coefficient of the dropwise mode is usually one order of magnitude higher than the other modes of condensation process. The preferred mode of condensation depends not only on the thermophysical properties of the fluid getting condensed, but also on the physicochemical properties of the cold substrate.

In this paper, a holistic view of the complete hierarchy of the processes involved in dropwise mode of condensation on plain and textured surfaces is presented. The state of the art on the subject has been scrutinized. The subject matter has been arranged in the following sequence:

(i) An atomistic viewpoint of the drop formation involving clusters of adatoms that eventually lead to thermodynamically stable nuclei was presented. A population balance model that captures the role of major engineering process parameters was highlighted.
(ii) Numerical analysis of thermofluid transport behavior of an individual droplet was discussed. Quantities reported are the three-dimensional fields of velocity, pressure, temperature, and transport fluxes of a single droplet. Fundamental information on wettability, apparent contact angle, its hysteresis, and contact line statics was also discussed.
(iii) Experimental heat transfer measurements by liquid crystal thermography under condensing droplets were discussed. Local heat transfer coefficient below a drop and the average heat transfer coefficient were presented.
(iv) A macroscopic model, incorporating the static analysis of an isolated individual droplet and dynamics of an ensemble of condensing droplets formed during dropwise condensation, was presented. Numerical computations were conducted for various contact angles and substrate inclination angle as a parameter. Drop size distributions and spatial patterns of condensation were presented for various liquids. The model predictions are compared to experimental data on chemically textured surfaces. Laboratory-scale surface preparation of such surfaces was briefly discussed.

Opting for dropwise condensation process in advanced engineering systems involves an understanding not only of the fundamental thermofluidic transport behavior but also of the microscale issues associated with the substrate material. With this background, the following major research issues are identified, among others:

1. Sustaining dropwise mode of condensation for prolonged periods of time on engineering surfaces by controlling the surface energy profile, so as to take the obvious advantage of high transfer coefficients, is a long-standing technology barrier faced by the industry.
2. As the ensuing driving temperature difference is very small in dropwise condensation, experimental determination of the heat transfer coefficient is a challenge. The statistical nature of droplet distribution in the ensemble further contributes to the intricacy of analysis and interpretation.
3. Individual droplet formation, shape, and resulting dynamics depend on microscale surface energy distribution. Hence, surface roughness, physicochemical thin film characteristics, and macroscale effects are intrinsically linked to microscale phenomena, necessitating a hierarchical modeling approach. Multiscale modeling of the entire dropwise condensation process, from atomistic level to macroscale individual droplet formation followed up by the creation of quasi-steady droplet population, is a topic of ongoing research.
4. Understanding of the contact line motion, droplet merging and instabilities, contact-angle hysteresis, and metastable thermodynamics are challenges at the macroscale models.

It is concluded that the understanding of dropwise condensation continues to pose difficulties, especially if the process has to be controlled. Breakthroughs in thin film coating, nanotechnology, physical and chemical texturing processes, advanced manufacturing, and superior experimental techniques have allowed deeper understanding of factors that decide the drop size distribution. Multiscale models starting from the condensing nuclei to unstable drops are in a state of development.

NOMENCLATURE

A	area of substrate (m^2)
C_p	specific heat of liquid (J/kg-K)
D	diffusion constant, m^2/s
d	diameter (m)
$f_i\,(s/S)$	scaling function for the island size distribution
f	degree of roughness of substrate
F	vapor flux, atoms/m^2-s
H	latent heat of vaporization of the liquid (kJ/kg)
h	heat transfer coefficient (W/m^2-K)
h_i	interfacial heat transfer coefficient, W/m^2-K
K	shape constant for contour of the droplet
k	thermal conductivity (W/m-K)
$\overline{M}$	molecular weight of the condensing liquid (kg/kmol)
M	maximum size of unstable clusters
m	mass of droplet (kg)
N	nucleation site density (1/cm^2)

N_A	Avogadro's number
n_s	number of clusters of size s at coverage ϑ
n_d	number of atoms/molecules
n_1	number density of monomers (monomers/m^2)
n_j	number density of clusters containing j atoms/molecules, number of clusters/m^2
n_i	number density of critical clusters (i refers to that cluster size which does not decay but may change due to growth by the addition of clusters), number of clusters/m^2
n_x	number density of stable clusters ($n_x = \sum_j n_j$ for all $j \geq i$), number of clusters/m^2
dn_1/dt	rate of change of monomers with time, monomers/m^2-s
dn_j/dt	rate of change of clusters containing j atoms, number of clusters/ m^2-s
dn_x/dt	rate of change of stable clusters ($n_x = \sum_j n_j$ for all $j > i$), number of clusters/ m^2-s
p	pressure (Pa)
q	surface heat flux (W/m^2)
$\bar{R}$	universal gas coefficient (J/kmol-K)
r	radius of droplet (m)
R	length scale (m)
$S = \frac{\sum s \cdot n_s}{\sum n_s}$	average island size; $s = 1, 2, 3\ldots$
T	temperature (K)
ΔT	temperature drop (K)
Δt	time step (s)
U	velocity of the wall droplet (m/s)
u	velocity (m/s)
V	volume of the drop (m^3)

Greek Symbols

α	inclination angle (deg)
δ_j	decay rate of clusters containing j atoms
η	dynamic viscosity (Pa-s)
$\bar{\eta}$	coefficient of friction (—)
λ	wavelength of light (m)
ν	specific volume at the saturation temperature (m^3/kg)
ϕ	azimuthal angle (deg)
ρ	density (kg/m^3)
σ	surface tension (N/m)
$\hat{\sigma}$	accommodation coefficient (—)
σ_1	capture rate of monomers by formation of dimers
σ_j	capture number of clusters containing j atoms
τ	shear stress (N/m^2)
τ_{ads}	mean residence time, s
θ	contact angle (deg)
$\vartheta = \sum_{s \geq 1} s \cdot n_s$	fractional area coverage of all the clusters

Subscripts

adv	advancing
avg	average
b	base
c	condensate
cond	conduction
crit	critical
curv	curvature
d	droplet
g	gravity
i	free indices
int	interfacial heat and mass transfer
l	liquid
lv	liquid vapor interface
max	maximum
min	minimum
prev	previous
r, θ, ϕ	spherical coordinates axis
rcd	receding
sat	saturation
sl	solid–liquid interface
s	shear
sc	spherical cap
t	total
v	vapor
w	wall
$\parallel$	parallel to the substrate
$\perp$	perpendicular to the substrate

Nondimensional Parameters

Ca	capillary number ($\frac{\mu \cdot U}{\sigma}$)
C_f	coefficient of friction($\frac{\tau_w}{\rho \cdot U^2}$)
Nu	Nusselt number ($\frac{h \cdot d_b}{k}$)
Po	Poiseuille number ($C_f \cdot \mathrm{Re}$)
Re	Reynolds number($\frac{\rho \cdot U \cdot d_b}{\mu}$)

REFERENCES

[1] Rose, J. W., Dropwise Condensation Theory and Experiments: A Review, *Proceedings Institution of Mechanical Engineers*, vol. 216, pp. 115–118, 2002.

[2] Lan, Z., Ma, X. Z., Zhang, Y., and Zhou, X. D., Theoretical Study of Dropwise Condensation Heat Transfer: Effect of the Liquid–Solid Surface Free Energy Difference, *Journal of Enhanced Heat Transfer*, vol. 16, pp. 61–71, 2009.

[3] Lee, L. Y., Fang, T. H., Yang, Y. M., and Maa, J. R., The Enhancement of Dropwise Condensation by Wettability Modification of Solid Surface, *International*

Communications in Heat and Mass Transfer, vol. 25(8), pp. 1095–1103, 1998.

[4] Boreyko, J. B., and Chen, C. H., Self-Propelled Dropwise Condensate on Superhydrophobic Surfaces, *Physical Review Letters*, vol. 103, pp. 184501–184504, 2009.

[5] Tanaka, H., A Theoretical Study of Dropwise Condensation, *Journal of Heat Transfer*, vol. 97(1), pp. 97–103, 1975.

[6] Leach, R. N., Stevens, F., Langford, S. C., and Dickinson, J. T., Dropwise Condensation: Experiments and Simulations of Nucleation and Growth of Water Drops in a Cooling System, *Langmuir*, vol. 22, pp. 8864–8872, 2006.

[7] Wu, Y., Yang, C., and Yuan, X., Drop Distribution and Numerical Simulation of Dropwise Condensation Heat Transfer, *International Journal of Heat and Mass Transfer*, vol. 44, pp. 4455–4464, 2001.

[8] Glassford, A. P. M., Practical Model for Molecular Containment Deposition Kinetics, *Journal of Thermophysics and Heat Transfer*, vol. 6, no. 4, pp. 656–664, 1992.

[9] Tien, C. L., Majumdar, A., and Gerner, M., *Microscale Energy Transport*, Taylor & Francis, New York, pp. 167–183, 1998.

[10] Hashimoto, H., and Kotake, S., In-situ Measurement of Clustering Process Near Condensate, *Thermal Science and Engineering*, vol. 3, pp. 37–43, 1995.

[11] Chen, L. H., Chen, C. Y., and Lee, Y. L., Nucleation and Growth of Clusters in the Process of Vapor Deposition, *Surface Science*, vol. 429, pp. 150–160, 1999.

[12] Carey, V. P., *Liquid–Vapor Phase–Change Phenomena*, 2nd ed., Hemisphere Publishing Corporation, New York, pp. 342–351, 1992.

[13] Bonner, R. W. III, Dropwise Condensation in Vapor Chambers, *26th IEEE Semi-Therm. Symposium*, pp. 224–227, 2010.

[14] Song, T., Lan, Z., Ma, X., and Bai, T., Molecular Clustering Physical Model of Steam Condensation and the Experimental Study on the Initial Droplet Size Distribution, *International Journal of Thermal Sciences*, vol. 48, pp. 2228–2236, 2009.

[15] Bentley, P. D., and Hands, B. A., The Condensation of Atmospheric Gases on Cold Surfaces, *R. Society London A*, vol. 359, pp. 319–343, 1978.

[16] Wang, X. D., Tian, Y., and Peng, X. F., Self-Aggregation of Vapor–Liquid Phase Transition, *Progress in Natural Science (Chinese)*, vol. 13, pp. 281–286, 2003.

[17] Tian, Y., Wang, X. D., and Peng, X. F., Analysis of Surface Inside Metastable Bulk Phase During Gas–Liquid Phase Transition, *Journal of Engineering Thermophysics (Chinese)*, vol. 25, pp. 100–102, 2004.

[18] Venables, J. A., *Introduction to Surface and Thin Film Processes*, Cambridge University Press, Cambridge, UK, pp. 144–165, 2000.

[19] Amar, J. G., Popescu, M. N., and Family, F., Self-Consistent Rate Equation Approach to Nucleation and Growth in Point/Extended Island Models of 1-D Homoepitaxy, *Proceeding of Material Research Society*, vol. 570, no. 3, 1999.

[20] Brune, H., Microscopic View of Epitaxial Metal Growth: Nucleation and Aggregation, *Surface Science Reports*, vol. 31, no. 3, pp. 121–229, 1998.

[21] Oura, K., Lifshits, V. G., Saranin, A. A., Zotov, A. V., and Katayama, M., *Surface Science*, Springer-Verlag, New York, July 2003.

[22] Shi, F., Shim Y., and Amar, J. G., Island-Size Distribution and Capture Numbers in Three-Dimensional Nucleation: Comparison with Mean-Field Behavior, *Physical Review B*, vol. 71, pp. 245411–245416, 2005.

[23] Venables, J. A., and Brune, H., Capture Numbers in the Presence of Repulsive Adsorbate Interactions, *Physical Review B*, vol. 66, pp. 195404–195419, 2002.

[24] Brune, H., Bales, G. S., Jacobsen, J., Boragno, C., and Kern, K., Measuring Surface Diffusion from Nucleation Island Densities, *Physical Review B*, vol. 60, pp. 5991–6006, 1999.

[25] Stroscio, J. S., and Pierce, D. T., Scaling of Diffusion Mediated Island Growth in Iron-On-Iron Homoepitaxy, *Physics Review B*, vol. 49, pp. 8522–8525, 1994.

[26] Ratsch, C., and Zangwill, A., Saturation and Scaling of Epitaxial Island Densities, *Physics Review Letters*, vol. 72, pp. 3194–3197, 1994.

[27] Bartelt, M. C., Tringides, M. C., and Evans, J. W., Island Size Scaling in Surface Deposition Processes, *Physics Review B*, vol. 47, pp. 13891–13894, 1993.

[28] Chen, L. Y., Baldan, M. R., and Ying, S. C., Surface Diffusion in the Low-Friction Limit: Processes, *Physics Review B*, vol. 54, pp. 8856–8861, 1996.

[29] Blochl, P. E., Smargiassi, E., Car, R., Laks, D. B., Andreoni, W., and Pantelides, S. T., First Principle Calculations Self-Diffusion Constants in Silicon, *Physics Review Letters*, vol. 70, pp. 2435–2438, 1993.

[30] Ratsch, C., Seitsonen A. P., and Scheffler, M., Strain Dependence of Surface Diffusion: Ag on Ag(111) and Pt(111), *Physics Review B*, vol. 55, pp. 6750–6753, 1997.

[31] DeGennes, P. G., Wetting: Static and Dynamics, *Review of Modern Physics*, vol. 57, pp. 827–863, 1985.

[32] Leger, L., and Joany, J. F., Liquid Spreading, *Reports on Progress in Physics*, vol. 57, pp. 431–487, 1977.

[33] Huh, C., and Mason, S. G., Effect of Surface Roughness on Wetting (Theoretical), *Journal of Colloids and Interface Science*, vol. 60, pp. 11–37, 1977.

[34] Wenzel, R. N., Resistance of Solid Surfaces to Wetting by Water, *Industrial and Engineering Chemistry*, vol. 28, pp. 988–990, 1936.

[35] Shibuichi, S., Onda T., Satoh, N., and Tsujii, K., Super-Water-Repellent Fractal Surfaces, *Journal of Physical Chemistry*, vol. 100, pp. 19512–19617, 1996.

[36] Dussan, E. B., On the Spreading of Liquid on Solid Surfaces: Static and Dynamic Contact Lines, *Annual Review Fluid Mechanics*, vol. 11, pp. 371–400, 1979.

[37] Briscoe, B. J., and Galvin, K. P., The Sliding of Sessile and Pendent Droplets the Critical condition, *Journal of Colloid and Interface Science*, vol. 52, pp. 219–229, 1991.

[38] Extrand, C. W., and Kumara, Y., Liquid Drop on an Inclined Plane: The Relation Between Contact Angles, Drop Shape and Retentive Forces, *Journal of Colloid and Interface Science*, vol. 170, pp. 515–521, 1995.

[39] Elsherbine, A. I., and Jacobi, A. M., Retention Forces and Contact Angles for Critical Liquid Drops on Non-Horizontal Surfaces, *Journal of Colloid and Interface Science*, vol. 299, pp. 841–849, 2006.

[40] Öner, D., and McCarthy, T. J., Ultra-Hydrophobic Surfaces: Effects of Topography Length Scales on Wettability, *Langmuir*, vol. 16, pp. 7777–7782, 2000.

[41] Krasovitski, B., and Marmur, A., Drops Down the Hill: Theoretical Study of Limiting Contact Angles and the Hysteresis Range on a Tilted Plate, *Langmuir*, vol. 21, no. 9, pp. 3881–3885, 2005.

[42] Pierce, E., Carmona, F. J., and Amirfazli, A., Understanding of Sliding and Contact Angles Results in Tilted Plate Experiments, *Colloids and Surfaces A: Physicochemical and Engineering Aspects*, vol. 323, pp. 73–82, 2008.

[43] ElSherbini, A. I., and Jacobi, A. M., Liquid Drops on Vertical and Inclined Surfaces I: An Experimental Study of Drop Geometry, *Journal of Colloid and Interface Science*, vol. 273, pp. 556–565, 2004.

[44] Elsherbine, A. I., and Jacobi, A. M., Liquid Drops on Vertical and Inclined Surfaces II. An Experimental Study of Drop Geometry, *Journal of Colloid and Interface Science*, vol. 273, pp. 566–575, 2004.

[45] Neeumann, A. W., Abdelmessihm, A. H., and Hameed, A., The Role of Contact Angles and Contact Angles Hysteresis in Dropwise Condensation Heat Transfer, *International Journal of Heat and Mass Transfer*, vol. 21, pp. 947–953, 1978.

[46] Sikarwar, B. S., Battoo, N. K., Khandekar, S., and Muralidhar, K., Dropwise Condensation Underneath Chemically Textured Surfaces: Simulation and Experiments, *ASME Journal of Heat Transfer*, vol. 133, Issue 2, p. 021501 (1–15), 2011.

[47] Leipertz, A., and Fröba, A. P., Improvement of Condensation Heat Transfer by Surface Modification, *Proceedings 7th ISHMT-ASME International Heat and Mass Transfer Conference*, IIT Guwahati (India), K7, pp. k85–k99, 2006.

[48] Lawal, A., and Brown, R. A., The Stability of an Inclined Pendent Drop, *Journal of Colloid and Interface Science*, vol. 89, pp. 332–345, 1982.

[49] Rose, J. W., Further Aspects of Dropwise Condensation Theory, *International Journal of Heat and Mass Transfer*, vol. 19, pp. 1363–1370, 1976.

[50] Zhao, H., and Beysens, D., From Droplet Growth to Film Growth on a Heterogeneous Surface: Condensation Associated With a Wettability Gradient, *Langmuir*, vol. 11, pp. 627–634, 1996.

[51] Mu, C., Pang, J., and Liu, T., Effect of Surface Topography of Material on Nucleation Site Density of Dropwise Condensation, *Chemical Engineering Science*, vol. 63, pp. 874–880, 2008.

[52] Battoo, N. K., Sikarwar, B. S., Khandekar, S., and Muralidhar K., Mathematical Simulation of Dropwise Condensation Exposed to Vapor Flux, *Proceeding 9th International ISHMT—ASME Heat and Mass Transfer Conference* Mumbai, India, 346, pp. 1330–1336, 2010.

[53] Andrieu, C., Beysens, D. A., Nikolayev, V. S., and Pomeau, Y., Coalescence of Sessile Drops, *Journal of Fluid Mechanics*, vol. 453, pp. 427–438, 2002.

[54] Wu, M., Cubaud, T., and Ho, C. M., Scaling Law in Liquid Drop Coalescence Driven by Surface Tension, *Physics of Fluids*, vol. 16, pp. L51–L54, 2004.

[55] Liao, Q., Zhu, X., Xing, S. M., and Wang, H., Visualization Study on Coalescences Between Pair of Water Drops On Inclined Surfaces, *Experimental Thermal and Fluid Science*, vol. 31, pp. 1647–1654, 2008.

[56] Narhe, R., Beysens, D., and Nikolayev, V. S., Contact Line Dynamics in Drop Coalescences and Spreading, *Langmuir*, vol. 20, pp. 1213–1221, 2004.

[57] Thoroddsen, S. T., Takehara, K., and Etoh, T. G., The Coalescence Speed of Pendent and a Sessile Drop, *Journal of Fluid Mechanics*, vol. 527, pp. 85–114, 2005.

[58] Furmidge, C. G., The Sliding Drop on Solid Surfaces and a Theory for Spray Retention, *Journal of Colloid Science*, vol. 17, pp. 309–324, 1962.

[59] Dussan, E. B., On the Ability of Drops or Bubbles to Stick to Non-Horizontal Surface of Solids, *Journal of Fluid Mechanics*, vol. 151, pp. 1–20, 1985.

[60] Sadhal, S. S., Ayyaswamy, P. S., and Chung, J. N., *Transport Phenomena With Drops and Bubbles*, Mechanical Engineering Series, Springer, New York, NY, pp. 218–230, 1997.

[61] Dimitrarakopoulos, P., and Higdon, J. J. L., On the Gravitational Displacement of the Three–Dimensional Fluid Droplets from Inclined Solid Surfaces, *Journal of Fluid Mechanics*, vol. 395, pp. 181–209, 1999.

[62] Suzuki, S., Nakajima, A., Sakai, M., Song, J., Yoshida, N., Kameshima, Y., and Okada, K., Sliding Acceleration of Water Droplets on a Surface Coated With Fluoroalkysline and Octadecyltrimethoxysilane, *Surface Science*, vol. 600, pp. 2214–2219, 2006.

[63] Annapragada, S. R., Garimella, V. S., and Murthy, Y. J., Experimental Characterization of Droplet Motion on Inclined Hydrophobic Surfaces, *Proceeding of the 9th*

International ISHMT–ASME Heat and Mass Transfer Conference, Mumbai, India, Paper #343, pp. 1298–1302, 2010.

[64] Kim, H., Lee, H., and Kang, B. H., Sliding of Drops Down an Inclined Solid Surface, *Journal of Colloid Science*, vol. 247, pp. 372–382, 2002.

[65] Huang, H., Liang, D., and Wetton, B., Computation of a Moving Drop/Bubble on a Solid Surface Using a Front-Tracking Method, *Communications in Mathematical Science*, vol. 2, pp. 535–552, 2004.

[66] Gao, L., and McCarthy, T. J., Contact Angle Hysteresis Explained, *Langmuir*, vol. 22, pp. 6234–6237, 2006.

[67] Sakai, M., Song, J., Yoshida, N., Suzuki, S., Kameshima, Y., and Nakajima, A., Direct Observation on Internal Fluidity in a Water Droplet During Sliding on Hydrophobic Surfaces, *Langmuir*, vol. 22, pp. 4906–4909, 2006.

[68] Grand, N. L., Daerr, A., and Limit, L., Shape and Motion of Drops Sliding Down an Inclined Plane, *Journal of Fluid Mechanics*, vol. 541, pp. 293–315, 2005.

[69] Yoshida, N., Abe, Y., Shigeta, H., Nakajima, A., Ohsaki, K., and Watanabi, T., Sliding Behavior of Droplet on Flat Polymer Surface, *Journal of American Chemical Society*, vol. 128, pp. 743–747, 2006.

[70] Denial, S., Chaudhury, M. K., and Chen, J. C., Fast Drop Movements Resulting From the Phase-Change on a Gradient Surface, *Science*, vol. 291, pp. 633–636, 2001.

[71] Sakai, M., and Hashimoto, A., Image Analysis System for Evaluating Sliding Behavior of a Liquid Droplet on a Hydrophobic Surface, *Review of Scientific Instruments*, vol. 78, pp. 045105–045109, 2007.

[72] Suzuki, S., Nakajima, A., Sakai, M., Song, J., Yoshida, N., Kameshima, Y., and Okada, K., Slipping and Rolling Ratio of Sliding Acceleration for a Water Droplet Sliding on Fluoroalkylsilane Coating of Different Roughness, *Chemistry Letters*, vol. 37, pp. 58–59, 2008.

[73] Das, A. K., and Das, P. K., Simulation of Drop Movement Over an Inclined Surface Using Smoothed Particle Hydrodynamics, *Langmuir*, vol. 25, pp. 11459–11466, 2009.

[74] Sikarwar, B. S., Muralidhar, K., and Khandekar, S., Flow and Heat Transfer in a Pendant Liquid Drop Sliding on an Inclined Plane, *Proceeding of the 9th International ISHMT–ASME Heat and Mass Transfer Conference*, Mumbai, India, Paper #345, pp. 1322–1329, 2010.

[75] Barth, T. J., and Jespersen, D. C., The Design and Application of Upwind Schemes on Unstructured Meshes, *AIAA* Paper #0366, vol. 89, 1989.

[76] Frink, N. T., Paresh, P., and Shahyar, P., A Fast Upwind Solver for the Euler Equations on Three Dimensional Unstructured Meshes, *AIAA* Paper #0102, vol. 91, 1991.

[77] Date, A. W., Solution of Transport Equations on Unstructured Meshes With Cell Centered Collocated Variables. Part I: Discretization, *International Journal of Heat and Mass Transfer*, vol. 48, pp. 1117–1127, 2005.

[78] Blackman, L. C. F., Dewar, M. J. S., and Hampson, H., An Investigation of Compounds Promoting the Dropwise Condensation of Stem, *Applied Chemistry*, vol. 7, pp. 160–157, 1957.

[79] Watson, R. G. H., Birt, D. C. P. Honour, C. W., and Ash, B. W., The Promotion of Dropwise Condensation by Montan Wax I. Heat Transfer Measurements, *Journal of Applied Chemistry*, vol. 12, no. 12, pp. 539–546, 1962.

[80] Erb, R. A., and Thelen, E., *Dropwise Condensation Characteristics of Permanent Hydrophobic System*, U. S. Department of Interior, R&D Report # 184, pp. 54–57, 1966.

[81] Erb, R. A., Promoting Permanent Dropwise Condensation, *Industrial and Engineering Chemistry*, vol. 57, pp. 49–52, 1965.

[82] Marto, P. J., Looney, D. J., and Rose, J. W., Evaluation of Organic Coating for the Promotion of Dropwise Condensation of Steam, *International Journal of Heat and Mass Transfer*, vol. 29, pp. 1109–1117, 1986.

[83] Mori, K., Fujita, N., Horie, H., More, S., Miyashita, M., and Matsuda, M., Heat Transfer Promotion of Aluminum–Brass Cooling Tube by Surface Treatment With Triazinethiols, *Langmuir*, vol. 7, pp. 1161–1166, 1991.

[84] Zhang, D. C., Lin Z. Q., and Lin, J. F., New Materials for Dropwise Condensation, *Proceedings 8th International Heat Transfer Conference*, vol. 4, pp. 1677–1682, 1986.

[85] Zhao, Q., Zhang, D. C., and Lin, J. F., Surface Materials With Dropwise Condensation Mode by Ion Implantation Technology, *International Heat and Mass Transfer*, vol. 34, pp. 2833–2835, 1991.

[86] Koch, G., Zhang, D. C., and Leiertz, A., Condensation of Steam on the Surface of Hard Coated Copper Discs, *Heat and Mass Transfer*, vol. 32, pp. 149–297, 1997.

[87] Grischke, M., Trojan, K., and Dimigen, H., Deposition of Low Energy Coating With DLC-Like Properties, *Proceedings 11th Conference on High Vacuum, Interfaces and Thin Films*, pp. 433–436, 1994.

[88] Zhao, Q., Zhang, D. C., Zhu, X. B., Xu, D. Q., Lin, Z. Q., and Lin, J. F., Industrial Application of Dropwise Condensation, *Proceedings 9th International Heat Transfer Conference*, vol. 4, pp. 391–394, 1990.

[89] Zhao, Q., and Burnside, B. M., Dropwise Condensation of Steam on Ion Implanted Condenser Surfaces, *Heat Recovery Systems & CHP*, vol. 14, pp. 525–534, 1994.

[90] Rausch, M. H., Fröba, A. P., and Leipertz, A., Dropwise Condensation on Plasma–Ion Implanted Aluminum Surface, *International Journal of Heat and Mass Transfer*, vol. 51, pp. 1061–1070, 2007.

[91] Vemuri, S., Kim, K. J., Wood, B. D., Govindraju, S., and Bell, T. W., Long Term Testing for Dropwise Condensation Using Self-Assembled Monolayer Coating on *n*-Octadecycl Mercaptin, *Applied Thermal Engineering*, vol. 26, pp. 421–429, 2006.

[92] Das, A. K., Kilty, H. P., Marto, P. J., The Use of an Organic Self-Assembled Monolayer Coating to Promote

Dropwise Condensation of Steam on Horizontal Tubes, *ASME Journal of Heat Transfer*, vol. 122, no. 2, pp. 278–286, 2000.

[93] Das, A. K., Kilty, H .P., and Marto, P. J., Dropwise Condensation of Steam on Horizontal Corrugated Tubes Using an Organic Self-Assembled Monolayer Coating, *Journal Enhanced Heat Transfer*, vol. 7, no. 2, pp. 109–123, 2000.

[94] Koch, G., Zhang, D., and Leipertz, A., Study of Plasma Enhanced CVD Coated Material to Promote Dropwise Condensation, *International Journal of Heat and Mass Transfer*, vol. 41, no. 13, pp. 1899–1900, 1998.

[95] Leipertz, A., and Choi, K. H., Dropwise Condensation on Ion Implanted Metallic Surfaces, *Proceedings 3rd European Thermal Sciences Conference*, pp. 917–921, 2000.

[96] Ma, X., and Wang, B., Life Time Test of Dropwise Condensation on Polymer-Coated Surfaces, *Heat Transfer–Asian Research*, vol. 28, no. 7, pp. 551–558, 1999.

[97] Rausch, M. H., Leipertz, A., and Fröba, A. P., Dropwise Condensation of Steam on Ion Implanted Titanium Surfaces, *International Journal of Heat and Mass Transfer*, vol. 53, pp. 423–430, 2010.

[98] Cras, J. J., Rowe-Tait, C. A, Nivens, D. A., and Ligler, F. S., Comparison of Chemical Cleaning Methods of Glass in Preparation for Silanization, *Biosensors and Bioelectronics*, vol. 14, pp. 683–688, 1999.

[99] Genzer, J., and Efimenko, K., Creating Long-Lived Super Hydrophobic Polymer Surface Through Mechanically Assembled Monolayer, *Science*, vol. 290, pp. 2130–2133, 2000.

[100] Ma, X. H., Wang, B., X., Xu, D. Q., and Lin, J. F., Life Time Test of Dropwise Condensation on Polymer-Coated Surfaces, *Heat Transfer—Asian Research*, vol. 28, no. 7, pp. 551–558, 1999.

[101] Ma, X., Tao, B., Chen, J., Xu, D., and Lin, J., Dropwise Condensation Heat Transfer of Steam on a Polytethefluoroethylene Film, *Journal of Thermal Science*, vol. 10, no. 3, pp. 247–253, 2000.

[102] Jain, V., and Nema, S. K., Deposition of Super-Hydrophobic Nanostructure Teflon-Like Coating Using Expanding Plasma Arc, *Applied Surface Science*, vol. 253, pp. 5462–5466, 2007.

[103] Bansal, G. D., Khandekar, S., and Muralidhar, K., Measurement of Heat Transfer During Dropwise Condensation of Water on Polyethylene, *Nanoscale and Microscale Thermophysical Engineering*, vol. 13, pp. 184–201, 2009.

[104] Collier, J. G., *Convective Boiling and Condensation*, 2nd ed., McGraw-Hill, New York, 1981.

[105] Rose, J. W., Condensation Heat Transfer Fundamentals, *Transactions of the AIChE*, vol. 76A, pp. 143–152, 1998.

[106] Rose, J. W., Condensation Theory, *International Journal of Heat and Mass Transfer*, vol. 24, pp. 191–194, 1981.

[107] Goldstein, R. J., Ibele, W. E., Patankar, S. V., Simon, T. W., Kuehn, T. H., Strykowski, P. J., Tamma, K. K., Heberlein, J. V. R., Davidson, J. H., Bischof, J., Kulacki, F. A., Kortshagen, U., Garrick, S., and Srinivasan, V., Heat Transfer—A Review of 2003 Literature, *International Journal of Heat and Mass Transfer*, vol. 49, pp. 451–534, 2006.

[108] Ma, X., Rose, J. W., Xu, D., Lin, J., and Wang B., Advances in Dropwise Condensation Heat Transfer, *Chinese Research—Chemical Engineering Journal*, vol. 78, pp. 78–93, 2000.

[109] Rose, J. W., Surface Tension Effects and Enhancements of Condensation Heat Transfer, *Chemical Engineering Research and Design*, vol. 82, pp. 419–429, 2004.

[110] Rose, J., Utaka, Y., and Tanasawa, I., Dropwise Condensation, in Randlikar, S. G., ed. *Hand Book of Phase Change: Boiling and Condensation*, Taylor & Francis, USA, pp. 581–594, 1999.

[111] Tsuruta, T., and Tanaka, H., A Theoretical Study on the Constriction Resistance in Dropwise Condensation, *International Journal of Heat and Mass Transfer*, vol. 34, no. 11, pp. 2779–2786, 1991.

[112] Tsuruta, T., Tanaka, H., and Togashi, S., Experimental Verification of Constriction Resistance Theory in Dropwise Condensation Heat Transfer, *International Journal of Heat and Mass Transfer*, vol. 34, no. 11, pp. 2787–2796, 1991.

[113] Tanner, D. W., Potter, C. J., Pope, D., and West, D., Heat Transfer in Dropwise Condensation: Part II—Surface Chemistry, *International Journal of Heat and Mass Transfer*, vol. 8, pp. 427–436, 1965.

[114] Tanner, D. W., Pope, D., Potter, C. J., and West, D., Heat Transfer in Dropwise Condensation at Low Stem Pressure in the Absence of Non-Condensable Gas, *International Journal of Heat and Mass Transfer*, vol. 11, pp. 181–190, 1968.

[115] Wilkins, D., and Bromley, L., Dropwise Condensation Phenomena, *AIChE Journal*, vol. 19, pp. 839–845, 1973.

[116] Tsuruta, T., Constriction Resistance in Dropwise Condensation, *Proceeding of the ASME Engineering Foundation Conference on Condensation and Condenser Design*, pp. 109–170, 1993.

[117] Stylianou, S. A., and Rose, J. W., Dropwise Condensation on Surface Having Different Thermal Conductivities, *ASME Journal of Heat Transfer*, vol. 102, pp. 477–482, 1980.

[118] Stylianou, S. A., and Rose, J. W., Drop-to-Filmwise Condensation Transition: Heat Transfer Measurements for Ethanediol, *International Journal of Heat and Mass Transfer*, vol. 97, pp. 72–98, 1975.

[119] McCormick, J. L., and Westwater, J. W., Nucleation Sites for Dropwise Condensation, *Chemical Engineering Science*, vol. 20, pp. 1021–1031, 1965.

[120] Peterson, A. C., and Westwater, J. W., Dropwise Condensation of Ethylene and Glycol, *Chemical Engineering Progress Symposium Series*, vol. 64, pp. 135–142, 1966.
[121] Umur, A., and Griffith, P., Mechanism of Dropwise Condensation, *ASME Journal of Heat Transfer*, vol. 87, pp. 275–282, 1965.
[122] Ivanovskii, M. N., Subbotin, V. I., and Milovanov, Y. V., Heat Transfer With Dropwise Condensation of Mercury Vapor, *Teploenergetika*, vol. 14, pp. 81–85, 1967.
[123] Rausch, M. H., Leipertz, A., and Fröba, A. P., On the Mechanism of Dropwise Condensation on Ion Implanted Metallic Surface, *ASME Journal of Heat Transfer*, vol. 132, pp. 94503(1–3), 2010.
[124] Le Fevre, E. J., and Rose, J. W., A Theory of Heat Transfer by Dropwise Condensation, *Proceedings of the 3rd International Heat Transfer Conference*, vol. II, pp. 362–375, 1966.
[125] Glicksman, R. L., and Hunt, W. A., Numerical Simulation of Dropwise Condensation, *International Journal of Heat and Mass Transfer*, vol. 15, pp. 2251–2269, 1972.
[126] Wu, W. H., and Maa, J. R., On the Heat Transfer in Dropwise Condensation, *Chemical Engineering Journal*, vol. 12, 225–231, 1976.
[127] Abu-Orabi, M., Modeling of Heat Transfer in Dropwise Condensation, *International Journal of Heat and Mass Transfer*, vol. 41, pp. 81–87, 1998.
[128] Rose, J. W., and Glicksman, L. R., Dropwise Condensation—The Distribution of Drop Sizes, *International Journal of Heat and Mass Transfer*, vol. 16, pp. 411–425, 1973.
[129] Gose, E., Mucciordi, A. N., and Baer, E., Model for Dropwise Condensation on Randomly Distributed Sites, *International Journal of Heat and Mass Transfer*, vol. 10, pp. 15–22, 1976.
[130] Burnside, B. M., and Hadi, H. A., Digital Computer Simulation of Dropwise Condensation From Equilibrium Droplet to Detectable Size, *International Journal of Heat and Mass Transfer*, vol. 42, pp. 3137–3146, 1999.
[131] Vemuri, S., and Kim, K. J., An Experimental and Theoretical Study on the Concept of Dropwise Condensation, *International Journal of Heat and Mass Transfer*, vol. 49, pp. 649–657, 2006.
[132] Chatterjee, J., A Criterion for Buoyancy Induced Drop Detachment Based on an Analytical Approximation of the Drop Shape, *Colloids and Surfaces A: Physicochemical and Engineering Aspects*, vol. 178, pp. 249–263, 2001.
[133] Chatterjee, J., Critical Eötvös Numbers for Buoyancy-Induced Oil Drop Detachment based on Shape Analysis, *Advances in Colloid and Interface Science*, vol. 98, pp. 245–283, 2002.
[134] Lexmond, A. S., and Geld, C. W. M., The Effect of Plate Thickness, Surface Tension and Fluid Flow on Detachment of Drop from a Plate, *Experimental Thermal and Fluid Science*, vol. 29, pp. 813–819, 2005.
[135] Sikarwar, B. S., Muralidhar, K., and Khandekar, S., Flow and Thermal Fields in a Pendant Droplet Moving on Lyophobic Surface, *Proceedings 14th International IHTC–ASME Heat and Mass Transfer Conference*, Washington, DC, Paper #IHTC14–22520, pp. 169–178, 2010.
[136] Mills, A. F., and Seban, R. A., The Condensation Coefficient of Water, *International Journal of Heat and Mass Transfer*, vol. 10, pp. 1815–1827, 1967.
[137] Sukhatme, S. P., and Rohsenow, W. M., Heat Transfer During Film Condensation of a Liquid Metal Vapor, *ASME Journal of Heat Transfer*, vol. 88, pp. 19–28, 1966.

APPENDIX: VAPOR ACCOMMODATION COEFFICIENT

When condensation occurs, kinetic theory of gases suggests that the flux of vapor molecules joining the liquid must exceed the flux of molecules escaping to the liquid phase. Hence, the accommodation coefficient, denoted as $\hat{\sigma}$, defines the fraction of the striking vapor molecules that actually get condensed on the vapor-liquid interface. The remaining fraction $(1 - \hat{\sigma})$ is due to reflection of vapor molecules that strike the interface but do not condense. Hence, the accommodation coefficient indirectly measures the interfacial resistance of the liquid–vapor interface to condensation. Higher the accommodation coefficient, lower the interfacial resistance of the liquid-vapor interface of condensed drop. Quoted values of $\hat{\sigma}$ in literature widely vary. Mills [136] reported that the accommodation coefficient is less than unity only when the interface is impure. For a pure liquid–vapor interface, value reported in the literature is unity. Because extreme purity is unlikely in most engineering systems, a value of less than unity can be expected. Sukhatme and Rohsenow [137] reported its values ranging from 0.37 to 0.61 for condensation of metallic vapor. For liquid ethanol, methanol, alcohol, and water, the reported value of accommodation coefficient range from 0.02 to 0.04. On the other hand, reported values for benzene and carbon tetrachloride are closer to unity. The accommodation coefficient decreases with increasing condensing temperature. The interfacial resistance may be particular important in the condensation of liquid metals.

Figure A1 presents the variation of interfacial heat transfer resistance per unit area $(1/h_i)$ at experimental conditions of $T_{sat} = 30^{\circ}$C and $p_{sat} = 0.015$ bar:

As can be seen, there is considerable variation of the interface heat transfer coefficient of over an order of magnitude for small values of the accommodation coefficient, $0.01 < \hat{\sigma} < 0.1$. Beyond $\hat{\sigma} > 0.1$ the interface heat transfer coefficient does not change appreciably. Next, the thermal resistance per unit area for drop diffusion (conduction heat transfer through an individual drop) and the interface heat transfer resistance per unit area (for $\hat{\sigma} = 0.01$ and as inset for $\hat{\sigma} = 0.1$) as a function of drop diameter are compared. The latter is a constant, while the former is a linear function on a semilog plot. As can be seen, the most dominant thermal resistance is due to drop conduction for practically the entire range of drop diameters. As the drop grows, heat transfer

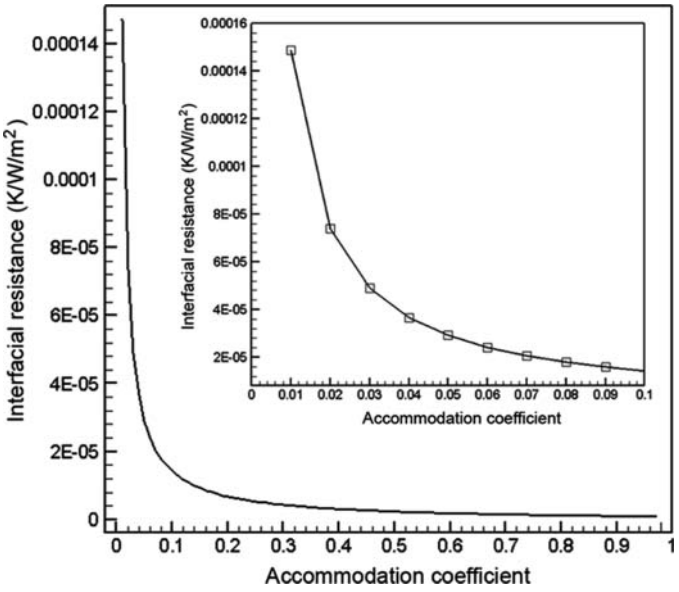

Figure A1 Variation of interfacial heat transfer coefficient with respect to the accommodation coefficient.

is progressively limited by the conduction resistance of the drop. The interfacial resistance plays a very minor role in the overall process, except immediately after nucleation when the drops are below a diameter of, say, 0.01–0.1 mm. Figures A1 and A2 clearly demonstrate that the accommodation coefficient plays a critical role only on very small range of nucleating and growing drops, i.e., in the very early stages of drop development. The major focus of the present study is long term dropwise condensation, in contrast to thin film deposition, vacuum CVD deposition of metal vapors, epitaxial growth in the early nucleation stages, etc. Thus, one can conclude that the sensitivity of the macroscopic numerical model to the accommodation coefficient is not predominant and a value of unity is acceptable.

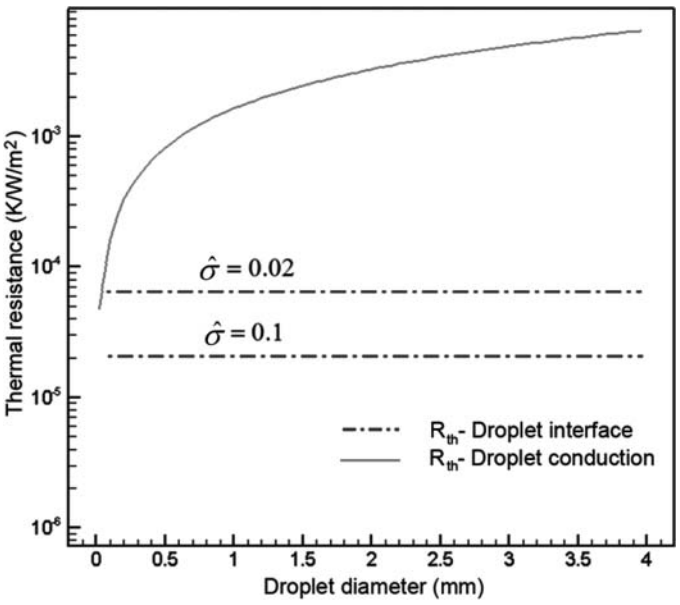

Figure A2 Comparison of conduction and interfacial thermal resistance per unit area of a drop. The condensation process is mostly limited by conduction resistance of the drop.

Basant Singh Sikarwar is a doctoral student at the Department of Mechanical Engineering, Indian Institute of Technology Kanpur, India. He received an M.Tech. degree from IIT Roorkee, India, in 2007. His doctoral research is focused on experimental and numerical simulation of dropwise condensation process.

Sameer Khandekar is an associate professor and P. K. Kelkar Research Fellow at the Department of Mechanical Engineering, IIT Kanpur, India. He completed a master's degree from IIT Kanpur, India, and earned a doctoral degree from Uni-Stuttgart, Germany. His current research interest is experimental microscale phase-change thermofluidic and energy systems. He is a recipient of the Prof. K. N. Seetharamu Award (Indian Society of Heat and Mass Transfer, 2010), George Grover Medal (International Heat Pipe Committee, 2007), and Young Scientist Award (Department of Atomic Energy, India, 2005).

Smita Agrawal is currently a doctoral candidate at the Department of Mechanical Engineering, University of Minnesota–Twin Cities, USA. She graduated with a bachelor's degree and master's degree from IIT Kanpur. Her area of interest is experimental fluid mechanics and heat transfer.

Sumeet Kumar is currently a doctoral candidate in the Mechanical Engineering Department, MIT, Cambridge, MA. He earned a B.Tech. degree in mechanical engineering from IIT Kanpur, India, and later completed his master's degree from MIT, USA, in 2009. His current research is in the design and implementation of sensor network for monitoring and addressing wastage in complex environments.

K. Muralidhar, a professor of mechanical engineering, IIT Kanpur, India, has conducted experiments and numerical simulation in fluid mechanics and heat transfer. He has contributed to improving the understanding of transport phenomena in porous media, wake dynamics, development of numerical algorithms, and laser measurement of flow and thermal fields. His research finds applications in enhanced oil recovery, regenerators, nuclear waste disposal, growth of optical crystals, and CVD reactors.